Rune Strandberg

Theoretical studies of the intermediate band solar cell

Thesis for the degree of Philosophiae Doctor

Trondheim, May 2010

Norwegian University of Science and Technology
Faculty of Natural Sciences and Technology
Department of Physics

NTNU
Norwegian University of
Science and Technology

NTNU
Norwegian University of Science and Technology

Thesis for the degree of Philosophiae Doctor

Faculty of Natural Sciences and Technology
Department of Physics

ISBN 978-82-471-2150-4 (printed ver.)
ISBN 978-82-471-2151-1 (electronic ver.)
ISSN 1503-8181

Doctoral theses at NTNU, 2010:94

Printed by NTNU-trykk

Abstract

This thesis presents theoretical work on the intermediate band solar cell (IBCS). It is divided into two main parts: The first part is an introduction to basic solar cell physics and a presentation of central parts of the physics of the IBSC. The intention is not to give a complete review of these topics, but to provide readers unfamiliar to solar cell physics the basic knowledge needed to understand the scientific papers that constitutes part two of the thesis.

The intermediate band solar cell is a photovoltaic concept with a theoretical efficiency limit of 63.2 %. This is over 50 % higher than the 40.7 % limit for conventional photovoltaic cells. The feature that distinguishes the IBSC from other photovoltaic concepts is that it allows electrons to be excited from low energy electron states to high energy states in a two-step process via an intermediate band (IB). This allows a more effective harvest of the energy of the photons impinging on the cell, than in ordinary solar cells where only transitions directly from the low energy states to the high energy states are allowed.

Theoretical efficiencies can be calculated for various combinations of band gaps and light concentrations. For conventional solar cells it has been shown that the theoretical efficiency of cells with band gaps lower than the optimal can be increased when spectral selectivity is applied. Spectral selectivity means that the cell absorptivity of certain photon energies above the band gap is set to zero. In this work it is shown that the theoretical efficiency increases for several band gap combinations and light concentrations for the IBSC, when spectral selectivity is applied. For some spectra, the efficiency of a spectrally selective IBSC can surpass the efficiency limit found without spectral selectivity. To give an example, the efficiency limit for an IBSC under the 1 sun 6000 K black body spectrum increases from 46.8 % to 48.5 % when spectral selectivity is applied. No change is found for the fundamental 63.2 % limit for fully concentrated black body radiation.

For the two-step generation process to work properly, the intermediate

band has to be partially filled with electrons to allow transitions both to and from the IB. It has previously been assumed that one either has to use materials that have a partially filled IB in thermal equilibrium or use doping to assure that the IB is partially filled. This work investigates the possibility of partially filling the IB with electrons that are photogenerated from the valence band, so called photofilling. In a model based on detailed balance principles it is found that a practically usable photofilling can be obtained when the density of states in the IB has values typical for IBs formed by quantum dot superlattices, particularly when the light is concentrated. It is also shown how the filling varies with the voltage of the solar cell and the position of the IB in the main band gap.

A drift-diffusion model for the IBSC which allows for photofilling, that is, the IB-filling is treated as a variable, is also developed. By use of this model it is shown how the mutual sizes of the absorption cross-sections for transitions over the sub-band gaps can give rise to spatial variations in the filling. These spatial variations will result in electric fields that can drive the carriers in the conduction band and valence band in opposite directions. If this effect is present in real cells this observation has the practical consequence that the cell should be designed in a way which assures that the electric field push the electrons in the right direction.

The drift-diffusion model is also used to determine whether an unfilled or a half-filled IB in thermal equilibrium results in the highest efficiency. This is found to depend on the mutual sizes of the absorption cross sections for transitions via the IB. The optimal filling is examined for a particular example.

To investigate the optimal filling further, models based on detailed balance principles are applied to see how the optimal filling is affected by various parameters. The optimal filling is found to vary with the band gaps, the overlap between the absorption coefficients, the light concentration and the mutual sizes of the absorption cross-sections for transitions over the sub-band gaps. The negative effect of a non-optimal filling is shown to depend on the absorptivity of the cell, the overlap between the absorption coefficients as well as the density of states in the IB. Two main effects are identified as determinative for the optimal filling. The first is the pursuit for a maximized net generation rate via the IB. The second effect is the irreversible losses due to overlapping absorption coefficients. These should be as small as possible.

An ideality that is assumed in most theoretical work on the IBSC is that the IB has no energetical width. Previously a fundamental limit has been found by Levy and Honsberg for the minimal effect of this width on the cell efficiency. In this thesis an attempt is made to investigate how

the thermalized nature of the IB-electrons affects the efficiency of IBSCs with a wide IB. To obtain numerical results, two sets of idealized absorption coefficients based on different assumptions are derived. For IBs with non-overlapping absorption coefficients, the efficiency deviates only slightly from the fundamental limit when the IB-width is below 0.15 eV. When the width increases, so does the difference between the fundamental limit and the efficiency calculated with the thermalized nature of the IB-electrons taken into account. One of the sets of absorption coefficients increases more steeply with the photon energy than the other. It is found that the reduction in efficiency is smaller for the absorption coefficients with the steeper increase.

Efficiencies are also calculated when the absorption coefficients are overlapping in the energy range which is assumed to be affected by the IB-width. The difference in efficiency between the fundamental limit and the efficiencies found in this work can be reduced, as compared to in the non-overlapping case, when the IB-width approaches 1 eV. In some of the investigated cases, the decrease in efficiency due to an increase in the IB-width is still significantly higher than the efficiency limit for single band gap cells. In other cases, however, the efficiency shows a devastating drop when the width of the IB goes from 0 to 1 eV.

The models presented in the thesis are idealized and based on assumptions that might not be fulfilled in real devices. Before transferring the results to real devices one should first be assured that the assumptions that have been made in the modeling are valid. If not, analyzes based on more advanced models might be required before conclusions can be drawn.

Preface

This thesis represents the final stop of a four and a half year academic and emotional roller coaster ride. A ride with peaks of inspiring work, small discoveries and the good feeling of doing something that gives you energy and pleasure. And a ride with valleys of frustration when things are not going as expected, when things are delayed and when the good idea turned out not to be good at all. Luckily, this is an unusual kind of roller coaster that stops at a peak.

The thesis has become very different from what was intended. Starting in August 2005, my work was supposed to be experimental with deposition of thin-films with pulsed laser deposition as the main field of research. Unfortunately, lab construction sometimes takes longer time than expected. When the lab was still not operating in January 2008, it was undoubtedly time to take action. While waiting for the lab to be completed, some initial theoretical ideas had started to form. A new research plan was made with these ideas as a base. They have now been extended and refined, and are presented in this thesis. Changing the objective of the thesis obviously causes strain in the time schedule. Hopefully, this is not reflected in premature conclusions or badly founded arguments. I hope that at least some of the work will turn out to be useful for the understanding of the intermediate band solar cell. Even if just a single person finds some of my work useful at a single occasion it has not been in vain.

A number of people deserves an acknowledgement for their support during my time as a PhD-student. First of all I would like to thank my supervisor Turid Worren Reenaas for her enthusiasm and never-ending optimism as well as the desirable ability to always look for opportunities and ways to solve unexpected problems. Co-supervisor Ola Hunderi deserves a thank for using his experience and knowledge to give me inputs while I was writing the thesis.

Sharing room with Sedsel Fretheim Thomassen for four years has been a true pleasure. I thought it would be hard to replace Sedsel when she had her

maternity leave, but then Maryam Gholami showed up and made my last few months just as nice as the first 48. Maryam also deserves recognition for discovering, or asking the questions that lead to the discovery, of some of the mistakes that have been found in paper II of the thesis. I wish both of you good luck in pursuing your PhD-degree!

Despite the fact that the thesis is purely theoretical, I would like to thank Randi Holmestad, Bjørn Soleim, Heimir Magnusson, John Walmsley, Per Erik Vullum, Heidi Nordmark and Cecile Ladam for learning me how to use a transmission electron microscope, a pulsed laser deposition system as well as equipment for X-ray diffraction. All of these techniques where initially supposed to be applied in my work.

Finally, I would like to thank everyone in NTNUI orientering, and particularly the guys at D-51, for making the last four and a half years an unforgettable time.

Contents

1 Introduction **1**

2 Solar cell physics **7**
2.1 Light spectra 8
2.2 Detailed balance theory 10
2.2.1 Radiative recombination 12
2.2.2 Generation rates 13
2.2.3 Theoretical efficiency limits 15
2.3 The pn-junction 17
2.4 Device modelling 19

3 The Intermediate Band Solar Cell **23**
3.1 Detailed balance theory for the IBSC 23
3.2 Non-idealities 25
3.2.1 Overlapping absorption coefficients 27
3.2.2 Width of the intermediate band 29
3.3 Practical implementation of the IBSC-concept 29
3.3.1 Quantum dot intermediate band solar cell 29
3.3.2 Bulk IB-materials 31
3.3.3 Molecular intermediate band solar cells 31
3.4 Device modeling of IBSCs 32

4 Summary of papers I to V **37**

Paper I **47**

Paper II **59**

Paper III **69**

Paper IV **101**

Paper V **127**

Chapter 1

Introduction

The more and more convincing evidence suggesting that anthropogenic emissions of greenhouse gases is rising the average global temperature [1], has induced a massive public interest in how to limit the negative impacts of these climate changes. The main source of the detrimental emissions is the worlds consumption of fossil fuels. This, combined with the inevitable fact that the amounts of fossil fuels are limited, is causing an increasing interest in the development of non-polluting renewable energy sources. It is understood that these issues cannot be solved by a single technology. Research and development of several environmentally friendly and sustainable energy sources are required to satisfy the energy demand of the world's increasing population. In this thesis, one of these technologies, the intermediate band solar cell, is explored theoretically. After a short introduction of the potential of solar cells as an energy technology, an overview of the physics of conventional solar cells is given in chapter 2. In chapter 3, the essential aspects of the intermediate band solar cell (IBSC) are presented to provide the reader with the necessary knowledge to comprehend papers I-V which presents new theoretical work on the IBSC and constitute the core of this thesis.

In 2007 the global electricity generation amounted to almost 20 000 TWh. Renewable energy technologies accounted for 18 % of the total generation [2]. Today hydropower and energy from biomass are the most important renewable energy sources, with solar and wind power as runner ups [3]. Solar power is divided into two main branches, thermal solar power - where the solar energy is transformed to heat before it is subsequently transformed to electricity, and photovoltaics - where the solar energy is transformed directly to electricity. The electricity producing panels that we call solar cells and mount on our roof tops are photovoltaic devices. Photovoltaic electricity

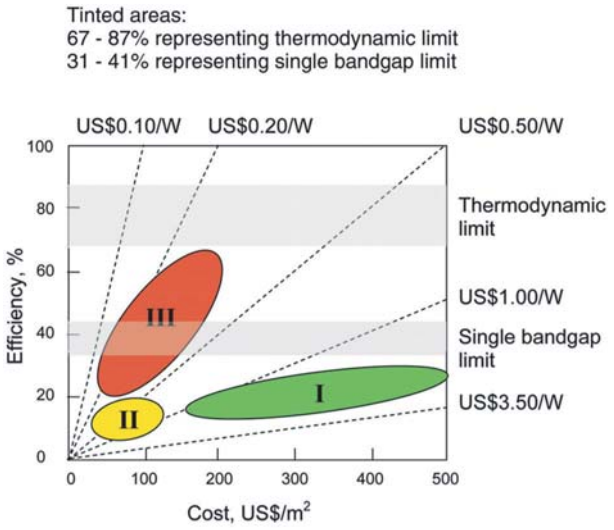

Figure 1.1: The tree generations of photovoltaic technologies position differently in an efficiency-cost plot. The figure is taken from Green [5].

production accounted for only a small fraction of the total global electricity production. The installed photovoltaic capacity corresponds to slightly above 1 % of the total installed renewable capacity [4].

A key to increase the installation of photovoltaic capacity is of course to make it economically competitive. The technologies constituting the photovoltaic branch of the solar energy technologies are often divided into three generations [5]. The division is done with respect to the various strategies that the generations represent to make photovoltaic energy conversion economically viable. A visualization of these generations is shown in figure 1.1. The first generation of photovoltaic solar cells is relatively expensive and typically give efficiencies from 15-20 %. Second generation technologies aim to produce devices which are sufficiently cheap to deliver electricity at a lower price per kWh. The last group, the third generation, are advanced technologies aiming to give cheaper energy due to high cell efficiencies. The third generation cells are more technologically advanced, and have higher theoretical efficiency limits, than first and second generation cells. Theoretical efficiency limits are described closer in section 2 and section 3.

Today the photovoltaic market is dominated by crystalline silicon cells - a first generation technology. Silicon is non-toxic and highly abundant, two very desirable properties. In fact, it is the second most common element

in the earth's crust, only beaten by oxygen. An important drawback of the silicon solar cells is the large amount of energy that is required in the production of high-quality silicon. The energy payback time[1] has been decreasing steadily, however, and are now approximately 1.5 years for state-of-the-art silicon cells [6]. With a guaranteed lifetime of typically 20-25 years, the silicon cells multiply the energy invested in manufacturing them, but the price of the energy delivered by solar cells is still relatively high.

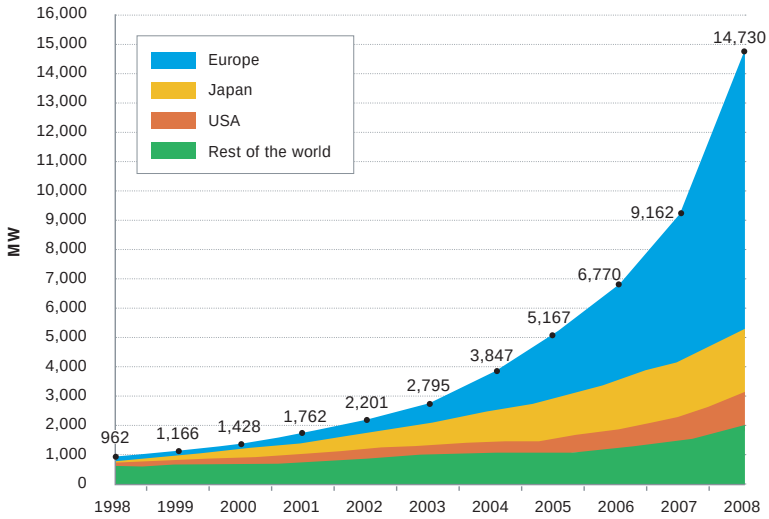

Figure 1.2: The global installed PV-power per region. The figure is taken from the European Photovoltaic Industry Association [7].

Despite today's high cost of photovoltaic energy, generous feed-in tariffs in countries like Germany and Spain, have caused a boom in the PV-market, as shown in figure 1.2 [7]. This has started a positive spiral of technology improvements and falling prices which fuels a hope that the PV-industry will be able to reach grid-parity[2] in more and more segments of the energy market. Today, grid-parity is reached in a few areas like California, but only during times of the day and times of the year when the electricity consumption is high. It has been forecasted, however, that by 2020 grid-parity will be reached in several countries, including Australia and southern Europe as well as large parts of northern Europe, Japan and the USA as

[1] The energy payback time is the time required for the solar cell to deliver the amount of energy it took to manufacture it.

[2] Grid-parity is the limit where the price of electricity produced by solar cells equals the price of electricity delivered by the electricity grid.

shown in figure 1.3 [8], due to reduced cost and increased efficiency of PV-modules.

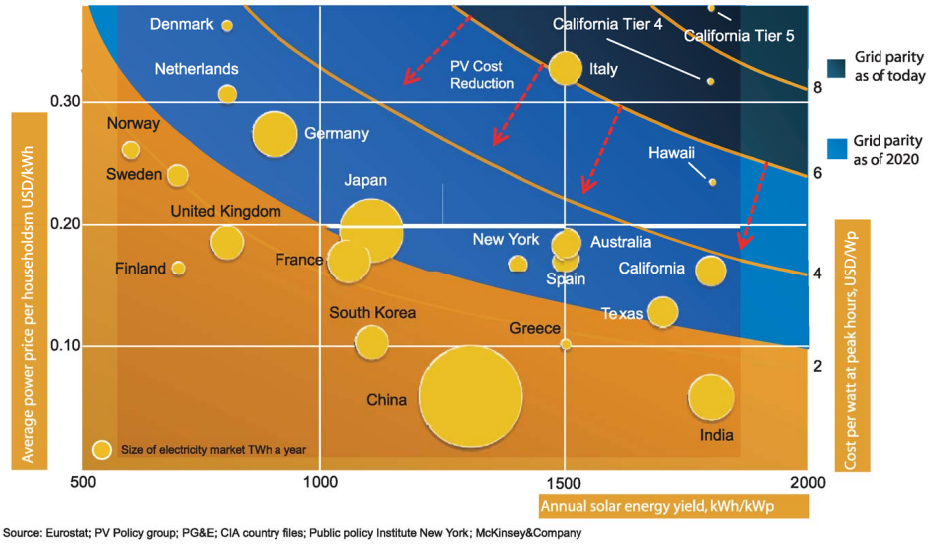

Figure 1.3: As the cost of silicon based photovoltaic modules decreases, grid-parity will be reached in a growing number of locations. The figure is re-printed with permission from the Renewable Energy Corporation [8].

The predictions of the silicon cells to reach grid-parity in important markets in only a decade is not stopping the development of and research on other PV-technologies. To address the energy needs and climate challenges at a broad front, a wide variety of photovoltaic technologies are being explored by scientists all over the world. This includes conventional cells made of materials such as gallium arsenide, cadmium telluride and copper indium gallium diselenide as well as more exotic technologies like dye sensitized solar cells, polymer based solar cells, tandem cells, hot carrier cells and intermediate band solar cells [9]-[14].

While commercial silicon cells typically has an efficiency in the range 13 to 20 %, the current world record for photovoltaic energy conversion is 41.6% and was reported by Spectrolab in 2009 [15]. The record was set using a triple-junction tandem cell. Triple-junction tandem cells are structures with three solar cells with different optical properties stacked on top of each other. The large gap between the record efficiency and the efficiency of commercial cells shows that it is technological possible to harvest much

more of the energy coming from the sun than what is the case today. As will be described in more detail later, the intermediate band solar cell is a particularly interesting photovoltaic concept because it has a theoretical efficiency limit of comparable size to the triple junction tandem cell, but can, if suitable materials are found, be implemented in a less complicated way. While the triple junction tandem cell consists of three cells stacked on top of each other, the intermediate band solar cell consists of a single cell.

Chapter 2

Solar cell physics

Before relevant parts of the physics of the intermediate band solar cell is reviewed in chapter 3, it is useful to go through some central parts of the physics of conventional solar cells. This chapter is describing the principles of the detailed balance theory which is widely used to calculate photovoltaic efficiency limits, as well as some basic features of semiconductor solar cell devices.

In photovoltaic cells, the energy in the sunlight is transformed directly to electric energy. Photons excite electrons from states with low energy to states higher in energy. Using appropriate devices, it is possible to extract some of the exited electrons and let them go through an external electric circuit before they end up in the low energy states of the solar cell, where they started. This effect, the photovoltaic effect, was first discovered by Alexandre-Edmond Becquerel in 1839 [16], and the first thin film photovoltaic cell was made in 1883 by C.E. Fritts [17]

In 1961 William Shockley and Hans J. Queisser published a paper that suggested a limit of 40.7% as the maximum theoretical conversion efficiency for conventional photovoltaic cells [18]. The core of the model is to omit all loss mechanisms but those which are truly physically unavoidable. Today this work forms the foundation of the detailed balance theory for photovoltaic cells. It took some time before their detailed balance model was accepted and appreciated by the scientific community. In 2008 Queisser wrote about the reactions to their model and a young scientist's meeting with a respected expert [19]:

> "Our paper on the detailed balance limit was ignored; it appeared of little help to the engineers trying busily to improve efficiencies. I gave oral presentations on our approach, the audi-

> ence usually listened politely and quietly, did not exactly demonstrate approval. I presented a contributed talk at the Cleveland 1960 March Meeting of the American Physical Society. In the discussion, Paul Rappaport remarked that any semiconductor with direct optical transitions, thus dominated by radiative recombination, should provide a good efficiency cell according to our approach. Was that not right? I stood there at the rostrum, thought a little and answered in the affirmative. Aha, retorted Rappaport, but GaAs has just been proven to be restricted to such direct transitions, yet still gives only a low efficiency. I shrugged, had to accept this rebuff silently, young greenhorn that I was against this solar cell expert from RCA Princeton [...]. Now, of course, it is obvious that I was right."

The work of Shockley and Queisser has later received the recognition it deserves, but it has also been improved by a modification of the equation used for the radiative recombination [20]. A review and generalization of the detailed balance theory has been given by Araujo and Martí [21].

2.1 Light spectra

Before jumping to the details of the solar cell theory it is useful to give a short description of the light spectra that are most commonly used in work on solar cells. The energy delivered by a solar cell depends on the incident light spectrum. In theoretical work it is common to use the black-body spectrum because this is described by analytical mathematical functions and resembles the solar spectrum satisfactorily, see figure 2.1. The actual surface temperature of the sun is 5762 K, but the 6000 K black-body spectrum is very often used.

For modeling aiming to approach the actual conditions under which a solar cell operates, standardized spectra based on empirical data are available. Of these, the AM1.5 spectrum is widely used. "AM" is an abbreviation for "air mass", and AM1.5 tells us that the spectrum is based on the solar spectrum after it has passed through air corresponding to 1.5 times the thickness of a standardized atmosphere of the earth. Similarly, the AM0 spectrum is based on the spectrum of the sunlight outside the atmosphere, resembling the conditions experienced by satellites orbiting the earth.

Flat plate solar cells without concentration systems will receive radiation scattered from the surroundings in addition to the radiation coming directly from the sun. For cells receiving the radiation through a concentrating

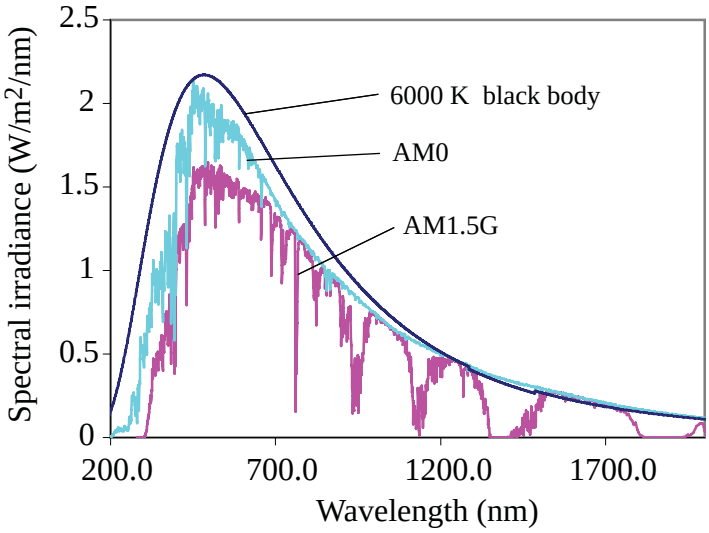

Figure 2.1: Various spectra relevant for PV-technology. The AM1.5G and AM0 data are available from the National Renewable Energy Laboratorium (NREL), Colorado, USA.

system, scattered light will not constitute a significant part of the incoming radiation. Two versions, the "global" AM1.5G and the "direct" AM1.5D, of the AM1.5 spectrum are therefore used. The AM1.5G takes into account scattered light while only the photons coming directly from the sun make up the AM1.5D spectrum. Figure 2.1 shows plots of the AM1.5G, AM0 and the 6000 K black body spectrum.

2.2 Detailed balance theory

The detailed balance theory is widely used to calculate limiting efficiencies of photovoltaic concepts. When calculating such limits one only takes into account effects that are physically unavoidable. For a solar cell, absorption of photons is an obvious effect to include. An inevitable physical property of an absorbing body is that it also is an emitting body [21]. In fact, absorption and emission of photons are the only two processes that needs to be considered when idealizing the photovoltaic cell to find its maximum efficiency limit.

The basic principle of a photovoltaic cell is that electrons are excited from electron states with low energy to electron states with higher energy by absorption of photons. If the electrons can be extracted from the high-energy states in some way , some of their increased energy can be harvested before they are re-inserted in the low-energy states. For simplicity, and with reference to the semiconductor implementation of the photovoltaic cell, the high-energy states will be referred to as the conduction band (CB) and the low-energy states as the valence band (VB), as shown in figure 2.2.

Since a system like this has to obey the laws of statistical mechanics, exciting an electron to the conduction band will not necessarily make all of the energy added to the solar cell in the absorption process available. Let us consider a system where there is no electrons in the conduction band and no empty states, in the following called holes, in the valence band at a temperature of 0 K. At room temperature there will be thermally excited electrons in the conduction band even when the cell is not exposed to sunlight. In a solar cell of a practical size, the number of electrons in the conduction band will be very large. Excitation of a single electron into the conduction band when the system is in thermal equilibrium, will only represent an infinitesimal disturbance of the system. Looking at the electrons in the CB and the holes in the VB as two populations of particles, the single excitation has only caused an infinitesimal change in the electrochemical potentials of the two populations. The populations are still infinitesimally close to being in mutual equilibrium. Therefore, removing an electron from the CB and

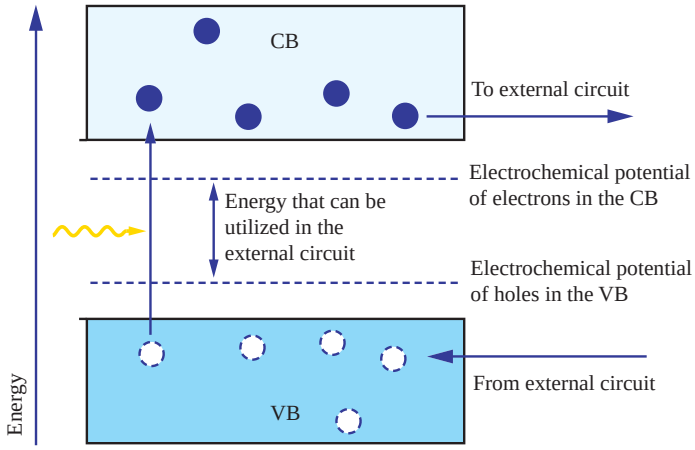

Figure 2.2: After being excited from the valence band to the conduction band, the electrons can be extracted to an external electrical circuit. The energy that can be delivered to the circuit by an electron is given by the difference in electrochemical potential between electrons and holes in the CB and VB.

inserting it in the VB will release only an infinitesimal amount of the energy brought to the cell by the absorbed photon.

To be able to harvest more of the energy that is transferred to the electron in the absorption process, there has to be a larger difference between the electrochemical potentials of the holes and the electrons. When many electrons are excited, but not immediately extracted from the CB to an external circuit, the difference in the electrochemical potential of the CB and VB can be increased as shown in figure 2.2. This allows us to harvest more of the energy transferred to the individual electrons. The larger the split between the electrochemical potentials, the more energy can be delivered to an external circuit by a single extracted electron. The drawback with a large difference in electrochemical potential is that the number of electrons recombining radiatively with a hole, that is, is de-excited to the VB by emitting a photon, will increase when the particle populations increase. At some point the energy losses related to increased recombination will surpass the gain achieved by a further increase in the splitting of the electrochemical potentials. Therefore there exists a splitting between the electrochemical potentials, where the energy delivered by the cell is maximized.

When an electron is excited to a CB-state high in energy, it will rapidly give away some of its energy as heat while it moves to states close to the

lower edge of the CB by emission of phonons. This process is called thermalization. Radiative recombination and other processes occurring in the solar cell happens very slow compared to the thermalization of carriers within each band. The electrons and holes are therefore in internal quasi-equilibriums where the carrier statistics can be described by the Fermi-Dirac distribution with a quasi-Fermi level having the role which in thermal equilibrium is played by the Fermi level. The quasi-Fermi level of a band equals the electrochemical potential of the electrons and holes in it. In solar cell physics the electrochemical potentials are therefore usually referred to as quasi-Fermi levels.

In the detailed balance theory one calculates the number of photons being absorbed in the cell and the number of photons that are emitted from the cell due to radiative recombination. The difference between the number of absorbed and emitted photons represent the number of electrons that can be driven through an external circuit while delivering an energy corresponding to the splitting between the electrochemical potentials. In the following this will be described mathematically.

2.2.1 Radiative recombination

The radiative recombination rate, i.e. the number of electron-hole pairs recombining per unit volume per unit time, is given by [20, 22]

$$r = 2\frac{4\pi n_{\mathrm{r}}^2}{h^3c^2}\int_0^\infty \frac{\alpha(E_\gamma)E_\gamma^2}{\mathrm{e}^{(E_\gamma-\Delta\mu)/kT_{\mathrm{c}}}-1}\,\mathrm{d}E_\gamma, \tag{2.1}$$

where h is Planck's constant, c the speed of light in vacuum, n_{r} the index of refraction in the cell material, $\alpha(E_\gamma)$ the absorption coefficient for photons with energy E_γ, k Boltzmann's constant and T_{c} the temperature of the solar cell. T_{c} is typically set to 300 K. $\Delta\mu$ is the splitting between the quasi-Fermi levels for electrons in the CB and holes in the VB.

Photons emitted in a recombination process can be re-absorbed before they leave the cell, a process called photon recycling. Recycled photons do not represent an energy loss. The degree of photon recycling depends on the geometry of the cell. The most commonly assumed geometry is a flat plate solar cell with a perfect mirror at the back side. Such a cell can receive and emit photons through a hemisphere as shown in figure 2.3. Photons are emitted homogeneously in all directions from all positions within the cell. The fraction of photons that escapes depends on the distance to the front surface from the location of emission, and on the direction in which the photons are emitted. Integrating over all positions and all directions one

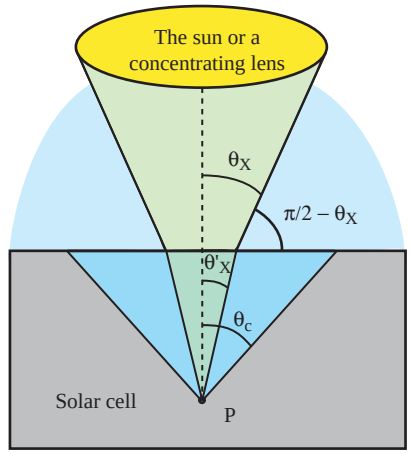

Figure 2.3: Radiation from the sun is received in the directions indicated with green color. Radiation from the surroundings are received from directions indicated by blue. The cell emits photons in every direction in which it is receiving photons. Due to total internal reflection, photons emitted outside the cone indicated by θ_c are not able to escape the cell.

finds that a cell with infinite thickness will emit a number of photons per unit time per unit area given by

$$R = \frac{2\pi}{h^3c^2}\int_{E_L}^{E_H} \frac{a(E_\gamma)E_\gamma^2}{e^{(E_\gamma-\Delta\mu)/kT_c}-1}\,dE_\gamma. \tag{2.2}$$

$a(E_\gamma)$ is the absorptivity for photons with energy E_γ. It is 1 for photon energies corresponding to an absorption coefficient larger than zero, and 0 when the absorption coefficient is zero. Equation (2.2) is used for the recombination when maximum efficiencies are calculated. The integration limits E_L and E_H restricts the integral to the energy interval where the absorption coefficients are non-zero. For an ordinary single gap solar cell we will have $E_L = E_g$ and $E_H = \infty$, where E_g is the band gap of the cell material, that is, the energy difference between the CB and the VB.

2.2.2 Generation rates

The solar radiation that is impinging on the solar cell comes either directly from the sun or from an optical system used to concentrate the sunlight. In addition, thermal radiation from the surroundings will make a small contribution to the generation of electron-hole pairs. The number of photons with

energy E_γ emitted per unit energy, solid angle, time and surface area by a black body with temperature T_r is given by [22]

$$\dot{N}(E_\gamma, T_\mathrm{r}) = \frac{2}{h^3 c^2}\left(\frac{E_\gamma^2}{\mathrm{e}^{E_\gamma/kT_\mathrm{r}} - 1}\right). \tag{2.3}$$

Rays of sunlight are hitting the cell at various angles of incidence as shown in figure 2.3. At a particular point inside the solar cell the contribution from photons coming from various directions should be summed when the generation rates are to be calculated. In addition, the radiation from the surroundings should be included. Without concentrating optics, the sun subtends a semiangle $\theta_\mathrm{sun} \approx 0.267\,^\circ$ as seen from the cell. When a light concentrating system is used, sunlight is received through a semiangle $\theta_\mathrm{X} = \sin^{-1}(\sqrt{X}\sin\theta_\mathrm{sun})$, where X is the concentration factor. The number of photons hitting the cell per unit energy, time and surface area can be calculated by

$$\phi(E_\gamma) = 2\pi\left[\int_0^{\theta_\mathrm{X}} \dot{N}(E_\gamma, T_\mathrm{s})\cos\theta\sin\theta\,\mathrm{d}\theta + \int_{\theta_\mathrm{X}}^{\pi/2} \dot{N}(E_\gamma, T_\mathrm{a})\cos\theta\sin\theta\,\mathrm{d}\theta\right], \tag{2.4}$$

where T_s is the temperature of the sun and T_a is the temperature of the surroundings. The factor 2π arises from the sylindrical symmetry of the illumination. Carrying out the integral yields

$$\phi(E_\gamma) = \pi\Big[X\sin^2\theta_\mathrm{sun}\dot{N}(E_\gamma, T_\mathrm{s}) + \big(1 - X\sin^2\theta_\mathrm{sun}\big)\dot{N}(E_\gamma, T_\mathrm{a})\Big]. \tag{2.5}$$

The highest possible light concentration is $X_\mathrm{max} = 1/\sin^2\theta_\mathrm{sun} = 46050$. This is equivalent to solar radiation being received through the entire hemisphere above the front surface.

When efficiency limits are calculated, the absorptivity for a particular photon energy should be either 1 or 0 [21]. The generation rate of electron and holes per unit area is then found by summing the number of photons, with an energy corresponding to an absorptivity of 1, that enter the cell. The absorptivity is obviously zero for photons with energy lower than the band gap. It should also be zero for energies where the number of emitted photons is larger than the number of absorbed photons [21]. It is very often assumed, however, that the absorptivity is unity for all photon energies above the band gap energy. In mathematical terms, the generation rate per unit area is

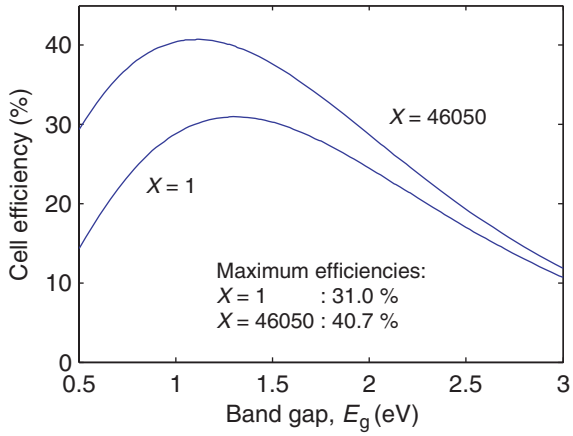

Figure 2.4: Efficiency limits as a function of the band gap for single band gap solar cells with a 6000 K black-body spectrum.

$$G = \int_{E_g}^{\infty} a(E_\gamma)\phi(E_\gamma)\,\mathrm{d}E_\gamma. \tag{2.6}$$

For an infinitely thick cell $a(E_\gamma)$ is either 1 or 0.

2.2.3 Theoretical efficiency limits

Having established expressions for the generation and recombination rates of electron-hole pairs, it is possible to calculate the efficiency of the solar cell. Since electrons cannot disappear, the number of electrons excited to the CB has to equal the number of electrons that are de-excited plus the number of electrons that are harvested and flow through an external circuit. That is, the current density J delivered by the solar cell, is given by

$$J = q(G - R), \tag{2.7}$$

where q is the elementary charge. As mentioned earlier, each electron harvested from the conduction band delivers an energy $\Delta\mu$ to the external circuit. $\Delta\mu$ is therefore related to the cell voltage V through $\Delta\mu = qV$. The recombination rate increases with V, as seen from eq. (2.2). The optimal quasi-Fermi level split corresponds to an optimal cell voltage V_m that gives the highest efficiency. This results in a cell efficiency

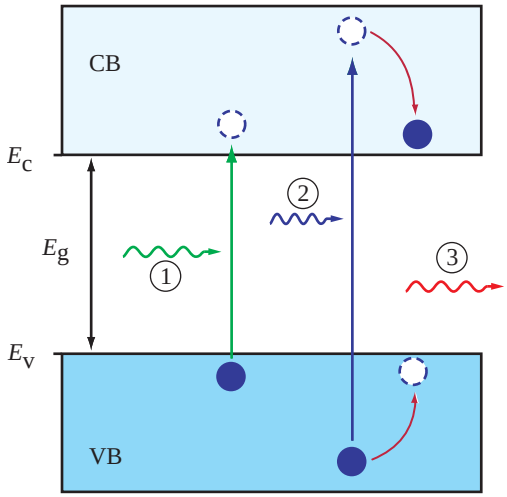

Figure 2.5: 1) The energy of photons with energy slightly above E_g will be most efficiently harvested. 2) Much of the energy of high energy photons will be lost when the generated electron-hole pair thermalizes to the band edges. 3) Photons with energy below E_g will not be absorbed.

$$\eta = \frac{J_m V_m}{E_{in}} = \frac{J_m V_m}{\pi X \sin^2 \theta_{sun} \int_0^\infty E_\gamma \dot{N}(E_\gamma, T_s)\, dE_\gamma}, \tag{2.8}$$

where J_m is the current density at $V = V_m$ and E_{in} is the energy which the cell receives from the sun per unit area. In figure 2.4 the efficiency limits[1] is plotted as a function of the band gap for light concentrations of 1 and 46050 suns. The maximum efficiencies are 31.0 % and 40.7 % respectively.

Less than half of the energy in the sunlight can be converted to useful energy by a conventional solar cell. What happens to the rest of the energy? Two very important loss mechanisms are absorption losses and thermalization losses. These are illustrated in figure 2.5. Absorption losses occur because some photons have a lower energy than the band gap energy. These can not induce VB to CB transitions, so their energy will be lost. Thermalization losses on the other hand, are large for high-energy photons. If the photon energy is higher than the band gap, an electron can be excited from low-energy states in the VB or to high-energy states in the CB (or

[1] Efficiency limits when the absorptivity is 1 for all photon energies above the band gap. For some non-optimal band gaps, the maximum efficiency is found when the absorptivity is zero for certain photon energies above the band gap [21].

even a combination). In either case, the excess energy will be lost when the carriers thermalize to the band edge. The energy of photons with energy close to the band gap will be most efficiently harvested. If we imagine that a multi band gap device is made in which all photons are absorbed over a band gap corresponding to their photon energy, the limiting efficiency is as high as 86.8 % [23].

2.3 The pn-junction

After the introduction to the fundamental physics of the solar cell, it is time to have a look at how electrons can be extracted from the conduction band in practice. The most common implementation of the photovoltaic concept is the semiconductor pn-junction solar cell which is described in this section. Semiconductors are materials which have a valence band and a conduction band, and a band gap typically between 0.5 and 3 eV. In intrinsic, that is undoped, semiconductors at a temperature of 0 K the conduction band is completely empty and the valence band is completely full. This is a property that can be modified by doping, small concentrations of other elements. Some dopants will give away one of their electrons to the conduction band, while other dopants can capture an electron from the valence band and by that create a hole.

The two ways of doping are designated n-doping and p-doping and results in semiconductor material of n-type and p-type. n-type and p-type materials have Fermi levels at different energies as shown in figure 2.6a). Since the Fermi level must be constant throughout a material in thermal equilibrium something has got to happen when n-type and p-type material is connected in a junction. This 'something' is a displacement of charge in layers on both sides of the border between the materials. Electrons will seek to minimize their energy by going from the CB in the n-type material to the VB in the p-type material, leaving behind a positive charge on the n-side. The charge displacement creates an electric field which counteracts further electron migration. The electric field implies a band bending which eventually aligns the Fermi levels on both sides. Figure 2.6 b) illustrates the charge displacements and resulting band bending. This structure where a p-type and n-type semiconductor are joined is called a pn-junction [24].

If an electron is excited to the CB on the p-side, it can diffuse to the pn-junction and be drifted over to the n-side by the electric field. In the same way, holes can be excited on the n-side and move to the p-side. The pn-junction acts as a charge separating structure which is what we need to be able to extract electrons from the solar cell. Unless all carriers are

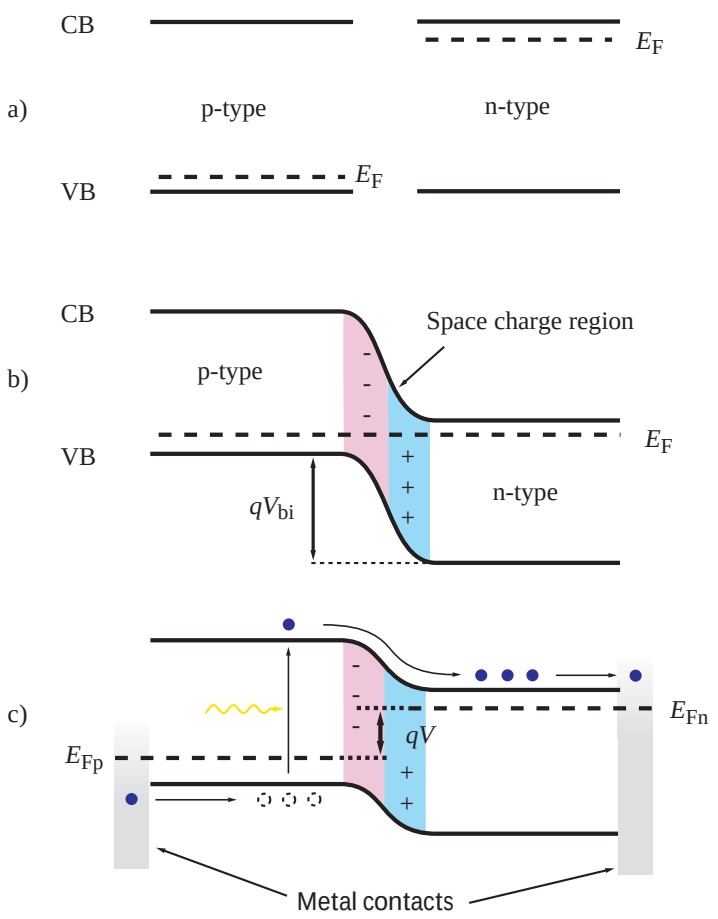

Figure 2.6: a) Semiconductors of n-type and p-type when separated from each other. b) pn-juncion in thermal equilibrium. c) pn-junction when subject to a voltage V as well as the route traveled by electrons that are contributing to the photocurrent.

extracted, there will be a build up of charge on each side of the junction. This causes the electrons in the CB on the n-side of the junction to have higher energy than the electrons in the VB on the p-side, as illustrated by a splitting of the Fermi levels on the two sides of the junction in figure 2.6c). The voltage of the cell is thus the difference between the Fermi level on the n-side and the Fermi level on the p-side divided by the elementary charge.

Absorption losses and thermalization losses where mentioned as two important loss mechanisms. Even if a monochromatic spectrum perfectly fitting the band gap is incident on the solar cell, only the energy corresponding to the split between the quasi-Fermi levels can be delivered to the external circuit, where does the rest go? Another fundamental energy loss also exist. A hint on what this loss is found by looking at figure 2.6c). When the electron is drifted across the pn-junction it looses energy. The energy is lost in the charge separation. The smaller the quasi-Fermi level split is, the more energy it costs to split electrons and holes and extract the electrons.

If no current is drawn from the cell, the voltage will stabilize when the total recombination rate in the cell equals the total generation rate. This voltage is called the open circuit voltage. If the metal contacts on either side of the junction are short circuited, the cell will deliver a current known as the short circuit current.

2.4 Device modelling

To facilitate the reader's understanding of paper III, an introduction to solar cell device modeling will now be given. Device modeling of solar cells can be done to various degrees of complexity. A complete treatment should incorporate carrier generation and all recombination mechanisms as well as carrier transport due to drift and diffusion in all regions of the cell. The mathematics involved in solving such a system is rigorous, but simplifications can be made which yields analytical expressions [25].

A widely used approximation is the depletion approximation. This implies assuming that there are no carriers in the space charge region (SCR) (see figure 2.6b). In practical terms this means assuming that no generation or recombination processes take place in the SCR, and that the carriers in each band are in equilibrium with the corresponding carriers on the other side of the SCR [24]. In many cases the number of photogenerated carriers will be small compared to the number of carriers introduced by the doping, so called low-injection conditions. In such cases one can assume that the electric field is zero outside the SCR [22]. The n- and p-regions are then said to be quasi-neutral and the carrier transport can be assumed

to be purely diffusive. A third approximation can be done if the n-region (or the p-region) is so thin that only a negligible fraction of the generation and recombination processes occur there. All generation and recombination processes can then be assumed to take place in the p-region (or n-region) of the cell.

Combining the three approximations makes it possible to construct a simple device model of the solar cell. Assuming a thin n-region so that practically all generation and recombination happen in the p-region, the current produced by the cell will equal the electron current entering the SCR from the p-side. In the general, the current has a drift and a diffusion component, but due to the quasi-neutrality this current can be assumed to consist solely of diffusing electrons. The current density then becomes

$$J = qD_{\mathrm{n}} \frac{\mathrm{d}n(x)}{\mathrm{d}x}\bigg|_{x=0}, \tag{2.9}$$

where D_{n} is the diffusion constant for electrons, n is the concentration of electrons in the conduction band and x is the distance from the edge of the SCR on the p-side as shown in figure 2.7.

To calculate $n(x)$ it is necessary to solve the continuity equation for the electrons. Assuming that the photons impinges normally to the cell surface this becomes [22]

$$D_{\mathrm{n}} \frac{\mathrm{d}^2 n(x)}{\mathrm{d}x^2} = \frac{n(x) - n_0}{\tau_{\mathrm{n}}} - \alpha\phi_0 \exp\big(-\alpha x\big), \tag{2.10}$$

where τ_{n} is the lifetime of the photoexcited electrons and n_0 is the density of electrons in the p-region in thermal equilibrium. The last term, where ϕ_0 is the flux of photons entering the solar cell and α is the absorption constant, describes the generation of electron hole pairs by Beer-Lambert's law. The lifetime τ_{n} is determined by the recombination rate. It is the time a photoexcited electron can be expected to stay in the conduction band before it recombines with a hole. In addition to the unavoidable radiative recombination, additional recombination processes can occur including Shockley-Read-Hall (SRH) recombination and Auger recombination [22]. SRH recombination occurs when an electron recombines with a hole via a localized state in the band gap. Such states can be present due to impurity atoms or lattice defects. Auger recombination is a mechanism where charge carriers collide and one of the carriers is de-excited while the other is lifted to states high in energy before giving away this excess energy through thermalization. The total recombination rate is the sum of all recombination rates, and the electron lifetime is found from this total recombination rate.

According to the depletion approximation the carriers on each side of the SCR are in equilibrium. The boundary condition for $x = 0$ thus becomes

$$n(0) = N_{\mathrm{d}} \mathrm{e}^{\frac{q(V-V_{\mathrm{bi}})}{kT}} = n_0 \mathrm{e}^{\frac{qV}{kT}}, \tag{2.11}$$

where N_{d} is the density of donor atoms used to dope the n-side and V_{bi} is the built-in-potential, that is, the difference in potential between the conduction band on the p-side and n-side in thermal equilibrium as shown in figure 2.6b). n_0 is the electron concentration on the p-side in thermal equilibrium.

On the rear side of the cell, the abrupt ending of the semiconductor leads to surface recombination - increased recombination due to the termination of the semiconductor lattice and defects related to this. The boundary condition for the rear side thus become

$$D_{\mathrm{n}} \frac{\mathrm{d}n}{\mathrm{d}x}\bigg|_{x=W} = S_{\mathrm{n}}(n(W) - n_0), \tag{2.12}$$

where S_{n} is the surface recombination velocity, a quantity describing the magnitude of the surface recombination. In idealized cells it can be set to 0.

Solving equation (2.10) with respect to $n(x)$ with the boundary conditions (2.11) and (2.12) gives analytical expressions from which the cell current, and subsequently the efficiency, can be calculated by equation (2.9) [22]. A qualitative plot of what the electron concentration and quasi-Fermi levels might look like are shown in figure 2.7.

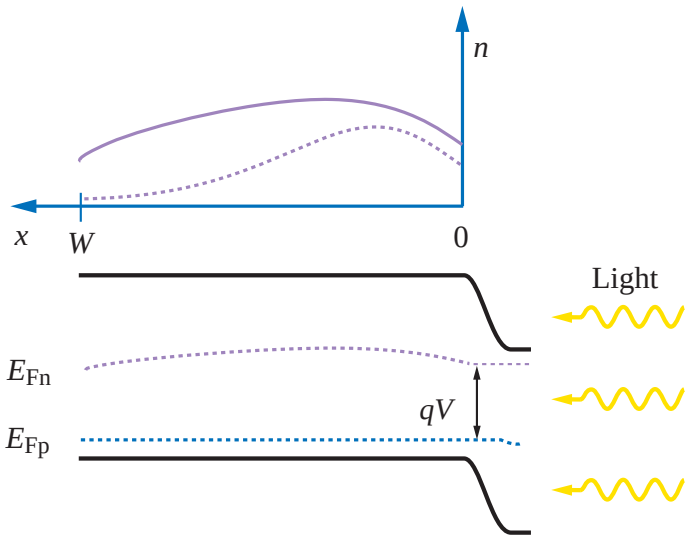

Figure 2.7: The light enters the cell on the n-side - that is, from the right. The n-region and the SCR are assumed to be very thin so that practically all generation and recombination takes place in the p-region. Typical spatial distributions of the electron concentration is plotted for two cases, a thick cell (dotted line) and a thin cell (solid line). The quasi-Fermi levels E_{Fn} and E_{Fp} for the thick cell are qualitatively indicated.

Chapter 3

The Intermediate Band Solar Cell

In 1997 Luque and Martí proposed a new photovoltaic concept, the intermediate band solar cell (IBSC), that has a theoretical efficiency of 63.2 % [14, 27] at full light concentration. Their work was a refinement of an early idea by Wolf [26]. In an IBSC there is a band of electron states, an intermediate band, in the main band gap of the solar cell material as shown in figure 3.1. This band allows electrons to be exited from the VB to the CB in a two-step process. Ideally, the IB should only be optically coupled to the VB and the CB, meaning that electrons should only be allowed to make transitions to or from the IB while absorbing or emitting a photon.

The increased efficiency of the IBSC compared to ordinary solar cells can be attributed to a reduction of both absorption losses and thermalization losses. The main band gap E_{cv} can now be larger than in conventional cells, providing a better utilization of the high energy photons. Photons with energy lower than the main band gap, can still be absorbed while exciting electrons over the two sub-band gaps E_{ci} and E_{iv}.

3.1 Detailed balance theory for the IBSC

With appropriate adjustments, the detailed balance theory can be applied to the intermediate band solar cell. In the IBSC, three recombination routes and three generation routes exist.

In the ideal IBSC the width of the IB, ΔE in figure 3.1, is zero. Another ideality that is commonly assumed is non-overlapping absorption coefficients. That is, for a given photon energy, no more than one absorption process is possible. The absorption coefficient for a given photon energy should be

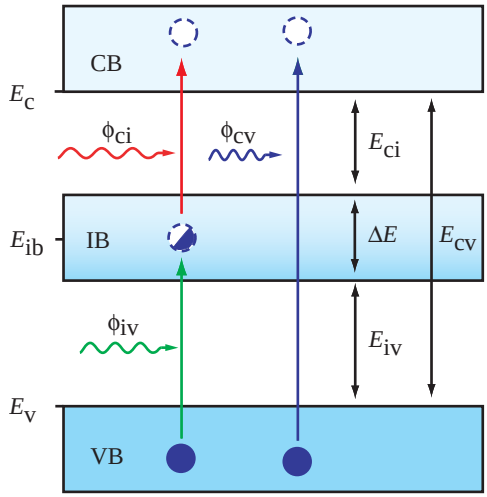

Figure 3.1: The intermediate band solar cell has an intermediate band situated in the main band gap. This allows for a two step excitation of electrons from the VB to the CB.

zero for excitations over all band gaps except the highest possible band gap, that is, the highest band gap with energy equal to or smaller than the photon energy. This correspond to a splitting of the solar spectrum into three fluxes, ϕ_{ci}, ϕ_{iv} and ϕ_{cv} which can be absorbed over the respective band gaps, E_{ci}, E_{vi} and E_{cv}. The generation rates over each band gap are then calculated from the respective photon fluxes in the same way as for the single gap solar cell. The recombination rates are still given by equation (2.2). If, as in figure 3.1, $E_{ci} < E_{iv}$, the integration limits $\{E_L, E_H\}$ becomes $\{E_{ci}, E_{iv}\}$, $\{E_{iv}, E_{cv}\}$ and $\{E_{cv}, \infty\}$ for R_{ci}, R_{iv} and R_{cv}, respectively, with non-overlapping absorption coefficients.

Like in the CB and the VB, the electron population in the IB is described by a quasi-Fermi level. As in the detailed balance theory for the single band gap cell, the quasi-Fermi level splitting over the main band gap, $\Delta\mu_{cv}$ is a parameter to be determined by choice through the cell voltage. But the quasi-Fermi level splittings over the two sub-band gaps, $\Delta\mu_{ci}$ and $\Delta\mu_{ci}$ which are used in the expressions for the respective recombination rates, are initially unknown [14]. To find their values, two equations has to be applied. The first of these equations is related to the electron current via the IB. The net generation, i.e. the generation rate subtracted the recombination rate, over E_{ci} is connected in series to the net generation over E_{vi}. In steady-state, the net generation rates over the sub band gaps have to equal each other,

fulfilling

$$G_{\mathrm{ci}} - R_{\mathrm{ci}} = G_{\mathrm{iv}} - R_{\mathrm{iv}}. \tag{3.1}$$

The second equation needed is also a result of the mentioned series connection. The quasi-Fermi level splittings over the two sub band gaps has to equal the total quasi-Fermi level split, i.e.

$$\Delta\mu_{\mathrm{cv}} = \Delta\mu_{\mathrm{ci}} + \Delta\mu_{\mathrm{iv}}. \tag{3.2}$$

Solving eq. (3.1) and (3.2) for $\Delta\mu_{\mathrm{ci}}$ and $\Delta\mu_{\mathrm{iv}}$ makes it possible to calculate the recombination rates and subsequently the current density which is given by

$$J = q\big(G_{\mathrm{ci}} - R_{\mathrm{ci}} + G_{\mathrm{cv}} - R_{\mathrm{cv}}\big). \tag{3.3}$$

This is, through eq. (3.1), equivalent to

$$J = q\big(G_{\mathrm{iv}} - R_{\mathrm{iv}} + G_{\mathrm{cv}} - R_{\mathrm{cv}}\big). \tag{3.4}$$

The cell efficiency is then calculated in the same way as for a conventional cell.

In figure 3.2 the detailed balance efficiencies for the 6000 K black body spectrum are plotted for various band gaps for $X = 1$ and $X = 46050$. An absorptivity of 1 for all photons with energy larger than the smallest sub-bandgap has been assumed. The efficiency limits are 63.2 % for full concentration and 46.8 % for unconcentrated light. For the AM1.5G spectrum, the efficiency limit for unconcentrated light is 49.4 % [28].

As mentioned, the efficiency of a single band gap cell with a non-optimal band gap can be increased if the absorptivity is set to zero for some photon energies that are larger than the band gap. This does not lead to efficiencies higher than the limit found with optimal band gaps [21]. For the intermediate band solar cell things are different. In paper I it will be shown that setting the absorptivity of some photons to zero will increase the efficiency limit for unconcentrated light from 46.8 % to 48.5 %, for the 6000 K black body spectrum. An increase is also seen for other light concentrations as well as for the AM1.5G spectrum, but the fundamental limit of 63.2 % is unchanged.

3.2 Non-idealities

Some of the idealities assumed when calculating the theoretical efficiency limit of intermediate band solar cells are similar to those assumed when

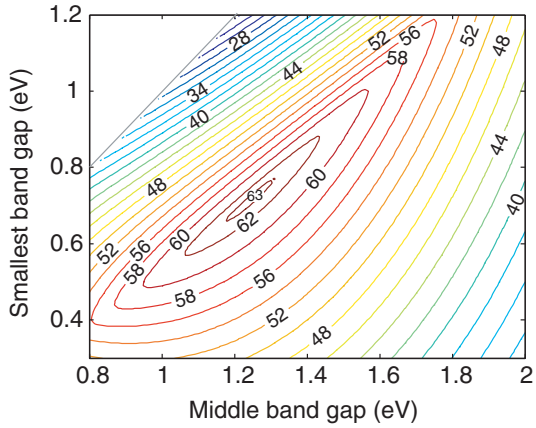

(a)

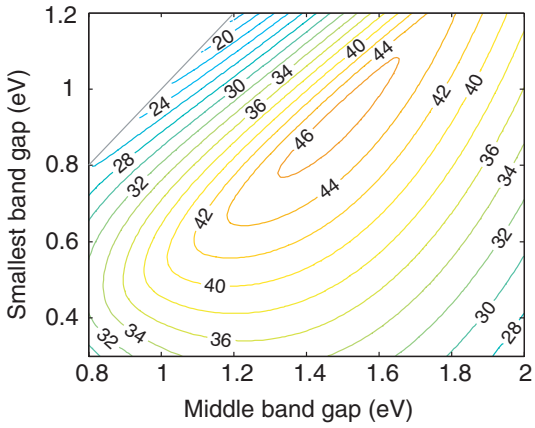

(b)

Figure 3.2: Efficiencies for intermediate band solar cells under a) 46050 suns and b) 1 sun. Complete absorption of all photons with energy higher than the band gap energy as well as non-overlapping absorption coefficients and $\Delta E = 0$ have been assumed.

single band gap cells are treated. Others are not, and it is interesting to see how the efficiencies are affected by non-idealities that are specific for the IBSC. Below, two such non-idealities, overlapping absorption coefficients and an IB with a non-zero width, are discussed.

3.2.1 Overlapping absorption coefficients

Non-overlapping absorption coefficients ensure that every photon is absorbed over the largest band gap energetically possible. If a photon is absorbed over a smaller band gap, energy will be lost when the generated electron-hole pair thermalizes, as shown in figure 3.3a [29].

Overlapping absorption coefficients are also reducing the positive effect of photon recycling, as shown in figure 3.3b). A photon emitted in a recombination process can be reabsorbed over a smaller band gap [29]. The photon is recycled, but there is not a full recycling of the energy, since some of it will be lost due to thermalization.

The total amount of recombination processes per unit area, and thus the degree of photon recycling, increases with the thickness of the cell. The cell thickness therefore becomes a parameter to optimize. There will be a trade off between a high absorptivity and minimized losses due to irreversible photon recycling.

The losses related to overlapping absorption coefficients can be reduced further if the probability of absorption and reabsorption of photons over the largest possible band gap is increased. That is, if the absorption coefficient over a band gap is larger than the absorption coefficient over the smaller band gaps, and smaller than the absorption coefficient over larger band gaps.

As mentioned above, for some combinations of band gaps, the efficiency will increase when the absorption coefficients are overlapping. This is particularly the case when the IB is placed in the middle, or close to the middle, of the main band gap. An example of this can be found in paper V.

It is necessary to modify the detailed balance theory to calculate the efficiencies of cells with overlapping absorption coefficients due to the new processes that occur. In general this leads to a rather complicated system of equations. But, as shown by Cuadra et al. [29], the system simplifies and reduces to a set of analytical expressions if the direction of the incoming photons is perpendicular to the cell surface. The reader is referred to the original source for these derivations. The simplified analytical expressions are used in papers IV and V to incorporate the effect of overlapping absorption coefficients.

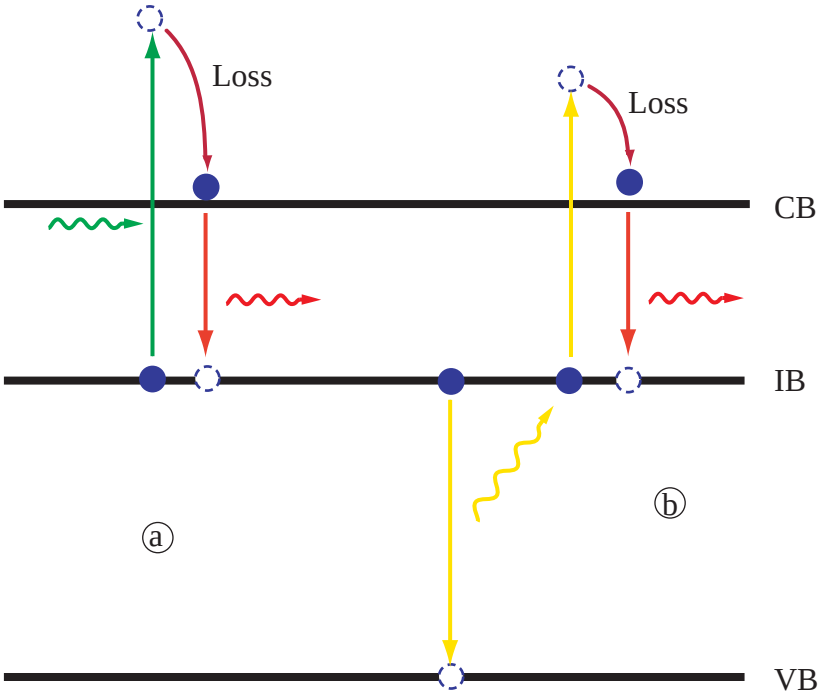

Figure 3.3: When the absorption coefficients are overlapping, a number of unfavourable processes can happen. Two of them are shown here. In a), a photon, energetically capable of exciting an electrons over E_{vi}, excites an electron over E_{ci} which, in this example, is smaller than E_{vi}. When this electron thermalizes to the band edge, an irreversible loss of energy has taken place. In b), a photon is emitted in a recombination process over E_{iv}. The photon is reabsorbed over E_{ci} before energy is lost in the thermalization.

3.2.2 Width of the intermediate band

When the intermediate band has a non-zero width, the possible combinations of band gaps is changed since $E_{\mathrm{cv}} = E_{\mathrm{ci}} + E_{\mathrm{iv}} + \Delta E$. This has consequences for the theoretical efficiencies. The minimal effect of the IB width on the cell efficiency has been calculated by Levy and Honsberg [30]. The minimal effect is found by making the same assumptions as for a case with non-zero width, but the calculations are made under the restriction that $E_{\mathrm{cv}} = E_{\mathrm{ci}} + E_{\mathrm{iv}} + \Delta E$. When ΔE goes toward infinity, the efficiency limit is reduced from 63.2 % to 55.5 %. But this is indeed a very theoretical observation and more realistic models can be developed. For example, when the IB gets wide, photons can possibly be absorbed by exciting electrons from states close to the lower band edge of the IB to IB-states higher in energy. When including this effect Levy and Honsberg has found that the efficiency will drop rapidly when the value of ΔE exceeds 1.5 eV [31].

An additional effect that is not taken into account when calculating the minimal effect of the IB-width, is the thermalized distribution of the electrons in the intermediate band. In a wide IB, the electrons will occupy states low in energy, while most states high in energy are unoccupied. As the IB-width increases, the absorption coefficients for transitions where electrons are excited from the VB to low-energy IB-states as well as transitions where electrons are excited from high-energy IB-states to the CB, will decrease. In idealized cases this is no problem because an absorptivity arbitrarily close to 1 can be achieved by choosing a sufficiently large cell thickness. In cases where the cell thickness is limited, however, the reduction of the absorption coefficients due to the IB-width will be important. In paper IV, an attempt is made to draw some general conclusions on how the thermalized distribution of the IB electrons affects the cell efficiency.

3.3 Practical implementation of the IBSC-concept

Despite the promising efficiency limit of 63.2 %, which is more than 50 % higher than the efficiency limit for conventional solar cells, the IBSC will never become more than a good idea unless ways are found to implement the concept in reality. Luckily, a number of possible implementations have been proposed. These are briefly presented in the following.

3.3.1 Quantum dot intermediate band solar cell

The first proposed implementation of the IBSC concept was the use of quantum dot superlattices [32]. Quantum dots (QDs) are nanosized particles of

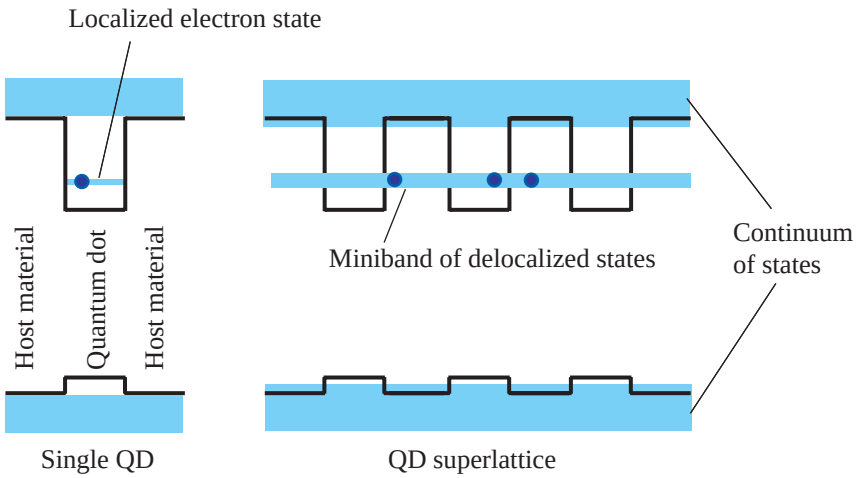

Figure 3.4: In quantum dots quantum effects give rise to new electron levels. In isolated dots electrons in such levels are confined to the QD. In a superlattice of QDs a miniband of delocalized electron states is formed.

a particular material. Due to quantum mechanical effects, particles of this size will have discrete energy levels. The position of the energy levels can be tuned by varying the size of the QDs. When many QDs are closely spaced, typically a few nanometers between the them, the electrons can tunnel from QD to QD. The electron wavefunctions have become delocalized and have formed a miniband as illustrated in figure 3.4.

A number of attempts have been carried out to make QD-based IBSCs using III-V semiconductors [33]-[43]. Unfortunately none of these cells have been able to achieve efficiencies higher than reference cells without QDs. Increased photocurrent due to absorption of low energy photons has been observed, however, proving the concept of the two-step photogeneration process via the IB [33, 35]. The most important reasons for the poor efficiencies of the experimental IBSCs are probably the material quality of the QD-structures as well as deviations from optimal cell design [34, 40].

If the IB arises from the conduction band of a QD, as in figure 3.4, the IB will be empty at 0 K and close to empty in room temperature. To assure that the IB is partially filled, it has been suggested to n-dope the region containing the superlattice at a concentration corresponding to the density of QDs [44]. Due to the spin degeneracy of the QD-states, this will half-fill the IB at 0 K. In papers II and III the possibility of photofilling is

investigated. By photofilling is meant that an IB which is close to empty in thermal equilibrium, is partially filled by electrons which are photoexcited from the VB. The papers show that this might be possible when the density of IB-states has values typical for QD-superlattices and concentrated light is used.

When using doping to partially fill the IB it will be useful to know if there exist an optimal filling and, if so, how large this filling is. Paper V shows that the optimal filling exists and that it varies with a number of parameters. It is also shown how deviations from the optimal filling will affect the cell efficiency.

3.3.2 Bulk IB-materials

Another way to implement the IBSC is to use so called bulk IB-materials. The principle behind this proposal is to use impurity atoms, rather than quantum dots, to form the intermediate band. Single impurity atoms with localized states in the band gap will act as centers for non-radiative recombination. However, when introduced into a host material at very high concentration, the electron states of the impurity atoms might form intermediate minibands. The delocalized nature of the states in the minibands will prevent the non-radiative recombination usually connected to intermediate states. Impurity densities of $10^{20}\,\mathrm{cm}^{-3}$, or above, are needed before the transition from localized to delocalized electron states takes place [45].

Transition metal substituted III-V semiconductors was the first group of materials to be launched as a candidate for bulk IB-materials, with $\mathrm{Ga_nAs_mM}$ and $\mathrm{Ga_nAs_mM}$ where M is a transition metal, as examples [46, 47]. Later, a variety of other potential materials have been investigated, including dilute II-VI oxide semiconductors, transition metal substituted chalcopyrites, transition metal substituted indium thiospinels, titanium doped silicon as well as doped nitride semiconductors. [47]-[60].

A major breakthrough in the IBSC research was recently achieved by Wang et al. when they managed to manufacture an intermediate band solar cell, based on oxygen doped ZnTe, that showed an efficiency increase of 50 % as compared to a reference cell made of ZnTe [61]. Their IBSC had a reduced open circuit voltage as compared to the reference cell, but this was more than compensated for by a doubling of the short circuit current.

3.3.3 Molecular intermediate band solar cells

Recently, a third way of implementing the IBSC-concept was proposed [62]; using organic molecules complexing metal atoms. Since the other proposed

implementations are based on inorganic semiconductors, the molecular approach is a step in a new and interesting direction. Good optical properties, low non-radiative recombination rates and a possiblility for spectrally selective absorption, that is low probability for a high-energy photon to excite electrons over a smaller band gap, are advantages that molecular IBSCs might have. A material group which might possess the desired properties are metalloporphyrins [62].

3.4 Device modeling of IBSCs

As for ordinary solar cells, the proposed implementation of semiconductor based IBSCs is by the use of pn-junctions [63, 64]. Some distinct features of IBSC devices, and the modelling of them, will be pointed out in this section.

To obtain a partially filled IB in the entire IB-region the IB-material should be placed in a flat band region, that is, a region with no, or very small, electric fields. This can be achieved by sandwiching the IB-material between an n-type and a p-type emitter as shown in figure 3.5. In addition to the emitters there should be two so-called field-damping layers bordering the IB-region. Their purpose is to counter balance the charge in the depleted zones of the emitters. Each of the emitter/field-damping layer pairs makes up a pn-junction. If the net charge in each of these junctions is zero, the IB-material will be in a flat band or a quasi-flat band region. (With quasi flat-band meaning that a small electric field is present due to internal charge displacement in the IB-region.) This assures a partial filling of the entire IB-region. The thickness of the field-damping layers resulting in flat band conditions will vary with the cell voltage and should be optimized for the voltage that gives the highest efficiency [64].

With flat band conditions it is possible to develop device models similar to the one in section 2.4. The following assumptions can be made to simplify the model:

1. The electron concentration in the IB is large compared to the concentration of electrons in the CB and holes in the VB.

2. The electrons in the IB have a high mobility so that the electron concentration in the IB can be treated as constant.

3. The rate of recombination processes between the CB and the VB is negligible compared to the recombination rates involving the IB.

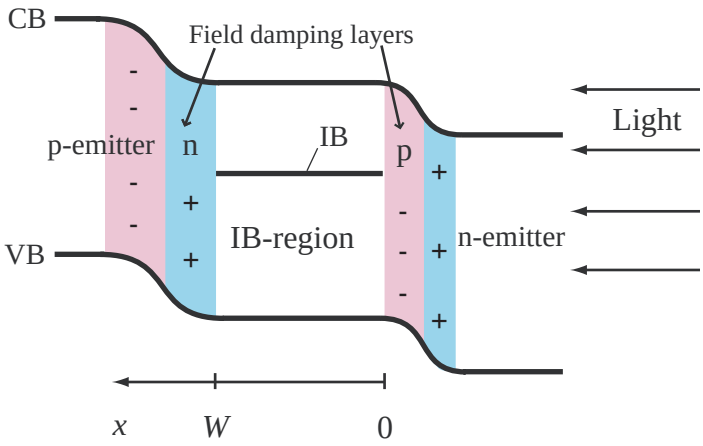

Figure 3.5: The IB-region should be sandwiched between the emitters and field-damping layers. The role of the field-damping layers is to keep the IB-material in a flat band region and prevent tunelling as shown in figure 3.6c).

4. The emitters and field-damping layers are very thin compared to the IB-region so that the number of generation and recombination processes in these regions are negligible.

The first two assumptions have the consequence that the electrons in the IB can screen any electric fields due to spatial variations in p and n with a negligible redistribution of the IB-electrons. The current will thus be purely diffusive in the IB-region.

Using the four assumptions, uncoupled continuity equations for electrons in the CB and holes in the VB can be established. For electrons it becomes

$$D_{\mathrm{n}}\frac{\mathrm{d}^2 n(x)}{\mathrm{d}x^2} = \frac{n-n_0}{\tau_{\mathrm{n}}} - \alpha_{\mathrm{cv}}\phi_{\mathrm{cv},0}\exp\left(-\alpha_{\mathrm{cv}}x\right) - \alpha_{\mathrm{ci}}\phi_{\mathrm{ci},0}\exp\left(-\alpha_{\mathrm{ci}}x\right) \quad (3.5)$$

when the photons impinges normally to the cell surface. The electron lifetime τ_{n} is now associated with recombination from the CB to the IB. α_{cv} and α_{ci} are the absorption coefficients related to transitions over the respective band gaps, and $\phi_{\mathrm{cv},0}$ and $\phi_{\mathrm{ci},0}$ are the corresponding photon fluxes at the cell surface. The continuity equation for the holes is completely analogous to the continuity equation for the electrons, but the generation over E_{ci} must

be replaced with generation over E_{iv}. The boundary condition for electrons at $x = 0$ is

$$n(0) = n_0 \mathrm{e}^{\frac{qV_\mathrm{n}}{kT}}. \tag{3.6}$$

And for holes at $x = W$ it is

$$p(W) = p_0 \mathrm{e}^{\frac{qV_\mathrm{p}}{kT}}. \tag{3.7}$$

p_0 and n_0 are the hole and electron (in the CB) concentrations in the IB-region in thermal equilibrium. V_n and V_p are the voltages over the sub-junctions. When the quasi-Fermi level of the IB is maintained at its equilibrium position during operation of the cell the sub-junction voltages equal the respective quasi-Fermi level splits as shown in figure 3.6a). In paper III it is shown that this is no longer the case if the quasi-Fermi level of the IB is shifted when the cell is illuminated.

Since the emitters and field-damping layers are assumed to be very thin, there is no hole current at $x = 0$ or electron current at $x = W$ (see figure 3.6b)). This can be used as additional boundary conditions when solving the continuity equations. It also has the consequence that the cell current is given either by the electron diffusion current at $x = 0$ or by the hole diffusion current at $x = W$. The value of the sub-junction voltages are found by equaling the electron current at $x = 0$ and the hole current at $x = W$.

Without field-damping layers the IB will not be partially filled in parts of, or even the entire, IB-region as illustrated in figure 3.6c). The figure also shows that without field-damping layers, the CB and IB can get quite close to each other. This opens for the possibility of tunneling between the two bands. Such a process is unwanted because it corresponds to short circuiting the two bands [64].

More complex device modeling can be done by introducing various types of recombination mechanisms, introducing electric fields, taking into account absorption and recombination in all parts of the cell, putting aside assumptions, etc. But the main principle described here of establishing continuity equations and solving these with appropriate boundary conditions remain.

Previous modeling allows to set assumptions 1 and 3 aside when the system is solved numerically [65]. In paper III the IBSC device modeling is taken one step further by setting aside assumption 2 as well.

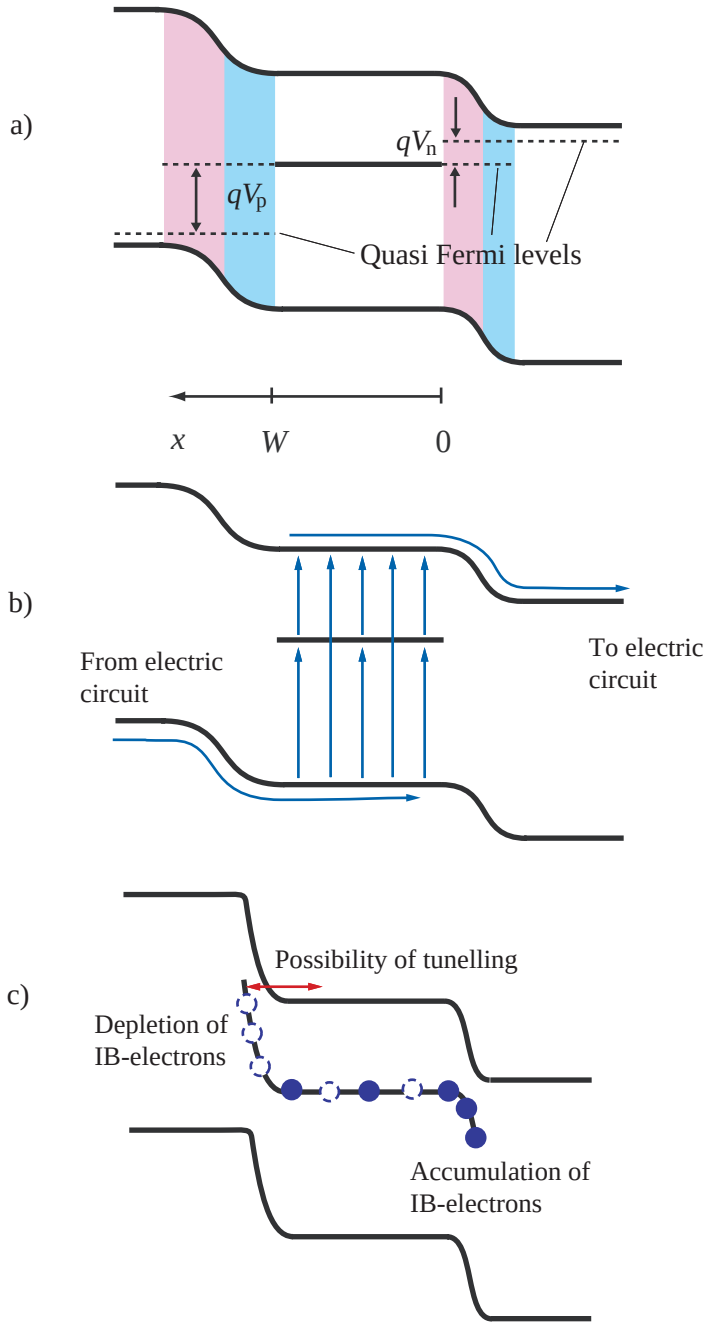

Figure 3.6: a) With a constant filling of the IB the sub-junction voltages equals the difference between the quasi-Fermi level of the IB and the quasi-Fermi levels of the carriers in the respective emitters. b) The paths traveled by electrons when the emitters and field-damping layers are very thin. c) Without field-damping layers, a uniform filling of the IB will not be obtained. A possibility for unwanted electron tunelling to occur also arises.

Chapter 4

Summary of papers I to V

Rune Strandberg and Turid Worren Reenaas are the authors of the five papers in this thesis. The mathematical modeling and numerical computations has been performed by Rune Strandberg who has also developed the ideas behind the papers. The writing has been done by Rune Strandberg in close cooperation with Turid Worren Reenaas whose contribution has also been to catalyze the work through discussions.

Paper I

Limiting efficiency of Intermediate Band Solar Cells with spectrally selective reflectors

In this paper, detailed balance efficiencies are calculated with a cell absorptivity of 0 for photon energies that would otherwise give a negative contribution to the cell current. That is, if the cell emits more photons, with a specific energy, than it absorbs, at the maximum power point, the absorptivity for this photon energy is set to zero. It is found that such a spectral selectivity can increase the efficiency limit for unconcentrated 6000 K black body radiation from 46.8 % to 48.5 %. The limiting efficiency for the AM1.5G spectrum increases from 49.4 % to 52.0 %. For full light concentration (46050 suns), the fundamental limit of 63.2 % is found to be unchanged.

Paper II

Photofilling of Intermediate Bands

This paper investigates the possibility of partially filling an initially empty[1] intermediate band with electrons that are photoexcited from the valence band. To fill the IB like this is denoted *photofilling*. The efficiencies calculated for photofilled cells are compared to efficiencies calculated for cells that have intermediate bands that are half-filled in thermal equilibrium, i.e. *prefilled* cells. Whether a cell based on photofilling can compete with a prefilled cell is found to depend on the density of states in the IB, the concentration of the light as well as the thickness of the cell. The concept of photofilling might work for cells with properties typical for quantum dot based IBSCs.

It is also investigated how the filling of photofilled and prefilled cells are changing with the cell voltage and the position of the IB in the main band gap. In both cases, the filling is found to be nearly constant for low voltages because the generation rates are much larger than the recombination rates and will determine the filling. Approximate analytical expressions for the filling at low voltages are derived. When the voltage approaches the maximum power point, the recombination rates becomes comparable in magnitude to the generation rates and the filling generally starts to change. The filling is also found to be highly dependent on the position of the IB in the main band gap, since this position determines the number of photons available for excitation of electrons over E_{ci} and E_{iv}.

Paper III

Drift-diffusion model for Intermediate Band Solar Cells including photofilling effects

This paper can be seen as a continuation of paper II. The concept of photofilling is here implemented into a drift-diffusion model to see how a varying filling is affecting intermediate band solar cells based on the design and principles described in section 3.4. The most important difference between the present model and other models is that the carrier concentrations in all three bands are allowed to vary.

It is found that light induced spatial variation of the IB-filling can occur and give rise to electrostatic fields. As a consequence, it is suggested that the

[1] To be precise, not completely empty, since a thermal population of electrons will be present in the IB, but practically empty unless elevated temperatures or unusually small band gaps are considered.

cells should have a design which assures that these fields drive electrons and holes in the right directions, that is towards the n- and p-emitter, respectively. It is also shown that cases exist where photofilled cells can perform better than cells that are initially half-filled. This will, for example, be the case if the absorption cross section for transitions from the IB to the CB is sufficiently large compared to the absorption coefficient for transitions from the VB to the IB.

For particular sets of parameters the optimal ratios between the absorption coefficients and the optimal filling of the IB is found.

Paper IV

When the IB has a non-zero width, the probability of occupation of various IB-states will be given by the Fermi-Dirac distribution. This will affect the number of electrons available for excitation from the IB to the CB by photons with energy slightly larger than E_{ci}, as well as the number of unoccupied IB-states available for electrons that are excited from the VB to the IB by photons with energy slightly larger than E_{iv}. Two sets of absorption coefficients are derived based on different assumptions. The absorption coefficients incorporate the thermalized nature of the IB-electrons and can be used to calculate cell efficiencies and draw some general conclusions. They are, however, based on very idealized assumptions which might not be found in real materials.

Efficiencies are calculated for cells where $E_{\mathrm{ci}} < E_{\mathrm{iv}}$ with either non-overlapping or overlapping absorption coefficients. The overlap is assumed to occur for photon energies where the thermalization limits the excitation of electrons across E_{iv}. That is, from E_{iv} to $E_{\mathrm{iv}}+\Delta E$, where ΔE is the width of the IB. The results are compared to the fundamental limit calculated in ref. [30], where all photons larger than the smallest sub-band gap are assumed to be absorbed. It is found that non-overlapping absorption coefficients gives the highest efficiencies for ΔE up to around 0.5 eV. When ΔE approaches 1 eV it is found that cells with overlapping absorption coefficients give the highest efficiencies.

It is also found that the energy dependence of the absorption coefficients is important for the efficiency. The absorption coefficients should go rapidly from very low values to high values with increasing photon energy.

Further it is concluded that the optimal band gaps decrease with the width of the IB for most of the investigated cases and values of ΔE. In the fundamental limit the optimal band gaps increase with the IB-width.

For some of the investigated cases, the calculated efficiency drops below

the limit for single band gap cells.

Paper V

The final paper is an investigation of the optimal filling of idealized IBSCs. Three cases are modeled using previously published models. The cases are: i) non-overlapping absorption coefficients and clamped quasi-Fermi level of the IB, ii)non-overlapping absorption coefficients and photofilling effects, and iii) overlapping absorption coefficients and clamping of the IB quasi-Fermi level.

It is found that the optimal filling depends on the band gaps, the light concentration, the mutual sizes of the absorption cross sections over the sub-band gaps as well as the degree of overlap between the absorption coefficients. The optimal filling is found to be determined by two main effects: The first is the need to maximize the net generation rate via the IB. The second is to minimize the negative effect of overlapping absorption coefficients.

When the effect of photofilling is included, the optimal filling in thermal equilibrium will, in general, deviate from the filling at the maximum power point. Cases have been identified where the optimal filling can not be reached at the maximum power point because the illumination removes too many electrons from the IB.

The impact of a non-optimal IB-filling on the cell efficiency is found to vary with the degree of overlap between the absorption coefficients, the size of the band gaps and the absorptivity of the cell. When photofilling effects are present, the negative effect of a non-optimal filling is found to decrease with increasing light concentration.

Bibliography

[1] Core Writing Team, R.K. Pachauri and A. Reisinger (Eds.), *Contribution of Working Groups I, II and III to the Fourth Assessment Report of the Intergovernmental Panel on Climate Change*, IPCC, Switzerland, ISBN 92-9169-122-4 (2008).

[2] International Energy Agency, *Key World Energy Statistics 2009* (2009).

[3] BP, *BP Statistical Review of World Energy 2009* (2009)

[4] Renewable Energy Policy Network for the 21st Century, *Renewable Global Status Report*, 2009 update (2009)

[5] M.A. Green, *Third Generation Photovoltaics: Ultra-High Efficiency at Low Cost*, Springer-Verlag, Berlin, ISBN 3540401377 (2003).

[6] Renewable Energy Corporation ASA, *REC Annual Review 2008* (2009) .

[7] European Photovoltaic Industry association, *Global market Outlook for photovoltaics until 2013*, www.epia.org (2008).

[8] A. Balzer, *Pioneering towards PV grid parity*, presentation, Renewable Energy Corporation (2009)

[9] A. Luque, S. Hegedus (ed.), *Handbook of Photovoltaic Science and Engineering*, John Wiley & Sons Ltd, England (2003).

[10] B. O'Regan, M. Grätzel, Nature **353**, 737-740 (1991).

[11] C.W. Tang, Applied Phyics Letters **48**, 183-185 (1986).

[12] A. Mayer, S. Scully, B. Hardin, M. Rowell, M. McGehee, Materials Today **10**, 28-33 (2007).

[13] R.T. Ross, A.J. Nozik, Journal of Applied Physics **53**, 3813-3818 (1982).

[14] A. Luque, A. Martí, Phys. Rev. Lett. **78**, 5014-5017 (1997).

[15] A. Chen, D. Ball, Press release from Boeing aug. 26, 2009.

[16] A.E. Becquerel, C. R. Acad. Sci. **9**, 145 (1839).

[17] C.E. Fritts Proc. Am. Assoc. Adv. Sci. **33**, 97 (1883).

[18] W. Shockley, H.J. Queisser, J. Appl. Phys. **32**, 510 (1961).

[19] H.J. Queisser, Materials Science and Engineering: B **159-160**, 322-328 (2008).

[20] A. de Vos, H. Pauwels, Appl. Phys. **25**, 119-125 (1981).

[21] G.L. Araujo, A. Martí, Sol. Energy Mat. and Sol. Cells **33**, 213-240 (1994).

[22] J. Nelson, *The Physics of Solar Cells*, Imperial College Press (2003), ISBN 1-86094-340-3.

[23] G.L. Araujo, A. Martí, Sol. Energy Mat. and Sol. Cells **43**, 203-222 (1996).

[24] B.G. Streetman, S. Banerjee, *Solid State Electronic Devices*, Prentice Hall, USA, ISBN 0-13-025538 (2000)

[25] C.T. Sah, R. Noyce, W. Shockley, Proceedings of the IRE **45**, 1228-1243 (1957).

[26] Wolf M, Proceedings of the Institute of Radio Engineers **48**, 1246-1263 (1960).

[27] A.Luque, A. Martí, Prog. Photovolt: Res. Appl. **9**, 73-86 (2001).

[28] S.P. Bremner, M.Y. Levy, C.B. Honsberg, Applied Physics Letters **92**, 171110 (2008).

[29] L. Cuadra, A. Martí, A. Luque, IEEE Transactions on Electron Devices **51**, 1002-1007 (2004).

[30] M.Y. Levy and C. Honsberg, J. Appl. Phys, **104**, 113103 (2008).

[31] M.Y. Levy and C. Honsberg, Phys. Rev. B **78**, 165122 (2008).

[32] L. Cuadra, A. Martí, A. Luque, Physica E **14**, 162-165 (2002).

[33] A. Luque, A. Martí, N. López, E. Antolín, E. Canovas, C. Stanley, C. Farmer, L.J. Caballero, L. Cuadra, J.L. Balenzategui, Applied Physics Letters **87**, 083505 (2005).

[34] A. Luque, A. Martí, N. López, E. Antolín, E. Cánovas, C.R. Stanley, C. Farmer, P. Díaz, Journal of Applied Physics **99**, 094503 (2006).

[35] A. Martí, E. Antolín, C.R. Stanley, C.D. Farmer, N. Lopez, P. Díaz, E. Cánovas, P.G. Linares, A. Luque, Physical Review Letters **97**, 247701 (2006).

[36] N. López, A. Martí, A. Luque, C. Stanley, C. Farmer, P. Diaz, Journal of Solar Energy Engineering **129**, 319-322 (2007).

[37] A. Martí, N. López, E. Antolín, E. Cánovas, A. Luque, C.R. Stanley, C.D. Farmer, P. Díaz, Appl. Phys. Lett. **90**, 233510 (2007).

[38] R.B. Laghumavarapu, A. Moscho, A. Khoshakhlagh, M. El-Emawy, L.F. Lester D.L. Huffaker, Applied Physics Letters **90**, 173125 (2007)

[39] R.B. Laghumavarapu, M. El-Emawy, N. Nuntawong, A. Moscho, L.F. Lester, D.L. Huffaker, Applied Physics Letters **91**, 243115 (2007)

[40] V. Popescu, G. Bester, M.C. Hanna, A.G. Norman, A. Zunger, Physical Review B **78**, 205321 (2008).

[41] R. Oshima, A. Takata, Y. Okada, Applied Physics Letters **93**, 083111 (2008).

[42] S.M. Hubbard, C.D. Cress, C.G. Bailey, R.P. Raffaelle, S.G. Bailey, D.M. Wilt, Applied Physics Letters **92**, 123512 (2008).

[43] E. Antolín, A. Martí, C.R. Stanley, C.D. Farmer, E. Cánovas, N. López, P.G. Linares, A. Luque, Thin Solid Films **516**, 6919-6923 (2008).

[44] A. Martí, L. Cuadra, A. Luque, IEEE Transactions on Electron Devices **48**, 2394-2399 (2001).

[45] A. Luque, A. Martí, E. Antolín, C. Tablero, Physica B **382**, 320-327 (2006).´

[46] P. Wahnón, C. Tablero, Phys. Rev. B **65**, 165115 (2002).

[47] C. Tablero, P. Wahnón, Applied Physics Letters **82**, 151-153 (2002).

[48] K.M. Yu, W. Walukiewicz, J. Wu, et. al., Phys. Rev. Lett. **91**, 246403 (2003).

[49] C. Tablero, Computational Materials Science **37**, 483-490 (2006).

[50] C. Tablero, Phys. Rev. B **74**, 195203 (2006)

[51] P. Palacios, J.J Fernandez, K. Sánchez, J.C. Conesa and P. Wahnón, Phys. Rev. B **73**, 085206 (2006)

[52] P. Palacios, K. Sánchez, J.C. Conesa, P. Wahnón, Phys. Stat. Sol. **203**, 1395-1401 (2006).

[53] P. Palacios, K. Sánchez, P. Wahnón, J. C. Conesa, Journal of Solar Energy Engineering **129**, 314-318 (2007).

[54] P. Palacios, I. Aguilera, K. Sánchez, J.C. Conesa, P.Wahnón, Physical Review Letters **101**, 046403 (2008).

[55] P. Palacios, I. Aguilera, P. Wahnón, Thin Solid Films **516**, 7070-7074 (2008).

[56] A. Martí, D. Fuentes Marrón, A. Luque, Journal of Applied Physics **103**, 073706 (2008).

[57] D. Fuentes Marrón, A. Martí, A. Luque, Thin Solid Films **517**, 2452-2454 (2008).

[58] J. Olea, M. Toledano-Luque, D. Pastor, G. González-Díaz, I. Mártil, Journal of Applied Physics **104**, 016105 (2008).

[59] K. M. Yu, W. Walukiewicz, J.W. Ager III, Applied Physics Letters **88**, 092110 (2006).

[60] A. Martí, C. Tablero, E. Antolín, A. Luque, R.P. Campion, S.V. Novikov, C.T. Foxon, Solar Energy Materials & Solar Cells **93**, 641-644 (2009).

[61] W. Wang, A.S. Lin, J.D. Phillips, Applied Physics Letters **95**, 011103 (2009).

[62] N.J. Ekins-Daukes, T.W. Schmidt, Applied Physics Letters **93**, 063507 (2008).

[63] A. Martí, L. Cuadra, A. Luque, Physica E **14**, 150-157 (2002).

[64] A. Martí, E. Antolín, N. López, P.G. Linares, A. Luque, C.R. Stanley, C.D. Farmer, Thin Solid Films **516**, 6716-6722 (2008).

[65] A. Martí, L. Cuadra, A. Luque, IEEE Transactions on Electron Devices **49**, 1632-1639 (2002).

Paper I

Limiting efficiency of Intermediate Band Solar Cells with spectrally selective reflectors

To be submitted.

Limiting efficiency of Intermediate Band Solar Cells with spectrally selective reflectors

Rune Strandberg*, Turid Worren Reenaas

Norwegian University of Science and Technology, Department of Physics, N-7491 Trondheim, Norway

Abstract

So far, theoretical efficiency limits for the intermediate band solar cell have been calculated under the assumption that the absorptivity of the solar cell is 1 for all photon energies larger than the smallest sub-band gap. In the present work, efficiency limits have been calculated under the assumption that the cell is covered by spectrally selective reflectors, i.e. materials that are perfect reflectors for certain photon energies, but otherwise perfectly transparent. It is shown that when the spectral selectivity is optimized, the cell efficiency is increased for several cases. It is of particular interest that the limiting efficiency for unconcentrated sunlight found with spectral selectivity exceeds the limit found without spectral selectivity. The efficiency limit for the 1 sun 6000 K black body spectrum is found to increase from 46.8 % to 48.5 % and the limit for the AM1.5G spectrum is found to increase from 49.4 % to 52.0 %. For full light concentration, the 63.2 % efficiency limit for the 6000 K black body spectrum is unchanged.

Keywords: intermediate band solar cell, spectral selectivity, AM1.5, detailed balance
PACS:

In the intermediate band solar cell (IBSC), electrons can be excited from the conduction band (CB) to the valence band (VB) either directly or in two steps via an intermediate band in the usually forbidden band gap [1]. This two-step process can increase the photocurrent and gives the IBSC a higher theoretical efficiency limit than the single band gap cell [2].

*Corresponding author. E-mail: strandbe@ntnu.no

The efficiency limits for the intermediate band solar cell published so far have been calculated under the assumption that the absorptivity for all photon energies larger than the smallest sub-band gap is 1 [1, 3]. For single band gap cells, it has been shown that when the band gap has a lower value than the optimum, the efficiency of the cell will be increased if the spectral absorptivity for some photon energies is smaller than one, and optimally zero [4]. Whether the optimal spectral absorptivity for a particular photon energy is one or zero depends on the net generation of such photons within the cell. That is, whether the cell absorbs more of these photons than it emits or not. A positive net generation of photons corresponds to a loss of energy and gives an optimal spectral absorptivity of 0. A negative net generation of photons gives an optimal absorptivity of 1. These arguments are also valid for the intermediate band solar cell, which is sketched in figure 1. Whenever the radiative recombination rate per unit area $R(E)$ related to emission of a particular photon energy E is larger than the generation rate per unit area $G(E)$ of electron hole-pairs induced by photons with this energy, the ideal absorptivity for this particular photon energy is zero.

One way to give a solar cell the desired properties is by the use of an ideal spectrally selective reflector. That is, a layer which is fully transparent for photons that give a positive contribution to the cell efficiency and act as a perfect reflector for photons that give a negative contribution. In the reflecting energy range(s), the reflector will prohibitit photons from the sun and the surroundings from entering the cell, but also recycle photons emitted by the cell, resulting in a net energy gain.

In this paper, cell efficiencies are calculated using detailed balance theory [1, 2, 4] while applying the concept of spectrally selective reflectors. Non-overlapping absorption coefficients are assumed, meaning that for a particular photon energy, only transitions over the largest band gap with band gap lower than, or equal to, the photon energy will be allowed. The IB is assumed to have zero energetical width.

Following ref. [1], two equations must be solved,

$$qV = \mu_{\mathrm{cv}} = \mu_{\mathrm{ci}} + \mu_{\mathrm{iv}}, \tag{1}$$

which describes the relation between the cell voltage V and the quasi Fermi level splittings across the three band gaps, and

$$G_{\mathrm{ci}} - R_{\mathrm{ci}} = G_{\mathrm{iv}} - R_{\mathrm{iv}}, \tag{2}$$

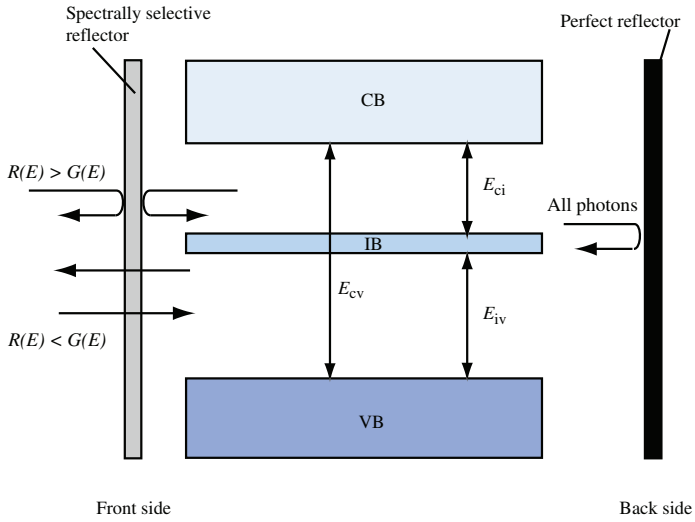

Figure 1: A sketch of an intermediate band solar cell with spectrally selective reflectors. Photons which are not giving a positive contribution to the cell efficiency are reflected by the spectrally selective reflector at the front surface.

the balance between the number of electrons entering and leaving the IB. q is the elementary charge. G_{ci} and G_{vi} are the generation rates per unit area over E_{ci} and E_{iv}, respectively, and R_{ci} and R_{iv} are the corresponding recombination rates per unit area. Knowing the solution of the pair of equations above, the current density of the cell is calculated by

$$J = q(G_{\mathrm{cv}} + G_{\mathrm{ci}} - R_{\mathrm{cv}} - R_{\mathrm{ci}}), \tag{3}$$

where G_{cv} and R_{cv} are the generation and recombination rates per unit area over the main band gap E_{cv}. The generation rates per unit area equal the number of photons with appropriate energy that are entering the cell per unit area and time. When the black body spectrum is used, the generation rates described mathematically in ref. [1] have been used after multiplication with the geometrical form factor π and a dilution factor $X/46050$, where X is the concentration factor of the light. When the AM1.5G spectrum is used, the generation rates are given by the photon fluxes in the respective energy intervals. The recombination rates per unit area are, in all cases, given by the generalized form of Planck's radiation law [5] and used as described in ref. [3]. Of course all integration limits have been adjusted to incorporate the spectral selectivity.

Calculating J for selected values of V allow us to find the maximum power per unit area delivered by the cell, P_{max}, from the resulting IV-curve. The efficiency η is then calculated by $\eta = P_{\mathrm{max}}/P_{\mathrm{in}}$, where P_{in} is the irradiance received by the cell. When the AM1.5G spectrum is used, P_{in} equals $1000\,\mathrm{W/m^2}$ due to the normalization of this spectrum. When the black body spectrum is used, P_{in} is given by

$$P_{\mathrm{in}} = \frac{X}{46050}\sigma T_{\mathrm{s}}^4, \tag{4}$$

where σ is the Stefan-Boltzmann constant and $T_{\mathrm{s}} = 6000\,\mathrm{K}$ is the temperature of the sun.

The calculations are first done with no reflective blocking, to identify photon energies with a negative contribution to the efficiency. Then the calculations are repeated with blocking of such photons. The reflective blocking might change the maximum power point of the cell. Therefore it is checked if the introduction of the blocking has changed what photon energies that give a negative and positive contribution to the efficiency. If so, the calculations are repeated until no such changes are found.

When the quasi Fermi level splitting over a band gap approaches the respective band gap energy, the absorption coefficients of photons with energy close to this band gap are reduced due to band filling which also leads to increased stimulated emission. For cells with a limited thickness, this has the consequence that the absorptivity of the cell is dependent on the cell voltage [6]. For a cell with infinite thickness, which is implicitly assumed in this work since the absorptivity is 1 for several photon energies, the quasi Fermi level split will always be smaller than the band gap because the recombination rate goes towards infinity when the quasi Fermi level split approaches the band gap [6]. The absorption coefficient will thus alway be positive and, due to the infinite cell thickness, the absorptivity of the cell will still be 1.

When a spectrally selective reflector is reflecting photons with the band gap energy, in an infinitely thick cell, the recombination rate will still go towards infinity when the quasi Fermi level split approaches the band gap. But, now some of the emitted photons cannot escape the cell. They are reflected and reabsorbed. Therefore the effective recombination rates do not necessarily approach infinity when the quasi Fermi level split approaches the band gap. Once the quasi Fermi level splitting gets infinitesimally larger than the band gap, a large, in fact infinite, number of photons will be emitted by stimulated emission. This valve effect prevents the quasi Fermi level split from becoming larger than the band gap also when spectrally selective reflectors are applied. The photons emitted this way will not be recycled by the cell nor can they escape the cell due to the spectrally selective layer. This results in an accumulation of photons in the cell. The system is not in steady state. When the situation is like this it is still possible to calculate the cell efficiency by setting $\Delta\mu_{\mathrm{x}} = E_{\mathrm{x}}$, where $\Delta\mu_{\mathrm{x}}$ is the quasi Fermi level split over the sub-band gap E_{x} in question and assume that the accumulation of photons does not affect the cell properties.

The cell temperature has been set to 300 K. The efficiencies plotted as a function of the sub-band gaps for the AM1.5G spectrum is shown in figure 2. Combinations of band gaps that result in a system that accumulates photons due to stimulated emission as described above are indicated by the shading. When spectrally selective reflectors are introduced, the theoretical efficiency limit increases from 49.4 % [3] to 52.0 % (this work). The efficiency peak is found for $E_{\mathrm{ci}} = 0.64\,\mathrm{eV}$ and $E_{\mathrm{iv}} = 1.41\,\mathrm{eV}$, and is obtained when photons with energy lower than 0.93 eV are subject to reflective blocking.

The efficiency limit for the black body spectrum plotted as a function of the concentration of the light is shown in figure 3. For the 1 sun black body

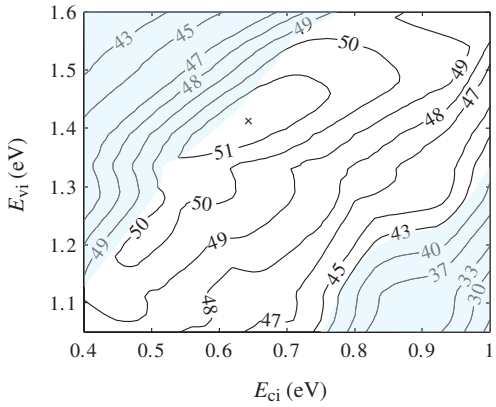

Figure 2: Efficiencies for IBSCs with spectrally selective reflectors for the AM1.5G spectrum. The shading indicates regions where the system is not in steady state due to accumulation of trapped photons. In the upper left corner there is accumulation of photons with energy E_{ci}, and in the lower right corner there is accumulation of photons with energy E_{iv} at the optimal cell voltage.

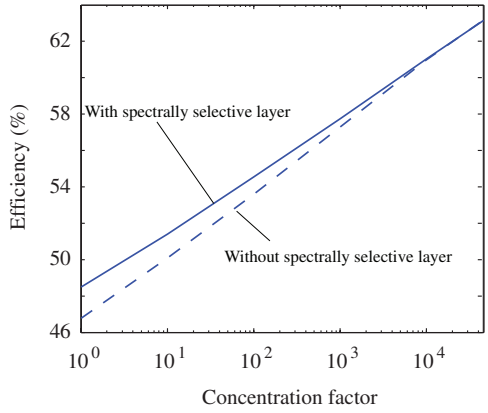

Figure 3: Limiting efficiencies as a function of the light concentration for the 6000 K black body spectrum for cells with and without ideal spectrally selective reflectors. The system is in steady state for all datapoints.

spectrum, the efficiency limit increases from 46.8 % to 48.5 % when an ideal spectrally selective reflector is applied. The optimal band gaps are shifted from $E_{\mathrm{ci}} = 0.92\,\mathrm{eV}$ and $E_{\mathrm{iv}} = 1.49\,\mathrm{eV}$ to $E_{\mathrm{ci}} = 0.67\,\mathrm{eV}$ and $E_{\mathrm{iv}} = 1.42\,\mathrm{eV}$. The limit is obtained when photons with energy below 0.945 eV are reflected. For 1000 suns, a limiting efficiency of 57.7 % is found for $E_{\mathrm{ci}} = 0.70\,\mathrm{eV}$ and $E_{\mathrm{iv}} = 1.29\,\mathrm{eV}$. This is slightly higher than the 57.3 % limit for cells without a spectrally selective reflector.

When the light concentration is increasing, the number of incoming photons increase and the number of photon energies that should be reflected decreases. At full concentration, spectrally selective reflectors are not changing the 63.2 % efficiency limit of the intermediate band solar cell.

For single band gap solar cells, spectral selectivity can not increase the efficiency limit for the black body spectrum at a given light concentration. But it can rise the efficiency limit for cells with a non-optimal band gap to the limit for cells with an optimal band gap [4]. As just shown, spectral selectivity can increase the efficiency limit of the IBSC for some light concentrations. The reason for this difference is as follows: A single band gap cell with a non-optimal band gap can be equipped with the spectral properties of a cell with the optimal band gap when spectral selectivity is applied. In an IBSC, spectral selectivity can give a cell spectral properties which can not be obtained without spectral selectivity. For the IBSC, the condition $E_{\mathrm{ci}} + E_{\mathrm{iv}} = E_{\mathrm{cv}}$ must be fulfilled. By applying spectrally selective reflectors, one ore more of the band gaps can be given the spectral properties of a higher band gap. IBSCs can thus be designed in a way that gives them optical properties like a cell where $E_{\mathrm{ci}} + E_{\mathrm{iv}} \neq E_{\mathrm{cv}}$.

To summarize, detailed balance theory has been used to calculate the limiting efficiencies of intermediate band solar cells with spectrally selective reflectors. The reflectors are reflecting photons that would otherwise give a negative contribution to the efficiency. This leads to increased efficiency limits for several cases, particularly when the light is not concentrated.

Acknowledgments

The authors would like to thank the Research Council of Norway for financial support through project no. 172905/S30.

References

[1] A. Luque and A. Marti, Phys. Rev. Lett. **78**, 5014-5017 (1997).

[2] W. Shockley and H.J. Queisser, J. Appl. Phys. **32**, 510 (1961).

[3] S.P. Bremner, M.Y. Levy, C.B. Honsberg, Applied Physics Letters **92**, 171110 (2008).

[4] G.L. Araujo and A. Mart, Sol. Energy Mat. and Sol. Cells **33**, 213-240 (1994).

[5] A. de Vos, H. Pauwels, Appl. Phys. **25**, 119-125 (1981).

[6] J.E. Parrott, IEEE Proceedings **133**, 314-318 (1986).

Paper II

Photofilling of Intermediate Bands

Journal of Applied Physics **105**, 124512 (2009);

Unfortunately, misprints occur in equations (2), (10) and (11). These equations should be

$$g_{\mathrm{if}} = 2\pi \int_0^{\theta_{\mathrm{C}}} \phi_{\mathrm{if}}(\theta)\alpha_{\mathrm{if}} \left[\exp\left(-\alpha_{\mathrm{if}} \frac{x}{\cos\theta} \right) + \exp\left(-\alpha_{\mathrm{if}} \frac{(2W - x)}{\cos\theta} \right) \right] \sin\theta \, \mathrm{d}\theta,$$

$$p = N_{\mathrm{v}} \mathrm{e}^{-\frac{E_{\mathrm{F,p}} - E_{\mathrm{v}}}{kT}}$$

and

$$n_{\mathrm{IB}} = \frac{N_{\mathrm{IB}}}{\mathrm{e}^{(E_{\mathrm{F}} - E_{\mathrm{F,IB}})/kT} + 1},$$

respectively. The equations have been correctly implemented in the script that is used for calculations. So the misprints do not influence the results or the conclusions presented in the paper.

Photofilling of intermediate bands

Rune Strandberg[a] and Turid Worren Reenaas[b]
Department of Physics, Norwegian University of Science and Technology, N-7491 Trondheim, Norway

(Received 2 March 2009; accepted 15 May 2009; published online 23 June 2009)

A detailed balance model for the intermediate band (IB) solar cell has been developed. The model allows the electron concentration in the IB to vary and assumes a linear relation between this concentration and the absorption coefficients related to transitions over the subband gaps. Numerical results show that for IBs with densities of states typical for quantum dot-superlattices it is possible to sustain a useful population of photogenerated electrons in the IB when the cell is exposed to concentrated light. For unconcentrated light the IB must be partially filled by means of doping to achieve high efficiencies within reasonable optical path lengths. The filling of the IB is shown to vary with light intensity, cell voltage, density of IB-states, and the positioning of the IB in the main band gap both for cells that are partially filled by doping and for photofilled cells. © *2009 American Institute of Physics*. [DOI: 10.1063/1.3153141]

I. INTRODUCTION

The intermediate band solar cell (IBSC) is a photovoltaic (PV) concept, suggested by Luque and Martí in 1997,[1] in which subband gap photons can excite electrons over a semiconductor band gap in a two-step process via an IB. Such a utilization of low-energy photons increases the maximum detailed balance efficiency from the Shockley–Queisser limit of 40.7%, to a significantly higher value of 63.2%.[1–3]

Proposed implementations of the IBSC-concept includes IB-formation by quantum dot superlattices (QD-IBSC) (Ref. 4) and use of materials intrinsically posessing an IB.[5,6] Although the IBSCs that have been made so far have had efficiencies below that of single band gap reference cells, recent research has shown progress by proving the concept of the two-step carrier generation.[7–10]

To have an efficient electron pumping via the IB, there must be both filled and empty electron states in this band.[11] So far it has been assumed and argued that the IB must be close to half-filled in thermal equilibrium to satisfy this requirement.[12,13] As a consequence, it has been proposed that QD-IBSCs should be doped at a concentration equalling the concentration of QDs.[14] Due to the spin degeneration this will equal half the concentration of electron states in the IB. In the following, cells with such doping will be referred to as prefilled cells.

The main aim of this paper is to examine whether or not a photogenerated electron population in the IB can be sufficient for the two-step generation process to work properly. To achieve this, a model based on detailed balance principles has been developed. A review on the detailed balance theory is given in Ref. 15. In the following, the model is presented and numerical results are presented and discussed.

The strategy of the modeling is to establish a set of equations from which the positions of the quasi-Fermi levels $E_{F,n}$, $E_{F,\mathrm{IB}}$, and $E_{F,p}$ (see Fig. 1) for each band can be calculated. This set consists of the continuity equation for the IB, the equation for concervation of charge neutrality and the dependence between the cell voltage and the split between the quasi-Fermi levels in the CB and the VB. Knowing the positions of the quasi-Fermi levels allows us to calculate the involved generation and recombination rates, also shown in Fig. 1, and subsequently the cell current and cell efficiency.

II. THE MODEL

A geometrical cell design as shown in Fig. 2 is considered. The light comes from an illuminating surface which is either the sun itself or a concentrating optical system. This surface extends over a semiangle θ'_{rad} as seen from the outside of the cell. Seen from the inside of the cell the surface extends over a smaller angle θ_{rad} due to refraction. θ_{rad} is thus related to θ'_{rad}, through Snell's law.

Infinite carrier mobilities, zero reflectivity at the cell surface and purely radiative recombination are assumed. Nonoverlapping, and, within each nonzero interval, constant absorption coefficients, are also assumed. The treatment of the IB is simplified by assuming it is a collection of electron states at a sharply defined energy E_{IB}. Finally, we restrict the model to consider cases where the energy gap E_{vi} between the VB and the IB is larger than the energy gap E_{ic} from the IB to the CB.

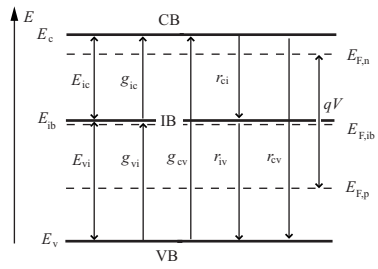

FIG. 1. Energy diagram for the IBSC with generation and recombination processes.

[a]Author to whom correspondence should be addressed. Tel.: +47 73 59 35 93. Electronic mail: rune.strandberg@ntnu.no.
[b]Tel.: +47 73 59 03 86. Electronic mail: turid.reenaas@ntnu.no.

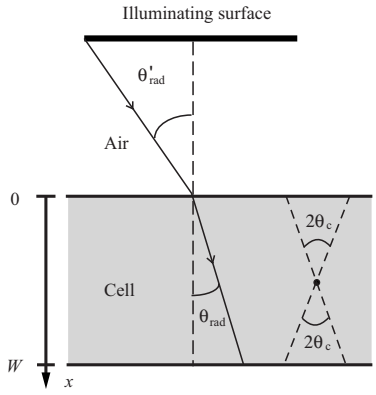

FIG. 2. Angles for light absorption or emission in the solar cell. The light comes from an illuminating surface, either the sun or an optical system, extending over a semiangle θ'_{rad}—as seen from the outer surface of the cell. Inside the cell, the light source subtends a smaller semiangle θ_{rad} because of refraction. To the right, the figure indicates the cones in which light, originating from recombination, must be radiated to be able to escape the cell.

The incorporation of photon recycling, reflection at the back surface and other geometry dependent processes resembles the model used by Cuadra *et al.*[16] in their detailed balance model developed to compare IBSCs with overlapping and nonoverlapping absorption coefficients.

The back side of the cell is assumed to be a perfect mirror. Due to total internal reflection, much of the photons emitted in recombination processes in the cell will not be able to leave it and will not represent a loss. Only photons propagating toward the front surface within a cone limited by the critical angle θ_c can leave the cell, as indicated in Fig. 2. Photons emitted toward the back surface within a cone limited by the same angle, but pointing in the opposite direction, can leave the cell after being reflected at the rear surface. Along their optical path toward the cell surface some of these photons will be reabsorbed by the cell, decreasing the actual energy loss.

The thickness of the PV device is usually not a parameter in detailed balance calculations. Here it is included to enable us to impose an actual difference between the photofilled and the prefilled IBSC. Any nonzero electron concentration in the IB will provide a nonzero absorption coefficient for allowed transitions from the IB to the CB. For an infinitely thick cell, nonzero absorption coefficients will be sufficient to absorb all photons. The interesting question to ask with respect to photofilling, is whether a photogenerated carrier density in the IB can provide as good absorption as a prefilled cell within a limited optical path length.

A. The continuity equation for the IB

The most complicated of the three equations determining the positions of the quasi-Fermi levels is the continuity equation for the IB. In steady-state, the total generation and recombination involving transitions to or from the IB has to has to balance each other. This balance includes generation from the VB to the IB, G_{vi} and from the IB to the CB G_{ic}, and recombination from the CB to the IB, R_{ci}, as well as recombination from the IB to the VB, R_{iv}. All rates being per unit area, i.e.,

$$G_{vi} - G_{ic} + R_{ci} - R_{iv} = \int_0^W (g_{vi} - g_{ic} + \rho_{ci} - \rho_{iv})dx = 0, \quad (1)$$

where the generation rates per unit volume g_{vi} and g_{ic} (see Fig. 1) and the effective recombination rates per unit volume ρ_{ci} and ρ_{iv} are disussed below. The integral over x and the distance from the cell surface is taken from the cell surface, at $x=0$, to the back of the cell where $x=W$. The integral is needed because locally there can be a net generation or net recombination of carriers to or from the IB. The sum of contributions from all positions, i.e., the sum of the rates per unit cell area, must, however, be zero in steady-state.

1. Generation rates

When considering the described cell, the photogeneration of electrons from band i to band f per unit volume will be given by the sum of excitations induced by the direct photons and those reflected at the back surface. Along the optical path, the generation follows Beer–Lambert's law. Since the optical path differs for light hitting the cell at different angles θ, the generation rates include an integral over θ. These rates then become

$$g_{if} = 2\pi \int_0^{\theta_C} \phi_{if}(\theta)\alpha_{if} \left\{ \exp\left(-\alpha_{if}\frac{x}{\cos\theta}\right) + \exp\left[-\alpha_{if}\frac{(2W-x)}{\cos\theta}\right] \right\} \cos\theta \sin\theta d\theta. \quad (2)$$

The $x/\cos\theta$-dependence on the distance traveled by the light incorporates the mentioned difference in optical path length. The integral over θ goes from $\theta=0$, which represents light rays normal to the surface to $\theta=\theta_C$ the critical angle of total internal reflection. $\phi_{if}(\theta)$ is the incoming flux, per unit solid angle and per unit cell area, of photons able to excite electrons from band i to band f, and α_{if} is the corresponding absorption coefficient. ϕ_{if} consists of two parts, radiation from the sun and thermal radiation from the surroundings. The radiation from the sun is recieved for $0<\theta<\theta_{rad}$. The radiation from the surroundings is recieved for $\theta_{rad}<\theta<\theta_C$. The photon fluxes are calculated from Planck's radiation law

$$\phi_{if}(\theta) = \frac{2n_r}{h^3c^2}\int_{E_L}^{E_U} \frac{E^2 dE}{e^{E/kT_{rad}(\theta)} - 1}, \quad (3)$$

where h is Planck's constant, c is the speed of light in vacuum, k is Boltzmann's constant, and n_r is the index of refraction of the cell material. $T_{rad}(\theta)$ is the temperature of the radiation source and is set to 6000 K for θ-values corresponding to radiation from the sun and 300 K for angles corresponding to radiation from the surroundings. The integral is taken over the photon energies E from E_L, the lowest photon energy that can drive the i to f transition, to E_U, the highest energy that will drive the transition, according to the nonoverlapping absorption coefficients.

The most important difference between this modeling and previous work done on IBSCs, is that previously the

filling of the IB or the absorption coefficients related to transitions via it, has been kept constant. As already mentioned, the main purpose of this work is to see whether or not a photogenerated carrier population in the IB can serve as a base for the two-step generation process present in IBSCs. To achieve this, it is necessary to establish a dependency between the absorption coefficients for transitions to and from the IB, and the concentration of IB electrons. The simplest way to implement this is to assume a linear dependence between IB-carrier densities and the absorption coefficients, i.e., we assume that the absorption coefficient for transitions from the IB to the CB is

$$\alpha_{\mathrm{ic}} = \sigma_{\mathrm{ic}} n_{\mathrm{IB}}, \tag{4}$$

where σ_{ic} is the absorption cross section for the transition and n_{IB} is the electron concentration in the IB. For transitions from the VB to the IB we analoguosly assume the absorption coefficient to be

$$\alpha_{\mathrm{vi}} = \sigma_{\mathrm{vi}}(N_{\mathrm{IB}} - n_{\mathrm{IB}}), \tag{5}$$

where σ_{vi} is the absorption cross section for this transition and N_{IB} is the number of electron states per unit volume in the IB. Similar forms of the absorption coefficients have been used by Keevers and Green[17] in the case of generation via impurity states and by Luque *et al.*[18] when treating impurities in nonideal IBSCs.

2. Recombination rates

The net rate r_{fi} of electrons deexcited, per unit volume, from band f to band i while radiating photons into a solid angle $d\Omega$ is given by the generalized Planck formula

$$r_{fi} d\Omega = \frac{2n_r^2}{h^3 c^2} \int_{E_L}^{E_U} \alpha_{fi} \frac{E^2}{e^{(E-\Delta\mu_{fi})/kT_c} - 1} dE d\Omega, \tag{6}$$

where $\Delta\mu_{fi}$ is the quasi-Fermi level split between the two involved bands, $T_c = 300$ K is the cell temperature and the integral is taken over all possibly emitted photon energies E, that is all energies with nonzero absorption coefficient α_{fi}. Since part of the radiation emitted by the cell will be reabsorbed, and thus not represent an energy loss, and since the number of photons leaving the cell is limited by total internal reflection, the *effective* recombination rates ρ_{fi} per unit volume will depend on the position x and an angular integral over the cone limited by the critical angle θ_c. ρ_{fi} can then be expressed as

$$\rho_{fi} = 2\pi \int_0^{\theta_c} r_{fi} \left\{ \exp\left(-\alpha_{fi} \frac{x}{\cos\theta} \right) + \exp\left[-\alpha_{fi} \frac{(2W - x)}{\cos\theta} \right] \right\} \cos\theta \sin\theta d\theta. \tag{7}$$

As in Eq. (2), the second exponential term is included to take into account photons that are reflected by the rear surface. This term will go to zero for thick cells.

B. Charge conservation

The second equation to be satisfied is the Poisson equation, which in the case of infinite carrier mobility reduces to an equation for conservation of charge neutrality. In the case of the described IBSC, this is given by

$$n + n_{\mathrm{IB}} - p - N_d^+ = 0, \tag{8}$$

where n and p are the concentrations of electrons and holes in the CB and VB, respectively, and N_d^+ is the concentration of ionized donor atoms used to prefill the IB. In the calculations it is assumed that all donor atoms are ionized. The entire difference between an IBSC with a doped IB and an IBSC without a doped IB is taken care of by the value of N_d^+. All other independent quantities will be the same for prefilled and photofilled cases.

For the electron and hole concentrations n and p the common approximations

$$n = N_c e^{-(E_c - E_{F,n})/kT}, \tag{9}$$

and

$$p = N_v e^{-(E_{F,p} - E_v)/}, \tag{10}$$

where $E_{F,n}$ is the quasi-Fermi level for electrons in the CB, $E_{F,p}$ is the quasi-Fermi level for holes in the VB and N_c and N_v are the effective densities of states in the respective bands, have been used. The energies E_c, E_{IB}, and E_v are the positions of the three energy bands, as shown in Fig. 1. For n_{IB} the full Fermi–Dirac distribution, i.e.,

$$n_{\mathrm{IB}} = \frac{N_{\mathrm{IB}}}{e^{(E_{F,\mathrm{IB}} - E_{\mathrm{IB}})/kT} + 1}, \tag{11}$$

must be used because the quasi-Fermi level $E_{F,\mathrm{IB}}$ will be close to, or at, E_{IB}.

C. Cell voltage

The voltage in an IBSC is determined as in conventional PV-devices. For a certain cell voltage V, the split between the quasi-Fermi level $E_{F,n}$ in the CB and the quasi-Fermi level $E_{F,p}$ in the VB is given by

$$E_{F,n} - E_{F,p} = qV, \tag{12}$$

where q is the elementary charge.

D. Cell current

Equations (1), (8), and (12) constitutes a set of equations which can be solved for the quasi-Fermi levels $E_{F,n}$, $E_{F,p}$, and $E_{F,\mathrm{IB}}$, which are the only independent unknowns in the system. This system of equations is, however, not trivial to solve, so this has to be done numerically. When the quasi-Fermi levels are found, the generation and recombination rates can be calculated, and the current density of the cell is found by

$$J = q(G_{\mathrm{vc}} + G_{\mathrm{ic}} - R_{\mathrm{cv}} - R_{\mathrm{iv}}). \tag{13}$$

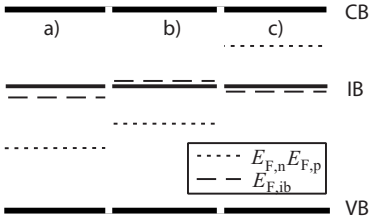

FIG. 3. Quasi-Fermi levels under illumination for a short circuited cell. (a) Cell with photofilled IB. (b) Prefilled IB where n_{IB} is increased to fulfill the continuity equation. (c) Prefilled IB where n_{IB} is decreased to fulfill the continuity equation.

E. Simplifications

The complexity of the continuity Eq. (1) makes simplifications of the system valuable, particularly when trying to get an understanding of the photofilling of the IB. Simplifications are indeed possible for some cases.

In a short circuited cell, the split between the VB and CB quasi-Fermi levels is zero. If the number of electrons entering the IB is larger than the number of electrons leaving it, n_{IB} will have to increase from its equilibrium value. If the opposite situation occurs, n_{IB} will decrease. This corresponds to a shift of $E_{F,IB}$ upwards or downwards, respectively. To satisfy the charge conservation, the quasi-Fermi level of the VB and CB will have to move in the opposite direction to account for the change of the charge in the IB. This leads to a split between the quasi-Fermi level for the IB and the other two quasi-Fermi levels.

A simplified band diagram for the short circuited cell is shown, for three different cases, in Fig. 3. The photofilled case where the IB is filled with electrons from the VB is illustrated in Fig. 3(a). The photofilling increases $E_{F,IB}$ and reduces $E_{F,n}$ and $E_{F,p}$. Figure 3(b) illustrates a prefilled case where $E_{F,IB}$ has to increase to fulfill the continuity equation for the IB. $E_{F,p}$ and $E_{F,n}$ must then decrease because the extra electrons in the IB are taken from these bands. Figure 3(c) illustrates the case where $E_{F,IB}$ has to decrease to fulfill the continuity equation. Now $E_{F,n}$ and $E_{F,p}$ must increase, because the electrons removed from the IB are now in these bands. The described quasi-Fermi level splits makes it possible to simplify the continuity Eq. (1), because $\Delta\mu_{iv}$ or $\Delta\mu_{ci}$ will be negative and the corresponding recombination rate R_{iv} or R_{ci} will be very small.

If the split between the quasi-Fermi levels is too small, neglecting one of the recombination rates might be erroneous. However, to get a non-negligible change in the filling of IBs with N_{IB} in the order of magnitude relevant for IBSCs, the split has to be several kT when N_v and N_c have values typical for semiconductors. Such splits will provide a major difference in the size of the recombination rates for band gaps relevant for PV-applications. In cases where the quasi-Fermi level split is not large enough to make one of the recombination rates negligible, the approximations to be derived might predict an incorrect shift in the filling of the IB. In such cases this shift will be very small, so the actual filling, in fact a filling very close to the equilibrium value, predicted by the approximations will nevertheless be good as long as the other assumptions made in the derivations below hold. The same kind of observation holds when in the following either n or p is treated as being negligible compared to the other.

By assuming a thick cell that absorbs all incoming photons we can set $G_{vi}=\Phi_{vi}$ and $G_{ic}=\Phi_{ic}$, where Φ_{ic} and Φ_{vi} are the total number of photons in the respective energy intervals hitting the cell per unit cell area per second. When $\Phi_{vi}-\Phi_{vi,0}>\Phi_{ci}-\Phi_{ci,0}$, where $\Phi_{vi,0}$ and $\Phi_{vi,0}$ are the photons recieved per unit cell area per second in thermal equilibrium, $E_{F,IB}$ have to increase from its equilibrium position for the continuity equation to be fulfilled. The concervation of charge neutrality will then drive $E_{F,n}$ and $E_{F,p}$ down. Due to the negative quasi-Fermi level split between the CB and the IB, the recombination between these bands, R_{ci}, will be very small, compared to R_{iv}, and can be neglected. When the difference between E_{vi} and $\Delta\mu_{iv}$ is larger than a few kT, it can be shown[19] that r_{iv} can be approximated by

$$r_{iv}=\frac{2n_r^2}{h^3c^2}\frac{pn_{IB}}{N_v(N_{IB}-n_{IB})}e^{E_{vi}/(kT)}\alpha_{vi}\int_{E_{vi}}^{E_{cv}}E^2e^{E/kT}dE. \quad (14)$$

Carrying out the integrals over x and Ω in Eqs. (1) and (6) for a wide cell yields a constant $\pi/(\alpha_{vi}n_r^2)$ that should be multiplied with Eq. (14) to get the effective recombination rate. In this case, due to the positioning of the quasi-Fermi levels, p has to be much larger than n. Using Eq. (8) which now becomes $n_{IB}-N_d^+\approx p$, we can express R_{iv} as

$$R_{iv}=K_{iv}\frac{(n_{IB}-N_d^+)n_{IB}}{N_v(N_{IB}-n_{IB})}, \quad (15)$$

where

$$K_{iv}=\frac{2\pi}{h^3c^2}e^{(E_{vi}/kT)}\int_{E_{vi}}^{E_{cv}}E^2e^{E/kT}dE. \quad (16)$$

The continuity equation $\Phi_{vi}-\Phi_{ci}=\Delta\Phi=R_{iv}$ can now be solved with respect to n_{IB}, yielding

$$n_{IB}=N_d^+-\frac{1}{2K_{iv}}[N_v\Delta\Phi-\sqrt{(N_v\Delta\Phi-K_{iv}N_d^+)^2+4K_{iv}N_vN_{IB}\Delta\Phi}]. \quad (17)$$

A similar derivation can be done when $\Phi_{vi}<\Phi_{ci}$. In this case $E_{F,IB}$ is lowered and $E_{F,n}$ and $E_{F,p}$ rises. The concervation of charge neutrality thus reduces to $n+n_{IB}-N_d^+=0$. When the difference between E_{ic} and $\Delta\mu_{ci}$ is larger than a few kT, it can also be shown[19] that

$$r_{ci}=\frac{2n_r^2}{h^3c^2}\frac{n(N_{IB}-n_{IB})}{N_cn_{IB}}e^{(E_{ic}/kT)}\alpha_{ic}\int_{E_{ic}}^{E_{vi}}E^2e^{E/kT}dE. \quad (18)$$

Carrying out the geometric integrals over x and Ω and using $n\approx N_d^+-n_{IB}$ gives the approximate expression

$$R_{ci}=K_{ci}\frac{(N_d^+-n_{IB})(N_{IB}-n_{IB})}{N_cn_{IB}}, \quad (19)$$

where

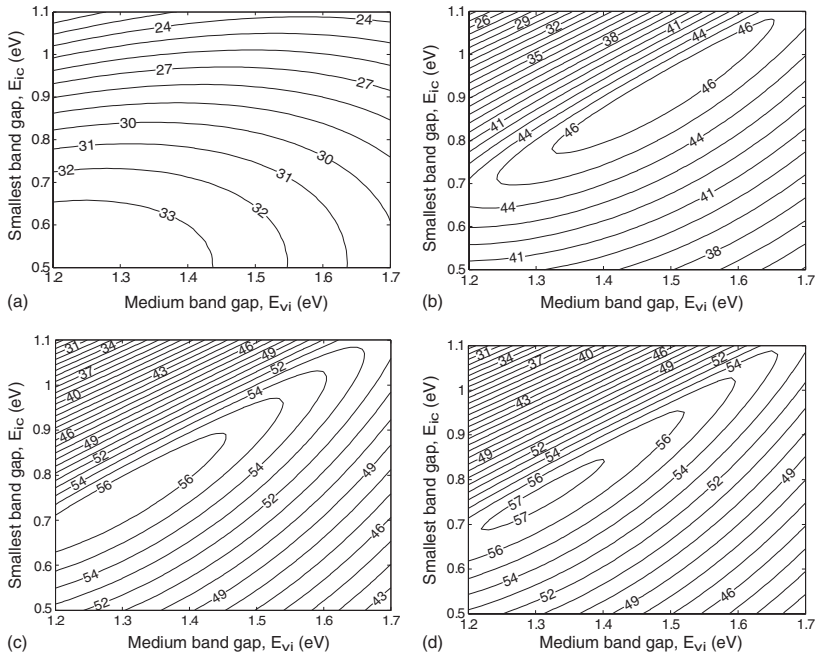

FIG. 4. Maximum efficiencies of a photofilled (a) and prefilled (b) IBSC as a function of the subband gaps E_{vi} and E_{ic} at 1 sun illumination. At 1000 suns the differences between the photofilled (c) and the prefilled (d) cells are reduced considerably.

$$K_{ci} = \frac{2\pi}{h^3 c^2} e^{(E_{ic}/kT)} \int_{E_{ic}}^{E_{vi}} E^2 e^{E/kT} dE. \tag{20}$$

Solving the continuity equation $\Delta\Phi = -R_{ci}$ with respect to n_{IB} yields

$$n_{IB} = N_d^+ + N_{IB} - \frac{1}{2K_{ci}}\{N_c\Delta\Phi + \sqrt{[N_c\Delta\Phi - K_{ci}(N_d^+ + N_{IB})]^2 - 4K_{ci}^2 N_d^+ N_{IB}}\}. \tag{21}$$

When $\Phi_{vi} > \Phi_{ci}$, the approximation (17) can be good both when $N_d^+ = 0$ and when $N_d^+ = N_{IB}/2$ for a cell with a limited thickness. When $\Phi_{vi} < \Phi_{ci}$, however, the approximation (21) will not be good when $N_d^+ = 0$ because the requirement of total absorption of the photons will be violated for the photons in Φ_{ic}.

III. NUMERICAL RESULTS

The full model described above has been used in numerical examples to evaluate the efficiencies achievable by photofilled IBSCs. The parameters used in the calculations have values close to those found in common semiconductors, and have been chosen as $N_v = N_c = 2 \times 10^{19}$ cm^{-3}, $n_r = 3.5$, and $\alpha_{vc} = 1 \times 10^4$ cm^{-1}. The cell temperature has been set to 300 K and N_{IB} to 5×10^{17} cm^{-3}, unless other values are specified, which corresponds to a center to center interdot distance of 16 nm in the case of a QD-IBSC. For the absorption cross sections no experimental data are available, but we have chosen $\sigma_{vi} = \sigma_{ic} = 3 \times 10^{-14}$ cm^2. This value gives $\alpha_{vi} = \alpha_{ic} = 7.5 \times 10^3$ cm^{-1} for a half-filled band when $N_{IB} = 5 \times 10^{17}$ cm^{-3}, which means that 99.9% of the photons will be absorbed for an optical path of 10 μm when the IB is half-filled. These values of α_{vi} and α_{ic} are between the values of the absorption coefficients used by Martí *et al.*[20] and those calculated by Tomic *et al.*[21]

A. Efficiencies

The efficiencies, as a function of the band gaps, of a photofilled and a prefilled IBSC with a thickness of 5 μm have been calculated for various light concentrations. Figures 4(a) and 4(b) show a contour plot of these efficiencies for unconcentrated sun light. The prefilled cell with the efficiencies in Fig. 4(b) and a maximum efficiency of 46.7% outclasses the photofilled cell, with efficiencies plotted in Fig. 4(a), showing a maximum efficiency of 33.9%. At 1 sun, the photogenerated electron population in the IB is too small to provide an effective absorption of the photons in ϕ_{ic}. In the case of a photofilled cell the efficiency peak is shifted toward smaller E_{vi} and E_{ic} than for the prefilled case. Smaller band gaps increases the number of photons capable of exciting electrons from the VB to the CB, which in this case is the most efficient generation process.

Increasing the illumination to 1000 suns reduces the differences between the photofilled and the prefilled IBSC, as shown in Figs. 4(c) and 4(d). The peak efficiency for the photofilled cell is now only slightly shifted to lower subband gaps, and the maximum efficiency is 56.8% compared to the 57.2% efficient prefilled cell.

The effect of light concentration on the efficiency is better seen in Fig. 5. The efficiencies of cells with E_{cv}

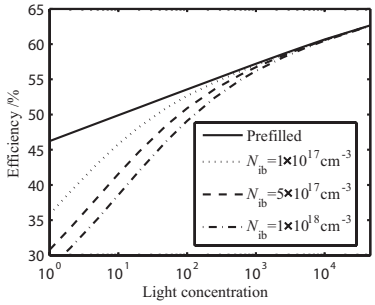

FIG. 5. Efficiencies as a function of light concentration for cells with different N_{IB}. The difference in efficiency between the prefilled and the photofilled cells, decreases whith decreasing N_{IB} and increasing light concentration.

=2.15 eV, E_{vi}=1.35 eV, and E_{cv}=0.8 eV, which is close to the efficiency peak at 1000 suns, has been calculated for various light concentrations and various density of electron states in the IB. For the results obtained with $N_{IB}=1\times10^{17}$ cm^{-3} and $N_{IB}=1\times10^{18}$ cm^{-3}, σ_{vi} and σ_{vi} have been adjusted to values maintaining absorption of 99.9% of the photons for an optical path of 10 μm with half-filled IB.

For low N_{ib}, the IB is easier to photofill, in accordance with Eq. (17), and the difference in efficiency between a photofilled and a prefilled cell will therefore be smaller for a cell with a low N_{IB} than for one with a larger N_{IB}. In Fig. 6 the cell efficiencies are plotted as a function of $\sigma N_{IB}W$, where $\sigma=\sigma_{vi}=\sigma_{ic}$, which is a measure of the absorbance of the cell. The horizontal axis ranges from 1, which gives $1-\exp(-\sigma N_{IB}W)=0.63$, to 10, giving $1-\exp(-\sigma N_{IB}W)=0.999\,95$. For a light concentration of 1000 suns the curves for $N_{IB}=1\times10^{16}$ cm^{-3} and $N_{IB}=1\times10^{17}$ cm^{-3} are not included in the figure because they are very close to the curve for the prefilled cell. This is also the case for the curve for $N_{IB}=1\times10^{16}$ cm^{-3} at 100 suns.

Note that the sizes of the absorption cross sections are not important to the conclusions that are made with respect to cell efficiencies. They will be important when determining the thickness needed for an efficient IBSC, but they do not directly affect the potential of photofilled IBSCs. The important parameters when considering the efficiency difference between a prefilled and a photofilled cell are N_{IB}, the light intensity and the absorptivity of the cell.

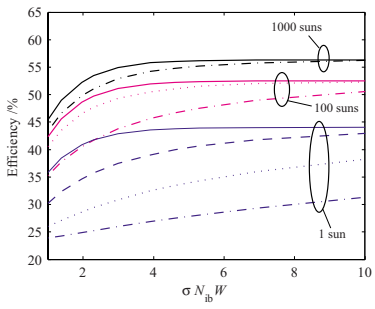

FIG. 6. (Color online) Efficiencies plotted for various light concentrations and N_{IB} as a function of $\sigma N_{IB}W$. The efficiencies of prefilled cells are plotted with solid lines and the efficiencies of photofilled cells with $N_{IB}=1\times10^{16}$ cm^{-3}, 1×10^{17} and 1×10^{18} cm^{-3} are plotted with dashed lines, dotted lines and dashed-dot lines, respectively.

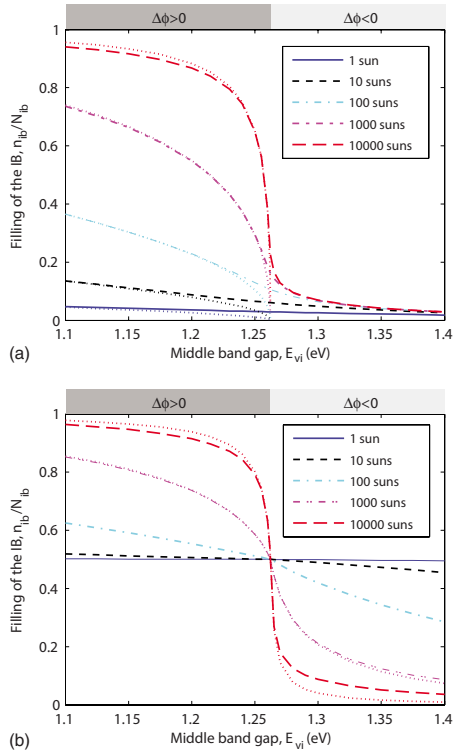

FIG. 7. (Color online) Filling of the IB in a (a) photofilled and (b) prefilled IBSC for various light concentrations. $\Delta\Phi=0$ for $E_{vi}\approx1.26$ eV. The dotted lines are the filling calculated by the approximations in (17) for $\Delta\Phi>0$ and (21) for $\Delta\Phi<0$.

For cells that are thick enough to absorb practically all incoming photons, the same absolute efficiency limit is obtained as by common detailed balance calculations.[1] This 63.2% limit is found regardless of the prefilling of the IB.

B. Filling of the IB

The filling of the IB is shown for various light concentrations in Fig. 7 for a photofilled (a) and prefilled (b) cell, with $E_{cv}=2$ eV, at zero cell voltage. The cell thickness has been set to 10 μm and N_{IB} to 5×10^{17} cm^{-3}. For higher N_{IB} the effect of the illumination on the filling will be reduced, and for lower N_{IB} the effect is increased, as can be seen from the N_{IB}-dependence of Eqs. (17) and (21). For this particular band gap $\Delta\Phi=0$ for $E_{vi}\approx1.26$ eV. From the figure it is clear that the filling of the IB varies with light intensity and the position of the IB in both cases. In the photofilled case, the filling is low for $E_{vi}>1.26$ eV which corresponds to $\Phi_{vi}<\Phi_{ic}$ and $\Delta\Phi<0$. For lower values of E_{vi}, however, the number of photons exciting electrons *to* the IB is larger than the number of photons exciting electrons *from* it, and a larger population of IB electrons can be sustained. In agreement

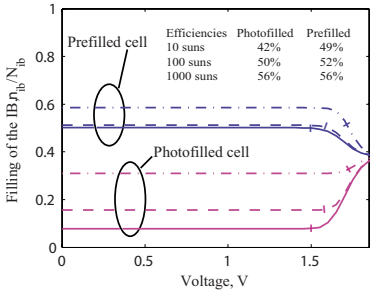

FIG. 8. (Color online) Calculated filling of the IB as a function of cell voltage for various light concentrations. The solid lines are for an illumination of 10 suns, the dashed lines for 100 suns and the bar-dot lines for 1000 suns. The voltages giving maximum efficiency are indicated with bars. Open circuit voltages for the cases are 1.66 V (10 suns), 1.77 V (100 suns), and 1.87 V (1000 suns).

with the curves in Fig. 5, a light concentration of at least a few hundred suns seems necessary to provide an IB-electron concentration giving an α_{ic} large enough [see Eq. (4)] to absorb most of the incoming photons within an acceptable optical path length for this particular value of N_{IB}. For high light intensities the difference between the filling in the photofilled and prefilled cases gets small for $\Delta\Phi > 0$, that is for $E_{vi} < 1.26$ eV.

The dotted lines in Fig. 7 are the result of the approximations in Eqs. (17) and (21). For the photofilled cell the approximation is not very good when $\Delta\Phi$ is too small, that is for E_{vi} around 1.26 eV. For both the photofilled and the prefilled cases the approximation becomes less accurate when the IB is nearly full or nearly empty. The reason for these discrepancies is that not all photons are absorbed in these cases, contradicting the assumption of full absorption that was made during the derivation of the approximations.

The approximate expressions for n_{IB} are derived under the assumption that the cell is short circuited. The arguments used in the derivation should also hold for small cell voltages. In Fig. 8 the filling of the IB is plotted as a function of cell voltage for the same cases as in Fig. 7 with $E_{vi} = 1.25$ eV, a value chosen to get $\Delta\Phi > 0$. For all illuminations, and for both the photofilled and prefilled IBSC, the filling keeps its low-voltage value for voltages up to around 1.5 V. In this voltage range one of the recombination rates is much smaller than the other one and can be neglected as is done in the derivation of the approximations. As the voltage approaches 2V, the recombination rates becomes very large compared to the generation rates. So when qV gets close to E_{cv}, the filling will therefore depend practically only on the recombination rates, and become independent on the illumination.

As can be seen from Eq. (17), n_{IB}/N_{IB} will decrease for the photofilled case when N_{IB} increases. Values of N_{IB} from 1×10^{16} to 1×10^{18} cm^{-3}, which have been used in the calculations above, corresponds to QD superlattice constants between 13 and 58 nm, which is quite typical for such nanostructures. Bulk IB-materials have N_{IB} orders of magnitude higher than this. They will thus be practically impossible to photofill.

A low filling of the IB as we have seen for several of the photofilled cases, can actually be an advantage. Cuadra *et al.*[16] have shown that the negative effect of overlapping absorption coefficients will be limited if $\alpha_{vi} > \alpha_{ic}$. A filling of 9% for example, will, when $\sigma_{ic} = \sigma_{vi}$ and the absorption coefficients have the form in Eqs. (4) and (5), give $\alpha_{vi}/\alpha_{ic} \approx 10$ which the mentioned authors outline as an appropriate ratio to suppress much of the negative overlap effect.

In Sec. II properties of an ideal IBSC were stated. In real IBSCs there will be deviations from these, so the results described above and the conclusions made below might not be valid for nonideal cells. Real cells will experience reflection losses, imperfect photon recycling, nonradiative recombination losses etc. that will lower the number of photons that can be utilized by the cell. In addition, terrestrial cells will experience a spectrum containing fewer photons than the black body spectrum used in the calculations above. This means that higher light concentrations than indicated will, in general, be needed to get an equivalent impact on the filling of the IB. The presence of absorption lines in the terrestrial spectrum might, however, cause deviations from this general observation. Nonradiative recombination losses will also affect the electron currents to and from the IB, and thus affect the filling of it and the cell performances. If nonradiative processes drain the IB of a photofilled cell, the IB will not be able to provide effective two-step generation.

Another important issue to keep in mind when transferring the results obtained in this work to real devices, is the assumption of an IB with zero width. For wide IBs, a quasi-Fermi level close to the lower edge of the band will imply a lower filling than what is the case for a narrow IB. A wide IB will therefore be harder to photofill. For prefilled cells, a shift in the IB quasi-Fermi level will have less impact on the filling of wide IBs than in narrow ones.

IV. CONCLUSIONS

A model, based on detailed balance principles, describing the IBSC has been developed. The major difference from existing models is that the electron concentration in the IB is allowed to vary. The present model has allowed us to examine whether or not a photofilled IB can allow an efficient two-step photogeneration of electrons, as well as to see how illumination affects the filling of the IB in prefilled cells.

The core of the model is charge conservation, the continuity equation for the IB and the relation between cell voltage and quasi-Fermi level splits. These equations are solved for the three quasi-Fermi levels present in the cell. The solutions determine the filling of the IB as well as the generation and recombination rates which are finally used to calculate the cell efficiency.

Numerical calculations show that a photofilled IBSC with a limited thickness can give efficiencies comparable to the efficiencies of a prefilled IBSC for concentrated light for N_{IB} typically found in QD-IBSCs, at least in the idealised setting for which the model is derived. This relieves the constraint of having a half-filled IB in thermal equilibrium in QD-IBSCs.

Despite the promising performance of the ideal photo-

filled IBSC, photofilling may not be easy to achieve in real cells. Nonradiative recombination processes can have a more devastating effect on the performance of a photofilled IBSC than in a prefilled one due to the possibility of draining of the IB.

A wide IB will also be harder to photofill than a narrow IB. In this model we only consider the extreme, and in fact unphysical, case of a sharply defined IB located at a single energy E_{IB}. The electron population in wide prefilled IBs will be less affected by changes in the IB quasi-Fermi level and therefore less influenced by the illumination it is exposed to than what is predicted by this model.

ACKNOWLEDGMENTS

The authors would like to thank the Research Council of Norway for financial support through Project No. 172905/S30.

[1]A. Luque and A. Martí, Phys. Rev. Lett. **78**, 5014 (1997).
[2]W. Shockley and H. J. Queisser, J. Appl. Phys. **32**, 510 (1961).
[3]A. S. Brown and M. A. Green, J. Appl. Phys. **94**, 6150 (2003).
[4]L. Cuadra, A. Martí, and A. Luque, Physica E (Amsterdam) **14**, 162 (2002).
[5]K. M. Yu, W. Walukiewicz, J. Wu, W. Shan, J. W. Beeman, M. A. Scarpulla, O. D. Dubon, and P. Becla, Phys. Rev. Lett. **91**, 246403 (2003).
[6]P. Wahnón and C. Tablero, Phys. Rev. B **65**, 165115 (2002).
[7]N. López, A. Martí, A. Luque, C. Stanley, C. Farmer, and P. Diaz, ASME J. Sol. Energy Eng. **129**, 319 (2007).
[8]A. Martí, N. López, E. Antolín, E. Cánovas, A. Luque, C. R. Stanley, C. D. Farmer, and P. Díaz, Appl. Phys. Lett. **90**, 233510 (2007).
[9]A. Martí, E. Antolín, C. R. Stanley, C. D. Farmer, N. López, P. Díaz, E. Cánovas, P. G. Linares, and A. Luque, Phys. Rev. Lett. **97**, 247701 (2006).
[10]E. Antolín, A. Martí, C. R. Stanley, C. D. Farmer, E. Cánovas, N. López, P. G. Linares, and A. Luque, Thin Solid Films **516**, 6919 (2008).
[11]A. Luque and A. Martí, Prog. Photovoltaics **9**, 73 (2001).
[12]A. Martí, L. Cuadra, and A. Luque, Physica E (Amsterdam) **14**, 150 (2002).
[13]A. Martí, E. Antolín, N. López, P. G. Linares, A. Luque, C. R. Stanley, and C. D. Farmer, Thin Solid Films **516**, 6716 (2008).
[14]A. Martí, L. Cuadra, and A. Luque, IEEE Trans. Electron Devices **48**, 2394 (2001).
[15]G. L. Araujo and A. Martí, Sol. Energy Mater. Sol. Cells **33**, 213 (1994).
[16]L. Cuadra, A. Martí, and A. Luque, IEEE Trans. Electron Devices **51**, 1002 (2004).
[17]M. J. Keevers and M. A. Green, J. Appl. Phys. **75**, 4022 (1994).
[18]A. Luque, A. Martí, N. López, E. Antolín, E. Cánovas, C. Stanley, C. Farmer, and P. Díaz, J. Appl. Phys. **99**, 094503 (2006).
[19]R. Strandberg and T. Worren Reenaas (to be published).
[20]A. Martí, L. Cuadra, and A. Luque, IEEE Trans. Electron Devices **49**, 1632 (2002).
[21]S. Tomic, T. S. Jones, and N. M. Harrison, Appl. Phys. Lett. **93**, 263105 (2008).

Paper III

Drift-diffusion model for Intermediate Band Solar Cells including photofilling effects

Accepted for publication in *Progress in Photovoltaics: Research and Applications*.

Drift-diffusion model for Intermediate Band Solar Cells including photofilling effects

Abstract

A novel drift-diffusion model for intermediate band solar cells (IBSC) is presented. The model differs from previous drift-diffusion models by allowing the carrier concentrations in all three bands to vary. It is developed for the idealized case where only radiative recombination occurs and where the IB has zero width. The model is used to compare the performance of IBSCs where the IB-region is doped to get a partially filled IB (prefilled IBSC) to IBSCs where the IB-region is not doped to partially fill the IB (photofilled IBSC). Numerical results show that a photofilled IBSC can achieve high efficiencies when operated under concentrated light. In fact, for some particular cases, a photofilled cell will perform better than a prefilled cell. The optimal degree of prefilling, i.e. the ratio of the concentration of doping atoms to the total number of IB-states, is found for a particular example. It is also examined how the carrier concentrations in all three bands, the conduction, the intermediate and the valence bands, vary in prefilled and photofilled IBSCs. Finally, the band diagrams of a prefilled and photofilled IBSC are discussed.

1 Introduction

The intermediate band solar cell (IBSC) is a third generation photovoltaic concept based on the principle of two-step photogeneration via an intermediate band (IB), situated in the usually forbidden semiconductor band gap. Research on this device is motivated by high theoretical efficiencies [1, 2, 3].

The IB has to be partially filled to allow photoexcitation both to it and from it [4]. So far, it has usually been assumed that the IB has to be, or at least be close to, half-filled in thermal equilibrium. In addition, a clamping of the quasi-Fermi level of the IB to its equilibrium value under operation of the IBSC has usually also been assumed in theoretical work [5, 6, 7, 8]. Clamping of the IB quasi-Fermi level gives a fixed filling of the IB, i.e. a filling constant in space and always equal to the filling in thermal equilibrium, which subsequently gives fixed absorption coefficients for transitions to and from

the IB.

It has been shown that the assumption of a fixed filling of the IB can be valid when the density of states in the intermediate band is sufficiently high [6, 9]. It has also been shown, however, that the filling of intermediate bands with densities of states typical for IBSCs based on quantum dot superlattices (QD-IBSCs)[10], can increase or decrease from the equilibrium filling when the cell is illuminated - particularly when the light is concentrated [11, 12]. In the following the, terms "photofilled cell" and "prefilled cell" are used. A photofilled cell is a cell where the intermediate band is only occupied by thermally excited electrons, i.e. it is practically empty, in thermal equilibrium. The IB is then partially filled by photoexitation. A prefilled cell is a cell that has been partially filled by means of doping. In some occasions the terms "photofilling" and "photofilling effects" are used. These refer to an increase or decrease of the filling under operation of the cell as compared to the filling in thermal equilibrium. While the model describing photofilling in ref. [12] is based on detailed balance principles, the present model investigates the possibilities of photofilling from a device modelling perspective. The difference between this work and previous drift-diffusion models [6, 13] is to allow the electron concentration in the IB, and thus the related absorption coefficients, to vary during operation of the cell.

The model treats an intermediate band solar cell sketched in figure 1. The intermediate band is sandwiched between the p and n emitters and two field-damping layers as proposed by Martí et al.[8]. To prevent tunnelling of electrons from the IB to the n-emitter, the field-damping layer of p-type can be substituted with an intrinsic region [14]. The purpose of the field-damping layers is to keep the IB-material in a flatband region of the cell to maintain a relatively even spatial distribution of electrons in the intermediate band. The optimal width of the field-damping layers depends on the cell voltage and should in practice be optimized for the voltage yielding the highest efficiency. For other voltages, parts of the intermediate band region will be depleted. With densities of states of the magnitude one can expect to find in QD-IBSCs, the thickness of the possibly depleted layers of the IB region will typically correspond to less than a few tens of nanometers. This is thin compared to the optical path length that seems to be necessary to absorb the majority of the sub-band gap photons in IB-materials based on QD-superlattices [15]. In the following, the cell is treated as if the field-damping layers are optimized with respect to the particular voltage at which the cell properties are evaluated.

The first step in the modeling is to determine the carrier concentrations in all three bands, the

conduction band (CB), the IB and the valence band (VB), in the IB-region by solving a set of differential equations that describes the device. The equations include the continuity equations for the bands plus the Poisson equation. The system is solved under the constraint that the net charge in the IB-region is zero. Zero charge is required to have an electrostatic field equal to zero at both edges of the IB-region, i.e. at $x = 0$ and $x = W$ as shown in figure 1. With optimized field-damping layers this will be the case.

For simplicity, the intermediate band is treated as a collection of electron states at a sharply defined energy level E_{ib}, still possessing the collective characteristics of a band of delocalized states. It is also assumed that all photons enter the cell normal to the cell surface and that the reflectivity of the cell is zero. The emitters and field-damping layers are assumed to be too thin to absorb a significant amount of photons, which makes it possible to neglect generation and recombination processes taking place in these regions.

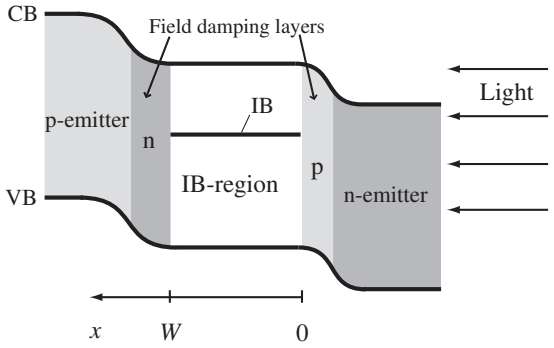

Figure 1: Schematic drawing of the intermediate band solar cell. The purpose of the field-damping layers is to obtain flat bands in the IB-region.

In section 2, the mathematical details of the model are presented, as well as a discussion of the differences in the band diagram of a photofilled and prefilled IBSC. The model is then used to investigate numerical examples in section 3.

2 Mathematical model

This section is divided into two subsections. In the first part, appropriate recombination and generation rates are derived. The model itself is then put together and discussed in section 2.2.

2.1 Generation rates and recombination rates

The absorption coefficients associated with electron transitions to and from an intermediate band depends on the number of electrons in this band. The simplest way to incorporate such dependencies mathematically is to assume a linear relationship between the absorption coefficients and the concentration of IB electrons. To be precise, the absorption coefficients are assumed to be

$$\alpha_{\mathrm{ci}} = \sigma_{\mathrm{ci}} n_{\mathrm{ib}}, \tag{1}$$

for excitations from the IB to the CB and

$$\alpha_{\mathrm{iv}} = \sigma_{\mathrm{iv}} (N_{\mathrm{ib}} - n_{\mathrm{ib}}), \tag{2}$$

for excitations from the VB to the IB, where σ_{ci} and σ_{iv} are the absorption cross-sections for the respective processes, N_{ib} is the total density of states in the IB and n_{ib} is the electron density in the IB. Linear relationships between the filling of the intermediate states and the absorption coefficients have previously been used while treating cases with localized intermediate states [11, 16, 17].

The three absorption coefficients of the system, α_{ci}, α_{iv} and α_{cv}, the latter being for transitions from the VB to the CB, are assumed to be non-overlapping. This implies that for a particular photon energy E there is at maximum one absorption coefficient with a non-zero value, namely the absorption coefficient related to excitations over the largest band gap with a band gap energy smaller than the photon energy. Non-overlapping absorption coefficients simplifies the model since overlapping absorption coefficients introduces irreversible processes that are not occurring otherwise [18, 19]. It is also assumed that the absorption coefficients are independent of the photon energy in their respective energy ranges.

The generation rates at a distance x from the surface of the cell are as usual given by $g_{\mathrm{if}}(x) = \phi_{\mathrm{if}}(x)\alpha_{\mathrm{if}}(x)$, where ϕ_{if} is the flux of photons energetically allowed to excite electrons from band i to

band f, and α_{if} is the absorption coefficient for this transition. The generation rates g_{ci}, g_{iv} and g_{cv} then become

$$g_{\mathrm{ci}}(x) = \sigma_{\mathrm{ci}} n_{\mathrm{ib}} \phi_{\mathrm{ci},0} \exp\Big(- \int_0^x \sigma_{\mathrm{ci}} n_{\mathrm{ib}}(x')\,\mathrm{d}x' \Big), \tag{3a}$$

$$g_{\mathrm{iv}}(x) = \sigma_{\mathrm{iv}} (N_{\mathrm{ib}} - n_{\mathrm{ib}}) \phi_{\mathrm{vi},0} \exp\Big(- \int_0^x \sigma_{\mathrm{iv}} (N_{\mathrm{ib}} - n_{\mathrm{ib}}(x'))\,\mathrm{d}x' \Big) \quad \text{and} \tag{3b}$$

$$g_{\mathrm{cv}}(x) = \alpha_{\mathrm{cv}} \phi_{\mathrm{vc},0} \exp(-\alpha_{\mathrm{cv}} x), \tag{3c}$$

where $\phi_{\mathrm{ci},0}$, $\phi_{\mathrm{vi},0}$ and $\phi_{\mathrm{cv},0}$ are the photon fluxes at $x = 0$. The integral in the exponents in eqs. (3a) and (3b) occurs because n_{ib}, and thus the absorption coefficients, are allowed to vary spatially. When the electron mobility in the IB is high, n_{ib} will be uniform throughout the IB-region and the integrals can be substituted with $\sigma_{\mathrm{ci}} n_{\mathrm{ib}} x$ and $\sigma_{\mathrm{iv}}(N_{\mathrm{ib}} - n_{\mathrm{ib}})x$, respectively. The respective fluxes at the surface of the cell are found by

$$\phi_{\mathrm{if},0} = \frac{X}{46050} \frac{2\pi}{h^3 c^2} \int_{E_{\mathrm{L}}}^{E_{\mathrm{H}}} \frac{E^2}{\exp\left(\frac{E}{kT_{\mathrm{s}}}\right) - 1}\,\mathrm{d}E, \tag{4}$$

where h is Planck's constant, k is Boltzmann's constant, c is the speed of light and T_{s} is the temperature of the sun, in this work assumed to be 6000 K. X is the concentration factor. The integration limits E_{L} and E_{H} are determined by the band gap in question and corresponds to the limits of the energy interval where the respective absorption coefficient is non-zero..

The radiative recombination rate from band f band to band i is given by [20]

$$r_{\mathrm{if}} = K \int \alpha_{\mathrm{if}} \frac{E^2}{\exp\left(\frac{E - \Delta\mu_{\mathrm{fi}}}{kT}\right) - 1}\,\mathrm{d}E, \tag{5}$$

where $\Delta\mu_{\mathrm{if}}$ is the quasi-Fermi level split between the involved bands and T is the temperature of the cell. The constant K equals $8\pi n_{\mathrm{r}}^2 / h^3 c^2$, where n_{r} is the index of refraction. The integral is to be taken over all possible energies E of the emitted photons.

In device modelling, a simplified version of the expression for the radiative recombination rates [21]

$$r_{\mathrm{if}} \approx K \mathrm{e}^{\frac{\Delta\mu_{\mathrm{if}}}{kT}} \int \alpha_{\mathrm{if}} E^2 \mathrm{e}^{-\frac{E}{kT}}\,\mathrm{d}E, \tag{6}$$

is usually used. The approximation is valid when $\Delta\mu_{\mathrm{fi}}$ is small compared to the smallest radiated photon energy, i.e. when $\exp((E-\Delta\mu)/kT) >> 1$. This approximation can also be used for the recombination rates involving the IB - with a little care, however. In photovoltaic devices based on ordinary semiconductors, both quasi-Fermi levels will be located within the band gap. In an IB-material the quasi-Fermi level of the IB can in principle be both over and under E_{ib}, the absolute energy of the center of the intermediate band, and thus potentially be outside the sub-band gap over which one of the recombination process takes place. Quasi-Fermi level splittings that do not meet the criterion for this approximation might therefore arise more easily in IB-devices than in traditional devices. In the numerical examples later in this paper, the resulting difference between a quasi-Fermi level split and the relevant band gap is always larger than $4kT$. This limits the error in the recombination rates to less than 2%. In most of the examples, however, the error is significantly lower than this.

It is useful to express the recombination rates by the carrier densities, for further simplification. Since the recombination rates used in ref. [6] are derived under the assumption of a fixed IB filling, a derivation of recombination rates that does not have this restriction is done in the following. The quasi-Fermi level of the intermediate band, $E_{\mathrm{F,ib}}$, will most likely be positioned at or close to E_{ib}. The Fermi-Dirac distribution should therefore be used, i.e.

$$n_{\mathrm{ib}} = \frac{N_{\mathrm{ib}}}{\exp\left(\frac{E_{\mathrm{ib}}-E_{\mathrm{F,ib}}}{kT}\right)+1}. \tag{7}$$

For the CB and VB, the relation between the carrier densities and the quasi-Fermi levels $E_{\mathrm{F,c}}$ and $E_{\mathrm{F,v}}$ are, as common in semiconductor physics, assumed to be described by the approximations

$$n = N_{\mathrm{c}}\mathrm{e}^{-(E_{\mathrm{c}}-E_{\mathrm{F,c}})/kT} \quad \text{and} \tag{8a}$$

$$p = N_{\mathrm{v}}\mathrm{e}^{(E_{\mathrm{v}}-E_{\mathrm{F,v}})/kT}, \tag{8b}$$

where n is the electron concentration in the CB, p is the hole concentration in the VB and N_{c} and N_{v} are the effective densities of states in the CB and VB, respectively.

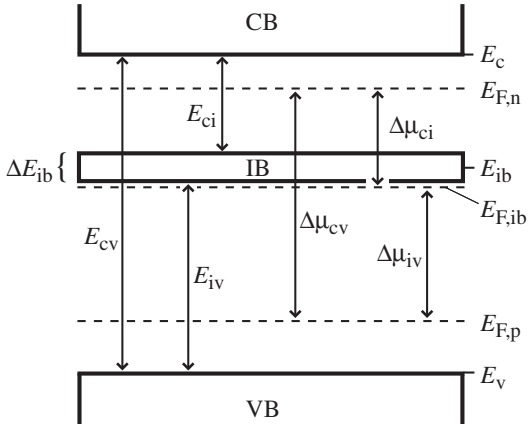

Figure 2: Simplified band diagram showing the energy band configuration of the IB-material as well as the quasi-Fermi level splits. In the modelling, the width of the IB, ΔE_{ib}, is assumed to be zero.

Using equation (7) and equations (8), while keeping an eye on the band diagram in figure 2, one finds

$$\mathrm{e}^{\Delta\mu_{\mathrm{ci}}/kT} = \mathrm{e}^{(E_{\mathrm{ib}}-E_{\mathrm{F,ib}}+E_{\mathrm{F,c}}-E_{\mathrm{c}}+E_{\mathrm{c}}-E_{\mathrm{ib}})/kT} = \frac{n}{N_{\mathrm{c}}}\left(\frac{N_{\mathrm{ib}}-n_{\mathrm{ib}}}{n_{\mathrm{ib}}}\right)\mathrm{e}^{E_{\mathrm{ci}}/kT}, \tag{9a}$$

$$\mathrm{e}^{\Delta\mu_{\mathrm{iv}}/kT} = \mathrm{e}^{(E_{\mathrm{F,ib}}-E_{\mathrm{ib}}+E_{\mathrm{v}}-E_{\mathrm{F,v}}+E_{\mathrm{ib}}-E_{\mathrm{v}})/kT} = \frac{p}{N_{\mathrm{v}}}\left(\frac{n_{\mathrm{ib}}}{N_{\mathrm{ib}}-n_{\mathrm{ib}}}\right)\mathrm{e}^{E_{\mathrm{iv}}/kT} \quad \text{and} \tag{9b}$$

$$\mathrm{e}^{\Delta\mu_{\mathrm{cv}}/kT} = \mathrm{e}^{(E_{\mathrm{F,c}}-E_{\mathrm{c}}+E_{\mathrm{v}}-E_{\mathrm{F,v}}+E_{\mathrm{c}}-E_{\mathrm{v}})/kT} = \frac{np}{N_{\mathrm{c}}N_{\mathrm{v}}}\mathrm{e}^{E_{\mathrm{cv}}/kT}, \tag{9c}$$

where equation (9c) is well known for regular semiconductors. Inserting equations (9a)-(9c) into their respective counterparts in (6a-c) and using (1) and (2) gives the following expressions for the radiative recombination rates:

$$r_{\mathrm{ci}} = K\sigma_{\mathrm{ci}}(N_{\mathrm{ib}}-n_{\mathrm{ib}})\frac{n}{N_{\mathrm{c}}}\mathrm{e}^{E_{\mathrm{ci}}/kT}I_{\mathrm{ci}}, \tag{10a}$$

$$r_{\mathrm{iv}} = K\sigma_{\mathrm{iv}}n_{\mathrm{ib}}\frac{p}{N_{\mathrm{v}}}\mathrm{e}^{E_{\mathrm{iv}}/kT}I_{\mathrm{iv}} \quad \text{and} \tag{10b}$$

$$r_{\mathrm{cv}} = K\alpha_{\mathrm{cv}}\frac{np}{N_{\mathrm{c}}N_{\mathrm{v}}}\mathrm{e}^{E_{\mathrm{cv}}/kT}I_{\mathrm{cv}}, \tag{10c}$$

where I_{fi}, with fi = ci, iv or cv, are the integrals given by

$$I_{\mathrm{fi}} = \int_{E_{\mathrm{L}}}^{E_{\mathrm{U}}} E^2 \mathrm{e}^{-E/kT}\,\mathrm{d}E, \tag{11}$$

i.e. the integrals over the possible energies of the emitted photons, where E_{L} and E_{U} are the lower and upper limits of the energy interval in which the absorption coefficient relevant for the transition is non-zero. The expressions for the two recombination rates involving the IB are, as one might expect, showing the same qualitative behaviour as the recombination from the CB to the VB described by the well known eq. (10c). The rates are linearly dependent on the product of the density of electrons in the upper band and the density of unoccupied states in the lower.

2.2 Model of the cell

Having derived appropriate recombination and generation rates makes it possible to develop a model that can be used to calculate the carrier densities and the cell performance. The mathematical details of the model used to calculate the results in section 3, is presented in the following.

If the spatial distribution of n, n_{ib} and p leads to net charges at any position, an electrostatic field F will occur. The magnitude of the field is found by the Poisson equation, which for this system becomes

$$\frac{\mathrm{d}F}{\mathrm{d}x} = \frac{q}{\epsilon}(p - n_{\mathrm{ib}} - n + N_{\mathrm{d}}^{+}), \tag{12}$$

where ϵ is the dielectric constant and N_{d}^{+} is the concentration of ionized donor atoms used to partially fill the intermediate band. All donor atoms are assumed to be ionized, so that N_{d}^{+} equals N_{d}, the density of donor atoms. In materials where the IB-electrons have a sufficiently high mobility and density, electrostatic fields will be screened by the IB-electrons [6]. In cases where the mobility of the IB-electrons is low, however, electrostatic fields can not be neglected.

Including both carrier diffusion and drift, the continuity equations for this three band system becomes

$$D_{\mathrm{n}}\frac{\mathrm{d}^2 n}{\mathrm{dx}^2}+\mu_{\mathrm{n}}\frac{\mathrm{d}(nF)}{\mathrm{d}x}+g_{\mathrm{ci}}+g_{\mathrm{cv}}-r_{\mathrm{ci}}-r_{\mathrm{cv}}=0, \tag{13a}$$

$$\frac{kT\mu_{\mathrm{ib}}}{q}\frac{\mathrm{d}}{\mathrm{dx}}\left(\frac{N_{\mathrm{ib}}}{N_{\mathrm{ib}}-n_{\mathrm{ib}}}\frac{\mathrm{d}n_{\mathrm{ib}}}{\mathrm{dx}}\right)+\mu_{\mathrm{ib}}\frac{\mathrm{d}(n_{\mathrm{ib}}F)}{\mathrm{d}x}+g_{\mathrm{iv}}-g_{\mathrm{ci}}+r_{\mathrm{ci}}-r_{\mathrm{iv}}=0 \quad \text{and} \tag{13b}$$

$$D_{\mathrm{p}}\frac{\mathrm{d}^2 p}{\mathrm{dx}^2}-\mu_{\mathrm{p}}\frac{\mathrm{d}(pF)}{\mathrm{d}x}+g_{\mathrm{iv}}+g_{\mathrm{cv}}-r_{\mathrm{iv}}-r_{\mathrm{cv}}=0, \tag{13c}$$

where D_{n} and D_{p} are the carrier diffusion constants and μ_{n}, μ_{ib} and μ_{p} are the carrier mobilities. The first term in equation (13b) differs from the first term in the two other equations because the Einstein relation $D = kT\mu/q$ is not applicable to the IB. A derivation of the first term in equations (13b) is shown in appendix A.

The system of equations, (12) and (13), should be solved with the constraint $\int_0^W (p - n - n_{\mathrm{ib}} + N_d^+)\,\mathrm{d}x = 0$ to preserve charge neutrality in the IB-region. In general, charge neutrality is not a requirement, but to comply with the boundary conditions presented below, the electrostatic field has to be zero at both edges of the IB-region. As mentioned above, this is equivalent to have optimized field-damping layers.

At $x = 0$ and $x = W$ there can be no current in the intermediate band due to its termination. Since the electric field is zero and the current has to be purely diffusive at these positions, $\frac{\mathrm{d}n_{\mathrm{ib}}}{\mathrm{dx}} = 0$ for $x = 0$ and $x = W$ are appropriate boundary conditions.

Given the assumption that the emitters and field-damping layers are too thin to absorb significant amounts of photons, there will be no hole current in the VB at $x = 0$ and no electron current in the CB at $x = W$. This leads to the boundary conditions $\frac{\mathrm{d}n}{\mathrm{dx}}\big|_{x=W} = \frac{\mathrm{d}p}{\mathrm{dx}}\big|_{x=0} = 0$.

In accordance with the depletion approximation, the boundary conditions

$$n(0) = n_0 \exp\left(qV_{\mathrm{n}}/kT\right) \tag{14}$$

and

$$p(W) = p_0 \exp\left(qV_{\mathrm{p}}/kT\right), \tag{15}$$

are also applied. n_0 and p_0 are the electron and hole densities in the IB-region in thermal equilibrium and V_{n} and V_{p} are the voltages over the two sub-junctions, as shown in figure 3 b) and c). These sub-junction voltages are related to the cell voltage V through

$$V = V_{\mathrm{n}} + V_{\mathrm{p}} + V_{\rho}, \tag{16}$$

where V_{ρ} is the potential difference between $x = 0$ and $x = W$ due to possible displacement of charge in the IB-region. V_{ρ} will be small whenever the carriers in one or more bands have a density and mobility high enough to screen electrostatic fields in the IB-region. In this paper, V_{ρ} is very small, and thus neglected, in all calculations except those in section 3.1.

The band diagrams in figure 3 illustrates some points that are worth mentioning. The figure shows a cell where the illumination increases the filling of the IB, b) and c), as compared to in thermal equilibrium, a), in a photofilled and a prefilled cell. In the figure it is assumed that the carrier mobilities are infinite. The quasi Fermi level splittings are then constant in the IB-region. It is useful to define the quantities $V_{\mathrm{n}}' = \Delta\mu_{\mathrm{ci}}/q$ and $V_{\mathrm{p}}' = \Delta\mu_{\mathrm{iv}}/q$. Now, in cells where the quasi-Fermi level for the IB is clamped to its equilibrium value, V_{n}' and V_{p}', will equal V_{n} and V_{p}, respectively. When $E_{\mathrm{F,ib}}$ is not clamped, these quantities will be decoupled. As shown in figure 3, the decoupling can happen when the cell is short circuited b) as well as when a bias is applied to the cell c). In other words, V_{n}' and V_{n}', which are the potential differences driving the recombination processes via the intermediate band does not equal the voltages V_{n} and V_{p} which determines the carrier concentrations in the CB and VB. We still have $V_{\mathrm{n}} + V_{\mathrm{p}} = V_{\mathrm{n}}' + V_{\mathrm{p}}' = V$, however. In terms of an equivalent circuit for an IBSC, see for example ref. [22], V_{n}' and V_{p}', not V_{n} and V_{p}, are the voltages over the two diodes associated with the sub-band gaps.

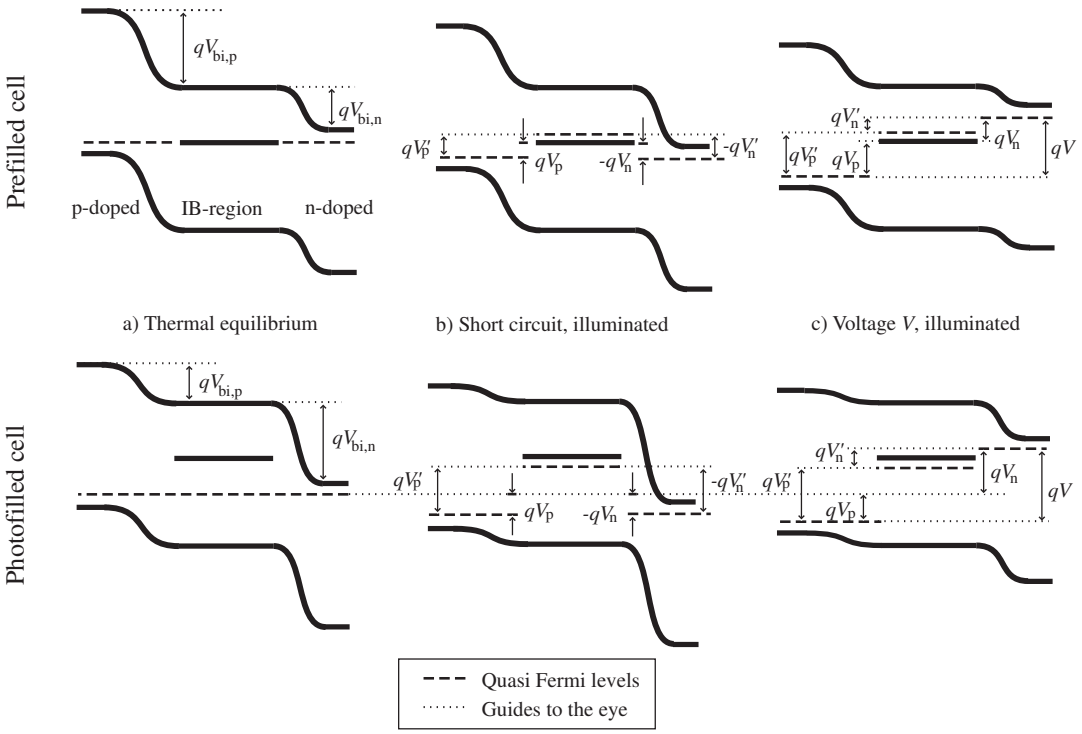

Figure 3: Schematic band diagrams for a prefilled (top) and a photofilled (bottom) IBSC in the dark a), illuminated and short-circuited b) and illuminated and subject to a cell voltage V b). The diagrams illustrate a situation where n_{ib} increase due to illumination, as discussed in more detail in ref. [12]. Infinite carrier mobilities are required to achieve spatially invariant V'_{n} and V'_{p}.

As illustrated in the left column of figure 3, the built-in potential $V_{\mathrm{bi,p}}$ between the p-emitter and the IB-region in a photofilled cell is smaller than in a prefilled cell, while the built in potential $V_{\mathrm{bi,n}}$ between the IB-region an the n-emitter is larger. The optimal thickness of the field-damping layers will therefore be different for the two cell types, as will be shown in section 3.4.

The current has to be constant throughout the cell. For $x = 0$ the current consists entirely of electron current in the CB and for $x = W$ it consists entirely of hole current in the VB. With zero electric field at the boundaries of the IB-region the current density thus becomes

$$J = qD_{\mathrm{n}}\frac{\mathrm{d}n}{\mathrm{dx}}\bigg|_{x=0} = -qD_{\mathrm{p}}\frac{\mathrm{d}p}{\mathrm{dx}}\bigg|_{x=W}. \tag{17}$$

When the current is found, the efficiency η is calculated by

$$\eta = \frac{I_{\mathrm{m}}V_{\mathrm{m}}}{E_{\mathrm{sun}}} = \frac{J_{\mathrm{m}}AV_{\mathrm{m}}}{E_{\mathrm{sun}}}, \tag{18}$$

where V_{m} is the voltage at the maximum power point, I_{m} is the cell current and J_{m} the current density at this voltage, and A is the area of the cell. The denominator $E_{\mathrm{sun}} = (X/46050)ST_{\mathrm{s}}^4$, where S is the Stefan-Boltzmann constant, is the energy brought to the cell by the photons in the solar spectrum.

In materials where the mobility of the IB-electrons is high, the modelling can be simplified due to screening of the electrostatic field, and the terms in the continuity equations that contain these fields can be neglected. For a half-filled IB with $N_{\mathrm{ib}} = 1 \cdot 10^{17}\,\mathrm{cm}^{-3}$, the number of states in the IB is high enough to provide screening, while maintaining a relatively flat distribution of n_{ib} throughout the cell, when the mobility exceeds $62\,\mathrm{cm}^2\mathrm{V}^{-1}\mathrm{s}^{-1}$, as discussed in ref. [6]. Equation (13b) can in such cases be replaced with

$$\int_0^W \Big(g_{\mathrm{iv}} - g_{\mathrm{ci}} + r_{\mathrm{ci}} - r_{\mathrm{iv}}\Big)\,\mathrm{d}x = 0, \tag{19}$$

i.e. an equation that can be used to find a spatially constant value for the filling of the IB.

In the following section, the full model, that is, with equation (13b), has been used in the calculations of the carrier concentrations in section 3.1. For calculations of cell performance, the electron mobility in the IB is assumed to be high, and the IB-region is treated as being quasi-neutral. The simplified model with equation (19) has been used in the latter cases.

In summary, the model resembles a previous model presented by Martí et al. [6] using basically the same geometry and boundary conditions, but represents a step towards a full model for IBSC-devices by introducing a non-constant electron concentration in the IB.

3 Numerical results and discussion

The described model is used to calculate carrier densities and performance characteristics of prefilled and photofilled IBSCs. First the carrier distributions are investigated in section 3.1. The performance

of photofilled and prefilled IBSCs are then compared in section 3.2. Section 3.3 discusses the optimal filling of the intermediate band and, finally, values of the sub-junction voltages and the optimal width of the field damping layers are discussed in section 3.4.

The calculations are made with band gaps $E_{\mathrm{cv}} = 2\,\mathrm{eV}$, $E_{\mathrm{iv}} = 1.2\,\mathrm{eV}$ and $E_{\mathrm{ci}} = 0.8\,\mathrm{eV}$. The cell thickness is $W = 5\mu\mathrm{m}$. The absorption coefficient α_{cv} is set to a value of $10^4\,\mathrm{cm}^{-1}$, and the photon fluxes are calculated from the 6000 K black body spectrum. The cell temperature is set to 300 K. Thermal generation caused by radiation from the surroundings is neglected. The density of IB-states is set to $2.5 \cdot 10^{17}\,\mathrm{cm}^{-3}$, which corresponds to a center to center interdot distance of 20 nm in a quantum dot superlattice. The absorption cross sections are set to $3 \cdot 10^{-14}\,\mathrm{cm}^2$ which will give absorption coefficients of $3750\,\mathrm{cm}^{-1}$ with a half-filled IB. This value is of the same order as the absorption coefficients calculated by Tomic et al. for a superlattice of InAs quantum dots embedded in GaAs [15]. In some of the numerical examples to follow, the values of the absorption cross-sections are varied, by varying the ratio of them (i.e. $\sigma_{\mathrm{ci}}/\sigma_{\mathrm{iv}}$) while keeping their geometrical average constant. The carrier mobilities in the VB and CB are set to $2000\,\mathrm{cm}^2\mathrm{V}^{-1}\mathrm{s}^{-1}$. N_{c} and N_{v} are both set to $2 \times 10^{19}\,\mathrm{cm}^{-3}$. The light concentration is varied from 10 to 1000. The concentration is specified for each of the presented cases.

The relative dielectric constant is set to 13 and the index of refraction to 1. This imposes an inconsistency, because ϵ_{r} should equal n_{r}^2. The dielectric constant have been given a value which is a typical for semiconductors, to incorporate the effect of potential electrostatic fields in a good way. Choosing an index of refraction larger than 1 will increase the recombination rates as well as reduce the solid angle through which photons can escape the cell. This will lead to an overestimation of the recombination losses unless photon recycling is incorporated into the model. To include photon recycling in a model like this will be complicated, and, as pointed out by Martí et al. [6], photon recycling effects are usually not incorporated in modelling of conventional semiconductor devices either. So to avoid overcomplicating the model, the index of refraction has been set to 1. It is the opinion of the authors that the results obtained by the model, although inconsistent on this particular point, give useful qualitative information about IBSC-devices. In the following, the electrons in the IB are assumed to have high mobilities in several of the numerical examples. In such cases the electric field in the IB-region can be neglected. The dielectric constant is then no longer a parameter in the model, and the inconsistency between the values of ϵ_{r} and n_{r} disappears.

3.1 Carrier distributions

To calculate the electron distribution in an IB with low electron mobilities, the full model, using equation (13b), is applied. Figure 4 shows the electron distribution in the IB at the open-circuit voltage for a photofilled cell with $\mu_{\mathrm{ib}} = 20\,\mathrm{cm^2V^{-1}s^{-1}}$. This is a rather low mobility compared to what is usually the case in the CB and VB of semiconductors, but if the origin of the intermediate band is a QD-superlattice one might probably expect rather low mobilities since the electrons will have to tunnel through the barriers between the quantum dots. As seen from the figure, the filling depends on the ratio $\sigma_{\mathrm{ci}}/\sigma_{\mathrm{iv}}$ of the absorption cross-sections. It can been shown [12] that in cases where the cell is thick enough to absorb all incoming photons, photon recycling is included and the carrier mobility is set to infinity, the filling of an IB will not depend on the absorption cross-sections. In the present case, however, the cell has a limited thickness so that not all incoming photons are absorbed.

When σ_{ci} is the larger of the two absorption cross sections, electrons will be excited from the IB to the CB more easily than from the VB to the IB. This results in a relatively low n_{ib}. When σ_{iv} is largest, that is $\sigma_{\mathrm{ci}}/\sigma_{\mathrm{iv}} < 1$, electrons are more easily pumped into the IB than removed from it, resulting in a larger n_{ib} than when $\sigma_{\mathrm{ci}}/\sigma_{\mathrm{iv}} > 1$.

In addition to affecting the average filling of the IB, the ratio of the absorption cross-sections also affects the spatial variation of n_{ib}. Looking at the case with $\sigma_{\mathrm{ci}}/\sigma_{\mathrm{iv}} = 0.1$, the solid line in figure 4, one finds that n_{ib} is lower near the front surface than near backside of the cell. The reason for this is that near the front surface, the net generation of electrons over E_{ci}, that is $g_{\mathrm{ci}} - r_{\mathrm{ci}}$, is larger than the net generation of electrons over E_{iv}. Due to the difference in the absorption coefficients, mainly caused by the difference in the absorption cross-sections, ϕ_{ci} will be absorbed more rapidly than ϕ_{iv}. This causes the number of electrons excited from the VB to the IB to increase relative to the number of electrons excited from the IB to the CB, and for increasing x, the net generation over E_{iv} will eventually become larger than the net generation over E_{ci}. n_{ib} is therefore increasing with increasing x.

For $\sigma_{\mathrm{ci}}/\sigma_{\mathrm{iv}} = 1, 2$ or 5, the situation is opposite. For small x, the net generation rate over E_{iv} is larger than the net generation over E_{ci}. For larger values of x, the net generation over E_{ci} is eventually becoming the larger, resulting in n_{ib}-profiles that are decreasing with increasing x.

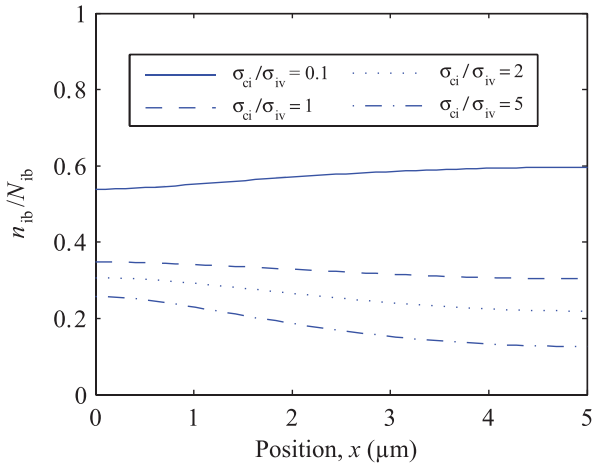

Figure 4: The electron distribution in the IB of a photofilled cell at V_{oc} at 1000 suns plotted for various $\sigma_{\mathrm{ci}}/\sigma_{\mathrm{iv}}$.

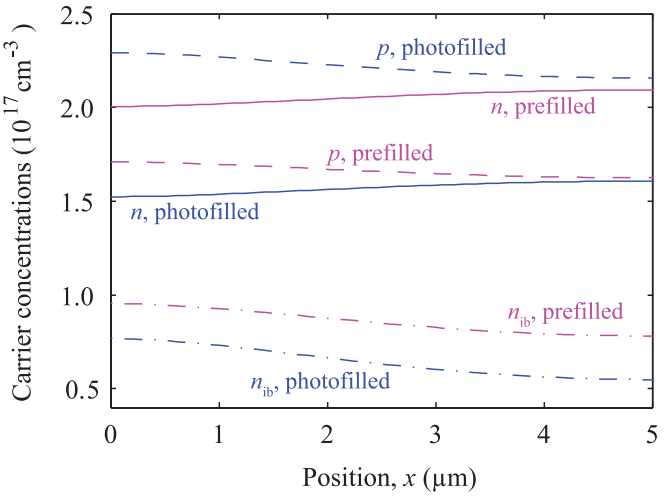

Figure 5: Electrons in the CB (solid lines), electrons in the IB (dash-dot lines) and holes in the VB (dashed lines) at V_{oc} at 1000 suns. The plots are made for a photofilled cell (blue) and for a prefilled cell (magenta) with $N_{\mathrm{d}}/N_{\mathrm{ib}} = 0.5$. $\sigma_{\mathrm{ci}}/\sigma_{\mathrm{iv}} = 2$ for both cells.

To compare the carrier concentrations in all three bands in a photofilled and a prefilled cell, with $N_d/N_{ib} = 0.5$, figure 5 shows calculated carrier distributions at the open circuit voltage at 1000 suns with $\sigma_{ci}/\sigma_{iv} = 2$. From the figure it is seen that the hole concentration is higher in the photofilled cell than in the prefilled one, because in the former, practically all the electrons in the IB have been excited from the VB, leaving behind a large hole population in the VB.

In both cases, the electrons in the CB are shifted towards the rear side of the solar cell while the holes in the VB are shifted towards the front surface of the cell. This is a result of the electrostatic field set up by the distribution of electrons in the IB. As seen from figure 4, the shape of the spatial distribution of n_{ib} reverses if σ_{ci}/σ_{iv} gets sufficiently small, like for the curve calculated for $\sigma_{ci}/\sigma_{iv} = 0.1$. So will the shape of the spatial distribution of n and p. This separation of carriers might have consequences for the device design of IBSCs. Electrons are extracted through the n-emitter, whereas the holes are extracted through the p-emitter. To give these carriers a small push in the right direction, one should decide whether the n-emitter or p-emitter should be placed at the front of the cell based on the spatial variation of n_{ib}. If $\sigma_{ci}/\sigma_{iv} = 1, 2$ or 5, the electrons and holes will be pushed in the correct direction if the n-emitter is on top of the cell. When $\sigma_{ci}/\sigma_{iv} = 0.1$, however, the carriers are pushed in the correct direction if the p-emitter is at the front of the cell.

It should be noted that the filling of the IB probably will be less affected by the light in an IB-material with a finite width of the IB ($\Delta E_{ib}>0$, see figure 2) than in the idealized case treated here. In a wide IB a shift in the quasi-Fermi level will not affect the number of electrons in the IB as much as in a narrow IB.

How the electron distribution in the IB will be affected by non-radiative recombination is another important issue that is not taken into account in this model.

3.2 Cell Performance

The results in this and the following sections are obtained by assuming a very high electron mobility in the IB, which allow us to treat the IB-region as quasi-neutral (that is, neglecting the electrostatic field). Equation (13b) is therefore replaced with equation (19).

Figure 6 shows the IV curves of a prefilled (with $N_d/N_{ib} = 0.5$) and photofilled IBSC for various light concentrations when $\sigma_{ci}/\sigma_{iv} = 1$. Performance data are also listed in table 1. The short-circuit

current divided by the concentration factor, J_{sc}/X, increases significantly with increasing light intensity in the photofilled case. For low light intensities, the photogenerated population of IB-electrons does not provide an α_{ci} that is sufficiently large to sustain an efficient step-wise generation process from the VB to the CB. For the prefilled cell, J_{sc}/X increases slightly with light concentration. This increase occurs because concentrated light causes a shift in n_{ib} to values that provide a better utilization of the sub-band gap photons. At 10 suns, n_{ib}/N_{ib} is still 0.50 at V_m, which means that the filling is not significantly affected by the illumination. At 1000 suns the prefilled cell has $n_{ib}/N_{ib} = 0.57$ at V_m, which is closer to the optimal filling that will be shown below to be n_{ib}/N_{ib} around 0.65.

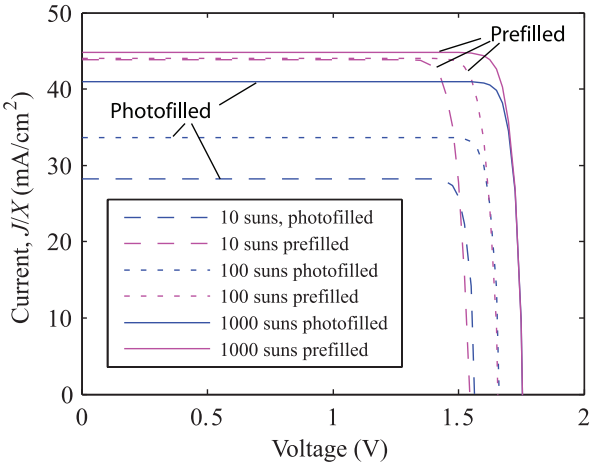

Figure 6: IV curves of a prefilled and a photofilled IBSC at 10, 100 and 1000 suns illumination. The current is divided by the concentration factor X. $\sigma_{ci}/\sigma_{iv} = 1$.

It is also apparent from figure 6 and table 1 that for 10 suns, the open-circuit voltage is slightly higher for the photofilled cell. The reason for this is that the low number of IB-electrons acts as a bottleneck for recombination via the IB. With only a few electrons in the IB, the recombination of electrons from the IB to the VB becomes small, as seen from eq. 10b, and recombination via the IB becomes a less effective process.

As seen from the table, a photofilled cell is capable of reaching high efficiencies for concentrated light, but the efficiency is lower than for the prefilled cell for all the three light concentrations in table

Table 1: Results for a prefilled cell with $N_{\rm d}/N_{\rm ib} = 0.5$ and a photofilled cell at various light concentrations. Both cells have $\sigma_{\rm ci}/\sigma_{\rm iv} = 1$.

	$J_{\rm sc}/X$ (mA/cm^2)	$V_{\rm oc}$ (V)	$n_{\rm ib}/N_{\rm ib}$ at $V_{\rm m}$	Efficiency (%)
Photofilled				
10 suns	28.2	1.57	0.05	25.4
100 suns	33.7	1.66	0.14	32.4
1000 suns	41.0	1.75	0.34	41.4
Prefilled				
10 suns	43.9	1.54	0.50	37.9
100 suns	44.0	1.66	0.51	41.2
1000 suns	44.8	1.75	0.57	44.8

1 and figure 6. If the value of σ_{ci} is increased relative to σ_{iv}, however, the picture is changing. This is shown in figure 7 where calculated efficiencies for a prefilled and a photofilled cell are plotted as a function of $\sigma_{\mathrm{ci}}/\sigma_{\mathrm{iv}}$, for $X = 100$ and $X = 1000$. With increasing $\sigma_{\mathrm{ci}}/\sigma_{\mathrm{iv}}$, a smaller population of IB-electrons is more favourable since that will give more equal absorption coefficients for transitions over the two sub-band gaps. For 1000 suns, the photofilled and prefilled cells have equal efficiencies for $\sigma_{\mathrm{ci}}/\sigma_{\mathrm{iv}} = 3.3$. The photofilled cell has a peak efficiency of 44.7 % for $\sigma_{\mathrm{ci}}/\sigma_{\mathrm{iv}} \approx 5$. The peak efficiency for the prefilled cell is 45.3 % when $\sigma_{\mathrm{ci}}/\sigma_{\mathrm{iv}} \approx 2$.

Qualitatively, the same observations can be made for 100 suns illumination, illustrated by the dashed lines in figure 7. The number of photogenerated electrons in the IB of the photofilled cell is now lower than for 1000 suns illumination. The highest efficiency for the photofilled cell is therefore found at a higher value of $\sigma_{\mathrm{ci}}/\sigma_{\mathrm{iv}}$, which, for this particular example, is slightly above 10.

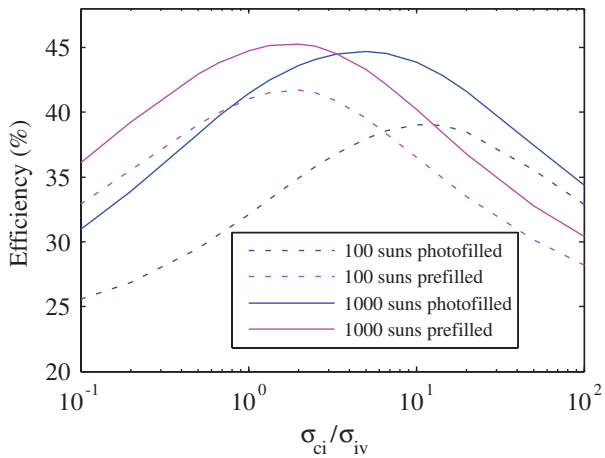

Figure 7: The efficiencies of a prefilled and a photofilled cell as a function of the ratio of the absorption cross sections.

In figure 8 the generation and recombination rates involving the IB, integrated over the cell thickness, are plotted as a function of $\sigma_{\mathrm{ci}}/\sigma_{\mathrm{iv}}$. The integrated rates are denoted with capital letters, G_{ci}, G_{iv}, R_{ci} and R_{iv}, and are calculated for a prefilled cell, with $N_{\mathrm{d}}/N_{\mathrm{ib}} = 0.5$ with the cell voltage set to V_{m}. The number of photons in ϕ_{ci} is smaller than the number of photons in ϕ_{vi} for the band gaps and the light

spectrum that are used. The size of ϕ_{ci} is therefore a limiting factor regarding the number of electrons that can be excited from the VB to the CB in a stepwise process via the IB. To harvest as many photons from ϕ_{ci} as possible, α_{ci} should be higher than α_{iv}. The optimal value of $\sigma_{\mathrm{ci}}/\sigma_{\mathrm{iv}}$ is therefore above 1. If this ratio gets too high, however, more electrons are eventually excited over E_{ci} than over E_{iv} and the number of electrons excited over E_{iv} becomes the limiting factor for the stepwise generation process.

To find the optimium ratio with respect to cell efficiency, requires an optimization of the net generation rate via the IB. In steady state, the net generation rates over each of the sub-band gaps equal each other (equation (19)), and will also equal the total net generation rate via the IB. We thus have for the net generation via the IB

$$G_{\mathrm{net}} = G_{\mathrm{iv}} - R_{\mathrm{iv}} = G_{\mathrm{ci}} - R_{\mathrm{ci}} = \int_0^W \left(g_{\mathrm{ci}} - r_{\mathrm{ci}}\right) \mathrm{d}x.$$

The integrated rates are plotted in figure 8. For the chosen case, the maximum net generation G_{net} is obtained for $\sigma_{\mathrm{ci}}/\sigma_{\mathrm{iv}} = 1.9$. For this ratio both the generation and the recombination over E_{iv} is larger than the generation and recombination over E_{ci}.

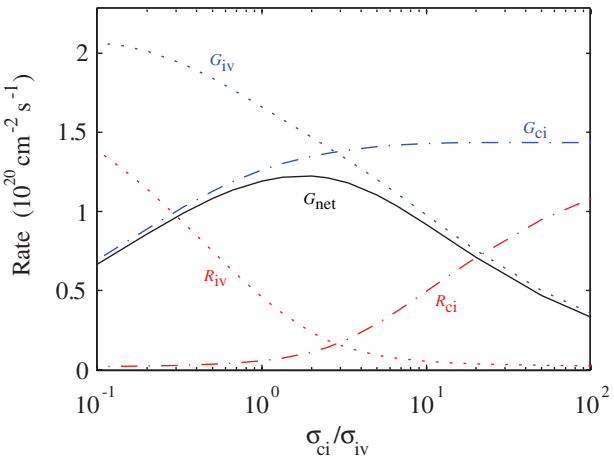

Figure 8: Generation and recombination rates integrated over the cell width at V_{m} for $X = 1000$. The sum of the generation rates subtracted the sum of the recombination rates peaks at the $\sigma_{\mathrm{ci}}/\sigma_{\mathrm{iv}}$-ratio yielding the highest cell efficiency.

3.3 Optimal filling of the IB

For real IB solar cells made of particular materials, the ratio of the absorption cross sections will appear as a material constant and is not a parameter to be determined by choice. We have seen that for a particular prefilling of the IB, i.e. half-filling, there exists an optimal value of $\sigma_{\mathrm{ci}}/\sigma_{\mathrm{iv}}$ yielding the highest efficiency. It will now be shown that for a particular $\sigma_{\mathrm{ci}}/\sigma_{\mathrm{iv}}$-ratio, there also exist an optimal prefilling of the IB, i.e. the filling that is giving the best combination of generation and recombination via the IB. The doping of the IB-region should be tuned to this optimal filling to achieve the highest possible cell efficiency.

A plot of the cell efficiency versus the degree of prefilling, that is the factor $N_{\mathrm{d}}/N_{\mathrm{ib}}$, for $\sigma_{\mathrm{ci}}/\sigma_{\mathrm{iv}} = 1$, is shown in figure 9 for $X = 100$ and $X = 1000$. From the figure it is seen that the optimal prefilling of the IB for the cell in consideration is $N_{\mathrm{d}}/N_{\mathrm{ib}} = 0.60$ at 10 suns and $N_{\mathrm{d}}/N_{\mathrm{ib}} = 0.65$ at 1000 suns. The reason why the optimal prefilling deviates from half-filling follows the same type of argument as used above when discussing the optimal value of $\sigma_{\mathrm{ci}}/\sigma_{\mathrm{iv}}$. Since ϕ_{ci} is smaller than ϕ_{iv}, it is important to utilize as many of these photons as possible to optimize the two-step generation process. A filling of over 50 % gives $\alpha_{\mathrm{ci}} > \alpha_{\mathrm{iv}}$ which ensures that a larger share of ϕ_{ci}, than of ϕ_{iv}, is absorbed. But again, if α_{iv} gets to low, it will eventually cause the generation rate over E_{iv} to be too small, and the cell efficiency will decrease.

The optimal filling depends on the $\sigma_{\mathrm{ci}}/\sigma_{\mathrm{iv}}$-ratio. With a larger value of this ratio, the photons in ϕ_{ci} are absorbed more easily and the optimal filling is reduced. And vice versa, a low ratio leads to a higher optimal filling.

Deviations from the optimal filling gives a larger drop in the cell efficiency for low light intensities than for high light intensities. High light concentration will more easily shift the filling of the IB from possibly unfavourable levels at thermal equilibrium, to more efficient levels under illumination. A more general discussion on how the filling is affected by the light intensity is given in ref. [12] where it is found that with no restrictions on the cell thickness, and full photon recycling, all prefillings will lead to the same limiting efficiency.

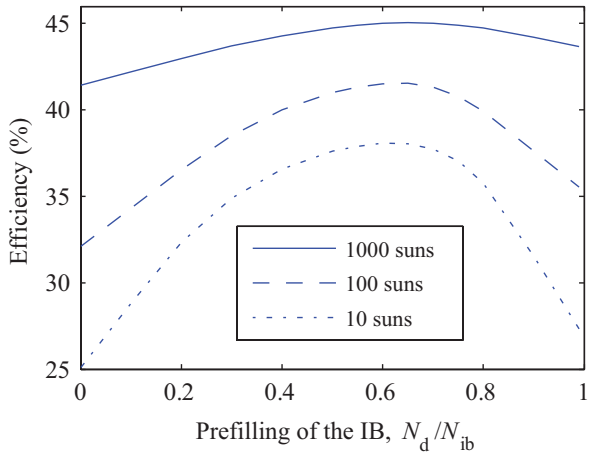

Figure 9: The cell efficiency plotted as a function of the degree of prefilling of the IB. The calculations are done with $\sigma_{ci}/\sigma_{iv} = 1$.

3.4 Sub-junction voltages and the thickness of the field-damping layers

As mentioned in section 2 and illustrated in figure 3, there is a possible decoupling between the quasi-Fermi level splits, divided by the elementary charge, V'_n and V'_p, and the voltages over the two sub-junctions, V_n and V_p. In figure 10, these quantities are plotted at V_m as a function of the prefilling factor N_d/N_{ib} for $X = 1000$ and $\sigma_{ci}/\sigma_{iv} = 1$.

It is seen from figure 10 that the curves for V_n and V_p crosses the curves for V'_n and V'_p, respectively, for $N_d^+/N_{ib} = 0.65$. The crossing points occurs at the degree of prefilling that the cell should have in order to keep the quasi-Fermi level of the IB at its equilibrium position at V_m. This occurs when the generation and recombination rates via the IB are well balanced, i.e. when (19) is fulfilled, at the equilibrium filling. With this prefilling, any electron excited from the valence band to the intermediate band will be passed on to the conduction band by a second photon. With higher degrees of prefilling, more electrons will be excited to the CB, but not all of these will be accompanied by electrons being excited to the IB. Instead they will contribute to a reduction of the filling, and thereby an increased quasi Fermi level split and recombination rate over E_{ci}. The situation is similar when the filling is

lower than the optimal filling, but now there is an excess number of photons excited over E_{iv}. The highest rate for the total stepwise generation process, i.e. the rate of electrons being excited all the way from the VB to the CB via the IB, is found when the net generation rates over the sub junctions are balanced at $n_{\mathrm{ib}} = N_{\mathrm{d}}$. In such cases no photons are used to support an excess population of carriers in the IB. The crossing points of the curves in figure 10 are therefore found at the degree of prefilling that yields the highest efficiency.

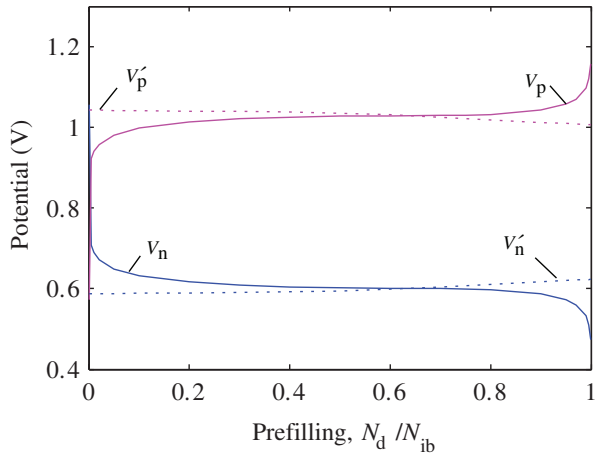

Figure 10: The voltages V_{n} and V_{p} over the two junctions plotted as a function of the degree of prefilling of the IB. The quasi-Fermi level splits divided by the elementary charge, V_{n}' at $x = 0$ and V_{p}' at $x = W$, are plotted as dotted lines. $\sigma_{\mathrm{ci}}/\sigma_{\mathrm{iv}} = 1$, $X = 1000$ and $V = V_{\mathrm{n}} + V_{\mathrm{p}} = V_{\mathrm{m}}$.

When $N_{\mathrm{d}}/N_{\mathrm{ib}}$ goes below 0.2 or above 0.8 the curves for the sub-junction voltages bends more and more. This is due to the fact that an increasing fraction of the electrons in the IB, when going below 0.2, or the holes in the IB, when going above 0.8, has been excited from the valence or conduction band, respectively. When the filling of the IB is shifted by the illumination, the carrier concentrations in the CB and VB, and thus V_{p} and V_{n}, are changed to preserve charge neutrality in the IB-region. In addition, the Fermi level, and thus n_0 and p_0, is dependent on the degree of prefilling, which is also affecting the values of the sub-junction voltages, as seen from (14) and (15).

When designing an IBSC one should optimize the thickness of the field damping layers. For a highly

doped p-emitter, the thickness of the field-damping layer of n-type is given by [14]

$$W_{\mathrm{n}} = \left[\frac{2\epsilon(V_{\mathrm{bi,p}} - V_{\mathrm{p}})}{qN_{\mathrm{n}}}\right]^{1/2}, \tag{20}$$

where N_{n} is the doping concentration in the field-damping layer. A highly doped p-emitter also implies that $V_{\mathrm{bi,p}}$ equals the difference between the equilibrium Fermi level and the valence band edge in the IB-region. For a cell with $N_{\mathrm{n}} = 1 \times 10^{16}\,\mathrm{cm}^{-3}$, the optimal thickness of the field-damping layer of n-type at $V = V_{\mathrm{m}}$ is plotted in figure 11 as a function of the degree of prefilling. The optimal thickness of the field-damping layer of a photofilled cell is found to be $0.14\,\mu$m, which is 10 % thinner than for a prefilled cell with $N_{\mathrm{d}}/N_{\mathrm{ib}} = 0.5$.

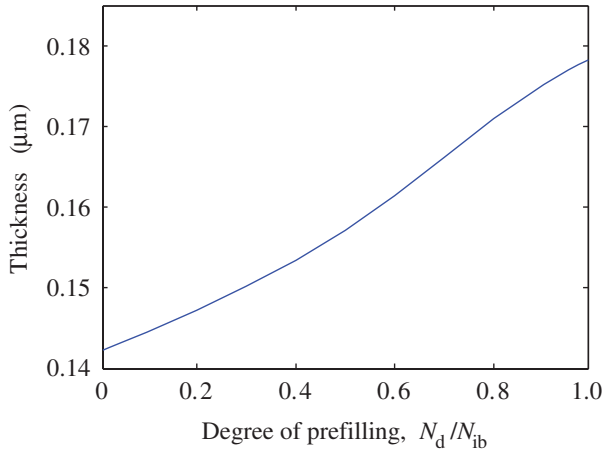

Figure 11: The optimal thickness of the field-damping layer depends on the degree of prefilling. The plot is done for the field-damping layer of n-type in a cell with $\sigma_{\mathrm{ci}}/\sigma_{\mathrm{iv}} = 1$ at 1000 suns.

4 Conclusions

A model has been developed that give new insight into the device modelling of intermediate band solar cells. The model includes photofilling effects and can be used to calculate the carrier concentrations in all three bands in an intermediate band material as well as the performance of solar cells based on such materials.

A photofilled cell is able to achieve high efficiencies. In fact, for some cases, a photofilled cell can perform better than a prefilled cell where the equilibrium filling equals half filling. Whether an initially half-filled or a photofilled cell gives the highest efficiency depends on the ratio of the absorption cross sections and on the light intensity.

Low electron mobility in the IB can lead to a light induced, spatial variation of the electron distribution in the IB. This will give rise to an electrostatic field that will drive electrons in the CB and holes in the VB in different directions. The shape of the electron distribution in the IB, and thus the direction of the electrostatic field and what directions the carriers will move, will determine whether the p or n-emitter should be placed at the front surface of the IBSC.

The optimal filling of the IB is calculated for a particular example. Illumination can drive the filling towards the optimal filling - an effect that becomes more important with increasing light intensity. The importance of optimized prefilling is therefore less important when the cell is exposed to highly concentrated light. The optimal prefilling is shown to equal the prefilling where the generation rates over the sub-band gaps are equally large. With such a prefilling, no photons are used to sustain a population of excess carriers in the IB.

When illumination is shifting the IB-filling from its equilibrium value, there will be a split between the voltages over the sub-junctions and the voltages over the diodes which in an equivalent circuit represents transitions via the IB.

Acknowledgements

The authors would like to thank the Research Council of Norway for financial support through project no. 172905/S30. We would also like to thank the anonymous reviewer who generously shared the derivation in appendix A with us.

A Derivation of the diffusion term in equation (13b)

The derivation made here has been done by one of the anonymous reviewers of this paper and has been slightly rephrased and adapted to the paper by the authors.

From equation (7) we have

$$\frac{E_{\mathrm{ib}} - E_{\mathrm{F,ib}}}{kT} = \ln(N_{\mathrm{ib}} - n_{\mathrm{ib}}) - \ln(n_{\mathrm{ib}}), \tag{21}$$

which gives

$$\frac{\mathrm{d}E_{\mathrm{ib}}}{\mathrm{d}x} - \frac{\mathrm{d}E_{\mathrm{F,ib}}}{\mathrm{d}x} = -\frac{kTN_{\mathrm{ib}}}{n_{\mathrm{ib}}(N_{\mathrm{ib}} - n_{\mathrm{ib}})}\frac{\mathrm{dn_{ib}}}{\mathrm{d}x}. \tag{22}$$

The electron current density in the IB is given by the gradient of the electrochemical potential of the electrons in this band, that is

$$J_{\mathrm{e,ib}} = \mu_{\mathrm{ib}} n_{\mathrm{ib}} \frac{\mathrm{d}E_{\mathrm{F,ib}}}{\mathrm{d}x} = \mu_{\mathrm{ib}} n_{\mathrm{ib}} \frac{\mathrm{d}E_{\mathrm{ib}}}{\mathrm{d}x} + kT\mu_{\mathrm{ib}} \frac{N_{\mathrm{ib}}}{N_{\mathrm{ib}} - n_{\mathrm{ib}}} \frac{\mathrm{dn_{ib}}}{\mathrm{d}x}, \tag{23}$$

where equation (22) has been used. With the current density given by equation (23), the continuity equation for the IB becomes

$$\frac{kT\mu_{\mathrm{ib}}}{q}\frac{\mathrm{d}}{\mathrm{dx}}\left(\frac{N_{\mathrm{ib}}}{N_{\mathrm{ib}} - n_{\mathrm{ib}}}\frac{\mathrm{d}n_{\mathrm{ib}}}{\mathrm{dx}}\right) + \mu_{\mathrm{ib}}\frac{\mathrm{d}(n_{\mathrm{ib}}F)}{\mathrm{d}x} + g_{\mathrm{iv}} - g_{\mathrm{ci}} + r_{\mathrm{ci}} - r_{\mathrm{iv}} = 0. \tag{24}$$

The Einstein relation $D_{\mathrm{ib}} = kT\mu_{\mathrm{ib}}/q$ will thus only be valid if $N_{\mathrm{ib}} >> n_{\mathrm{ib}}$. If so, equation (13b) will be similar to equations (13a) and (13c).

References

[1] Luque A, Martí A *Physical Review Letters* 1997; **78**: 5014-5017, DOI: 10.1103/PhysRevLett.78.5014.

[2] Brown AS, Green MA *Journal of Applied Physics* 2003; **94**: 6150-6158, DOI: 10.1063/1.1610774.

[3] Bremner SP, Levy MY, Honsberg CB *Applied Physics Letters* 2008; **92**: 171110, DOI:10.1063/1.2907493.

[4] Wolf M *Proceedings of the Institute of Radio Engineers* 1960; **48**: 1246-1263.

[5] Martí A, Cuadra L, Luque A *IEEE Transactions on Electron Devices* 2001; **48**: 2394-2399, DOI: 10.1109/16.954482.

[6] Martí A, Cuadra L, Luque A *IEEE Transactions on Electron Devices* 2002; **49**: 1632-1639, DOI: 10.1109/TED.2002.802642.

[7] Luque A, Martí A *Progress in Photovoltaics: Research and Applications* 2001; **9**: 73-86, DOI: 10.1002/pip.354.

[8] Martí A, Cuadra L, Luque A *Physica E* 2002; **14**: 150-157, DOI: 10.1016/S1386-9477(02)00368-5.

[9] Levy MY, Honsberg C *Journal of Applied Physics* 2009; **106**: 073103, DOI: 10.1063/1.3213337.

[10] L. Cuadra, A. Martí, A. Luque, Physica E **14**, 162-165 (2002).

[11] Luque A, Martí A, López N, Antolín E, Cánovas E, Stanley C, Farmer C, Díaz P *Journal of Applied Physics* 2006; **99**: 094503, DOI: 10.1063/1.2193063.

[12] Strandberg R, Worren Reenaas T *Journal of Applied Physics* 2009; **105**: 124512, DOI: 10.1063/1.3153141.

[13] Lin AS, Wang W, Phillips JD *Journal of Applied Physics* 2009; **105**: 064512, DOI: 10.1063/1.3093962.

[14] Martí A, Antolín E, Cánovas E, López N, Linares PG, Luque A, Stanley CR, Farmer CD *Thin Solid Films* 2008; **516**: 6716-6722, DOI: 10.1016/j.tsf.2007.12.064.

[15] Tomic S, Jones TS, Harrison NM *Applied Physics Letters* 2008; **93**: 263105, DOI: 10.1063/1.3058716.

[16] Keevers MJ, Green MA *Journal of Applied Physics* 1994; **75**: 4022, DOI: 10.1063/1.356025.

[17] Aroutiounian V, Petrosyan S, Khachatryan S *Solar Energy and Materials* 2005; **89**: 165-173, DOI: 10.1016/j.solmat.2005.02.011.

[18] Cuadra L, Martí A, Luque A *IEEE Transactions on Electron Devices* 2004; **51**: 1002-1007, DOI: 10.1109/TED.2004.828161.

[19] Navruz TS, Saritas M *Solar Energy Materials & Solar Cells* 2008; **92**: 273-282, DOI: 10.1016/j.solmat.2007.08.012.

[20] Ruppel W, Würfel P *IEEE Transactions on Electron Devices* 1980; vol. ED-27, no. 4: 877-882.

[21] van Roosbroeck W, Shockley W, *Physical Review* 1954; **94**: 1558-1560

[22] Luque A, Marti A, Stanley C, López N, Cuadra L, Zhou D, Pearson JL, McKee A *Journal of Applied Physics* 2004; **96**: 903-909, DOI: 10.1063/1.1760836.

Paper IV

Initial theoretical study of solar cells with an intermediate band of non-zero width and a thermalized electron population

To be submitted.

Is not included due to copyright

Paper V

Optimal filling of Intermediate Bands in Intermediate Band Solar Cells

To be submitted.

Optimal filling of the intermediate band in idealized intermediate band solar cells

Rune Strandberg*, Turid Worren Reenaas

Norwegian University of Science and Technology, Department of Physics, N-7491 Trondheim, Norway

Abstract

The optimal filling of the intermediate band of an intermediate band solar cell is investigated. Using models based on detailed balance principles, it is shown that the optimal filling varies with the size of the sub-band gaps, the absorptivity of the cell, the degree of overlap between the absorption coefficients as well as the mutual sizes of the absorption cross sections for transitions over the sub-band gaps. The results of calculations that show how a non-optimal filling affects the cell efficiency are also presented. In several cases, a deviation from the optimal filling will only result in small changes in the efficiency. However, cases where the efficiency is dramatically reduced due to a non-optimal filling are also identified. For some cases the negative impact of a non-optimal filling can be reduced by increasing the absorptivity of the cell, or, the effect of photofilling is significant, increasing the light concentration.

Keywords: intermediate band solar cell, IBSC, optimal filling, IB-filling, detailed balance
PACS:

1. Introduction

In the intermediate band solar cell (IBSC), electrons can be excited from the valence band (VB) to the conduction band(CB) in a two-step process via an intermediate band (IB) as sketched in figure 1. This allows this type of solar cells to utilize more of the solar spectrum, resulting in a theoretical

*Corresponding author. E-mail: strandbe@ntnu.no

efficiency limit of 63.2 % [1] - significantly higher than the 40.7 % limit of conventional single band gap photovoltaic cells [2].

For an intermediate band solar cell to work properly, the intermediate band has to be partially filled with electrons [3, 4, 5]. While some proposals for promising photovoltaic IB-materials results in a partially filled IB without the need for any manipulations of the material [6, 7, 8, 9, 10, 11, 12], other materials, e.g. quantum dot superlattices, have to be partially filled by means of doping [13]. If the density of electron states in the IB is not too high, the intermediate band can also be photofilled, i.e. the IB can be sufficiently filled by electrons that have been photoexcited from the valence band [14].

The optimal filling has recently been calculated for a couple of IBSC-devices [15], [16]. To our knowledge, no general examination of the optimal filling has been made so far. In the present work it is investigated how the optimal filling of the intermediate band in an idealized IBSC varies with band gaps, the degree of photofilling, absorption cross sections and overlapping absorption coefficients. What is meant by overlapping absorption coefficients is shown in figure 1.

The existence of an optimal filling adds another factor to be optimized when designing IBSCs. This is particularly interesting for materials in which the filling can be adjusted by doping or other types of manipulation. The results to be presented are based on models that are idealized with respect to the energy dependence of the absorption coefficients, the width of the IB as well as the assumption that the recombination is purely radiative. The work is therefore to be regarded as an initial study to identify how some basic parameters affects the optimal filling. More advanced models allowing a more detailed incorporation of material parameters like the absorption coefficients will have to be developed in order to determine the optimal filling of real IBSCs.

It can be argued that when the thickness of an IBSC is unrestricted, it is not important to optimize the filling of the IB [14]. No matter how small any non-zero absorption coefficient is, the absorptivity of the cell can always be made arbitrarily close to 1 by making the cell thicker. When the absorption coefficients are overlapping or when non-radiative recombination is present, the optimal absorptivity, and thus the optimal thickness of the cell, is restricted [17]. The amount of photons absorbed over each of the sub-bandgaps will then depend on the filling of the IB, which should be optimized.

The modeling in this paper is divided into three cases: i) non-overlapping

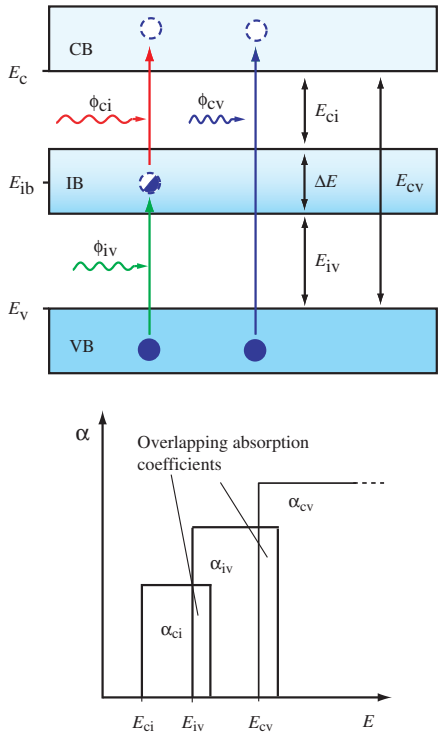

Figure 1: In intermediate band solar cells, electrons can be excited from the VB to the CB in two steps via an intermediate band. The absorption coefficients are assumed to have the energy dependence indicated in the lower part of the figure.

absorption coefficients without photofilling, ii) non-overlapping absorption coefficients with photofilling, and iii) overlapping absorption coefficients. The assumptions made in each case are described in detail in the following section.

In this work, we use the word photofilling to describe the effect when illumination causes a non-negligible shift in the in the filling of the IB as compared to in thermal equilibrium. By this definition photofilling can mean both an increase and a reduction of the filling. This implies a modification of the use of the word compared to how it has been used in previous work, where it has denoted the effect where an IB which is practically empty in thermal equilibrium gets partially filled by photoexcited electrons under operation of the cell [14, 16]. In cases where photofilling is an issue, it is necessary to distinguish between the equilibrium filling, which we will denote the *prefilling*, and the filling under optimal operation conditions, which is simply denoted the *filling*. In cases i) and iii), the filling of the IB is assumed to be clamped to its value in thermal equilibrium during operation of the cell. This will be a valid assumption provided that the IB has a high number of states [14, 18]. In these cases the denotation *filling* is solely used since there is no difference between the prefilling and the filling.

2. Mathematical models

The mathematical models used in this work are combinations of approaches to the IBSC theory that have been published previously. These models include the model used to investigate photofilling of intermediate bands [14], and the model used to investigate the effect of overlapping absorption coefficients [17]. The base for these models is the theory of detailed balance [2, 19]. Certain modifications are done to adapt the models to this study of the optimal filling.

The first modification is that the relationships between the filling and the absorption coefficients for transitions *from* the IB, α_{ci}, and transitions *to* the IB, α_{iv}, have been incorporated by

$$\alpha_{\mathrm{ci}} = \alpha_{\mathrm{ci},0} f \tag{1}$$

and

$$\alpha_{\mathrm{iv}} = \alpha_{\mathrm{iv},0}(1 - f), \tag{2}$$

in all three cases i)-iii). f, the occupation factor, has a value between 0 (totally empty) and 1 (completely full) and describes the degree of IB-filling. $\alpha_{\mathrm{ci},0}$ and $\alpha_{\mathrm{iv},0}$ are the values that the absorption coefficients will have when $f = 1$ or $f = 0$, respectively. In either case, the absorption coefficients have a constant value in the energy range where they are non-zero. That is, the energy range from the respective band gap edge to the next band gap edge plus the possible overlap (see fig. 1).

In case ii), where photofilling is incorporated, the parameters $\alpha_{\mathrm{ci},0}$ and $\alpha_{\mathrm{iv},0}$ are assumed to be proportional to the respective absorption cross-sections and the density of electron states in the IB, as is done in ref. [14]. That is $\alpha_{\mathrm{ci},0} = \sigma_{\mathrm{ci}} N_{\mathrm{ib}}$ and $\alpha_{\mathrm{iv},0} = \sigma_{\mathrm{iv}} N_{\mathrm{ib}}$.

As argued in the introduction, an optimal filling will only exist when the thickness of the cell is limited. Instead of introducing the cell thickness as a parameter, the thickness is limited indirectly through a limitation of the absorbance of the cell. Being proportional to the absorption coefficients, the absorbance will have the same dependence on the filling of the IB as the absorption coefficients. The value of the absorbance related to transitions between the IB and the CB when $\alpha_{\mathrm{ci}} = 1/2\,\alpha_{\mathrm{ci},0}$, that is when the IB is half-filled, has been set to 3 unless other is mentioned. This corresponds to absorption of 95 % of the incoming photons. The absorbance related to transitions from the VB to the IB has also been set to 3 with a half-filled IB. The sub-band gap absorbances with a half-filled IB are denoted the *main absorbances* in the following. Unless other is mentioned, $\alpha_{\mathrm{ci},0} = \alpha_{\mathrm{iv},0}$. The absorbance for transitions directly from the valence band to the conduction band is set to 10 times the main absorbance for transitions over E_{iv}.

In case iii), the model for overlapping absorption coefficients derived by Cuadra et al. [17] has been implemented with the absorption coefficients being on the form presented above. The absorbance of the cell is assumed to be independent on the angle of incidence of the incoming light. This simplifies the modeling of a system with overlapping absorption coefficients considerably by allowing the use of analytical expressions. This assumption is also made in case i) and ii).

As in all detailed balance models for the IBSC, the models used here basically implies finding expressions for the net generation rates to the CB and VB, equaling these rates and solve the resulting equation together with $\Delta\mu_{\mathrm{cv}} = \Delta\mu_{\mathrm{ci}} + \Delta\mu_{\mathrm{iv}}$. The latter equation states that the sum of the quasi-Fermi level splittings over the sub-band gaps, has to equal the quasi-Fermi level splitting over the main band gap, which is related to the cell voltage

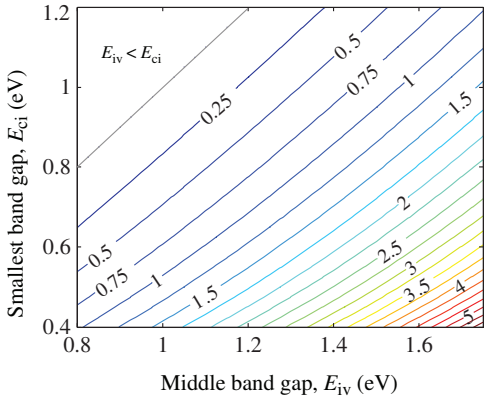

Figure 2: A plot of $\Phi = \phi_{ci}/\phi_{iv}$ for the 6000 K black body spectrum as a function of the sub-band gaps.

V through $\Delta\mu_{cv} = V/q$, where q is the elementary charge. We refer to the original papers, refs. [14] and [17], for the details involved.

3. Results and discussion

Calculations of the optimal filling have been performed using the 6000 K black-body spectrum with, unless other is clearly stated, a concentration factor of 1000. The temperature of the cell is assumed to be 300 K. When photofilling is included, N_{ib} is set to $1 \cdot 10^{18}\,\mathrm{cm}^3$. The index of refraction, which is a parameter in the modeling of a cell with overlapping absorption coefficients as in case iii), is set to 3.5.

i) Non-overlapping absorption coefficients without photofilling

The first case to be investigated is IBSCs with the quasi-Fermi level of the IB clamped to its equilibrium position and non-overlapping absorption coefficients.

The net generation via the IB is limited by the smallest of the two photon fluxes allowed to excite electrons over the sub-band gaps. It is therefore of importance to absorb as many photons from the smallest flux as possible. Any excess photons absorbed from the larger flux will not increase the net

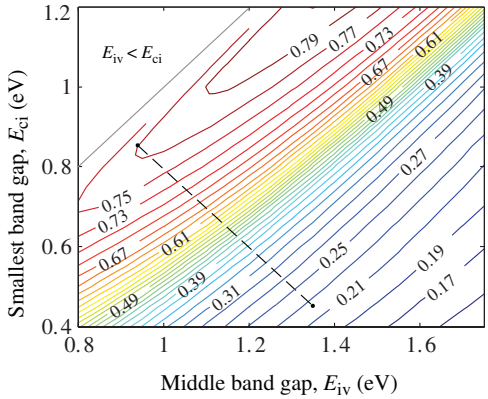

Figure 3: The optimal filling for cells with non-overlapping absorption coefficients. The plot in figure 5 is along the dashed line indicated in this figure.

generation via the IB. Figure 2 shows a plot of the ratio $\Phi = \phi_{ci}/\phi_{iv}$ for various band gaps. ϕ_{ci} is the flux of photons allowed to excite electrons over E_{ci}, and ϕ_{iv} is the flux of photons allowed to excite electrons over E_{iv}. The corresponding optimal filling for a cell with non-overlapping absorption coefficients is shown in figure 3. It becomes clear that the optimal filling is closely related to the ratio between the fluxes. With a large Φ it is important to absorb as many photons from ϕ_{vi} as possible, leading to a low optimal filling to maximize the absorption over E_{vi}. With a small Φ, it becomes more important to absorb as many photons as possible from ϕ_{ci}, which results in a higher optimal filling to get a large α_{ci} and a good absorption of photons over E_{ci}.

The efficiencies as a function of the sub-band gaps are plotted in figure 4. The highest efficiencies are found for combinations of band gaps where Φ is close to one. When Φ is close to one, a balanced net generation is achieved around half-filling. If $\alpha_{ci,0} \neq \alpha_{iv,0}$, the optimal filling will be shifted: $\alpha_{ci,0} < \alpha_{iv,0}$ results in a higher optimal filling, and $\alpha_{ci,0} > \alpha_{iv,0}$ results in a lower optimal filling, due to the same argument as above: the net generation rate via the IB should be maximized.

Variations in the optimal filling are also found when the light concentration is varied. A change in the illumination will maintain the ratio between

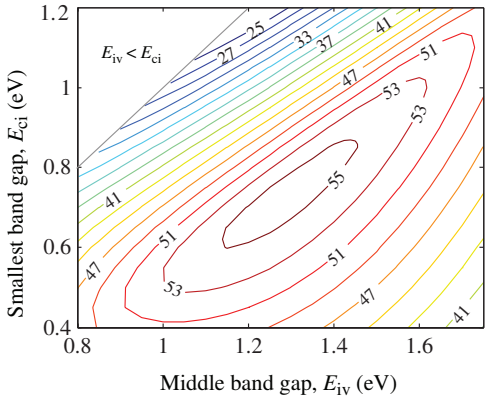

Figure 4: Cell efficiencies with optimal filling of the IB for cells in case i).

the photon fluxes. But increasing the light intensity also means that the optimal cell voltage increases. The dependence of the recombination rates on the respective quasi-Fermi level splittings will disturb the balance between generation rates and recombination rates when the light concentration is varied. Depending on how the ratio between the recombination rates changes with a variation in the voltage, the optimal filling can both increase and decrease with a change in the light concentration. If $\frac{\partial}{\partial V}(G_{ci} - R_{ci} - G_{iv} + R_{iv}) < 0$, where G_{ci} and G_{iv} are the generation rates and R_{ci} and R_{iv} are the recombination rates over the sub-band gaps, the optimal filling will increase with the light concentration. If this quantity is positive, the optimal filling will decrease with the light concentration.

ii) Non-overlapping absorption coefficients and photofilling

If the density of states in the IB is not too high, the illumination can increase or decrease the filling [14, 18]. To repeat a couple of important points, in this work the optimal filling in thermal equilibrium will be denoted the optimal *pre*filling, to distinguish it from the optimal filling which we reserve for the filling that gives the highest efficiency when the solar cell is operated at the maximum power point. Depending on the conditions, the filling of the IB can both increase or decrease due to the illumination. The term photofilling is used to describe the deviation between the filling in

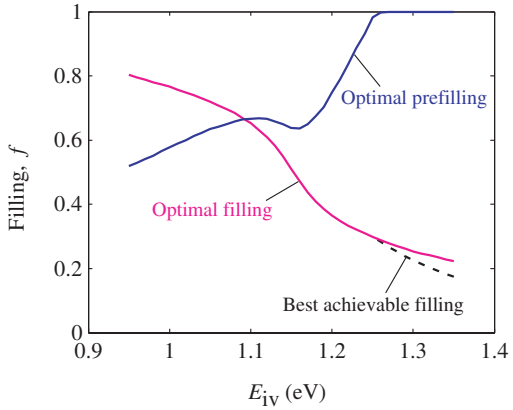

Figure 5: The optimal filling and the optimal prefilling of cells with a main band gap of 1.8 eV and varying position of the IB, corresponding to a plot along the dashed line in figure 3. When the optimal prefilling goes to one for the cell with photofiling, the optimal filling can not be obtained. The best achievable filling is shown by the dashed line.

thermal equilibrium and the filling under illumination. There can thus be both negative and positive photofilling. In the discussion in this subsection the cells are supposed to be operated at the maximum power point.

Figure 5 shows the optimal prefilling and the optimal filling for a cell with $N_{\mathrm{ib}} = 1 \cdot 10^{18}\mathrm{cm}^{-3}$ and effective densities of states in the CB and VB $N_{\mathrm{c}} = N_{\mathrm{v}} = 2 \cdot 10^{19}\mathrm{cm}^{-3}$. The total band gap, E_{cv} is kept constant at 1.8 eV, which means that the plot is done along the dashed line indicated in figure 3.

The curves for the optimal prefilling and the optimal filling have a crossing point where there is a perfect match between the number of electrons entering and leaving the cell at the optimal prefilling. To the left of this point, an excess number of electrons will enter the IB if the prefilling matches the optimal filling, resulting in an optimal prefilling that is lower than the optimal filling. To the right of the crossing point, there is an excess number of electrons leaving the IB, if the prefilling matches the optimal filling, resulting in an optimal prefilling that is higher than the optimal filling.

To the right of the crossing point, the curve for the optimal prefilling has a striking shape. Starting at the crossing point, the curve first reaches a

local maximum, then a local minimum before it rises steeply and eventually goes to 1. Between the crossing point and the local maximum, the optimal prefilling increases. As one moves to the right in this region, the increase in the net number of electrons leaving the IB, if the prefilling matches the optimal prefilling, is larger than the reduction of the optimal filling. This is also the case to the right of the local minimum. Between the local maximum and the local minimum, the increase in the net number of electrons leaving the IB if the prefilling matches the optimal prefilling, is smaller than the change in the optimal filling. Note that the difference between the optimal prefilling and optimal filling increases all the way due to the increasing Φ.

For $E_{\mathrm{iv}} > 1.27\,\mathrm{eV}$, the optimal prefilling reaches 1. For such combinations of band gaps it is not possible for the cell to achieve the optimal filling. The illumination removes too many electrons from the IB. The dotted line in figure 5 shows the best achievable filling. Since the optimal filling can not be reached, the efficiency is slightly lower than found in case i) for these particular band gaps. For $E_{\mathrm{vi}} = 1.35\,\mathrm{eV}$, the difference in efficiency is 0.55 percentage points. For combinations of band gaps where the optimal filling can be obtained, the efficiency equals the efficiency plotted in figure 4.

In ref. [16] it was found that the optimal prefilling was the one where the illumination did not change the filling. This turns out to be a mere coincidence. The combination of band gaps and other parameters resulted in a situation corresponding to the crossing point in figure 5. It should, however, be noted that the absence of photon recycling in the model described in [16] is likely to be of importance when discussing the optimal filling.

The effect of the illumination on the filling of the IB will be reduced if N_{ib} increases [14]. With higher N_{ib} the optimal prefilling will therefore be closer to the optimal filling and vice versa. Oppositely, an increase in the light concentration will increase the effects of photofilling and therefore increase the difference between the optimal prefilling and the optimal filling. (With, of course, the exceptions that the optimal prefilling already has one of the extreme values 0 or 1.)

Figure 6 shows how a deviation from the optimal prefilling will affect the cell efficiency for a cell where photofilling is *not* occurring (dashed lines) and a cell where it *is* occurring (solid lines). The plot is done for $E_{\mathrm{iv}} = 1.3\,\mathrm{eV}$ and $E_{\mathrm{ci}} = 0.8\,\mathrm{eV}$ which is close to the efficiency peak in figure 4. Main absorbances of 1 and 5 are selected to get more 'extreme' values than with the rather moderate absorbance of 3 used earlier in this paper. Plots are also made for light concentration factors of both 10 and 1000.

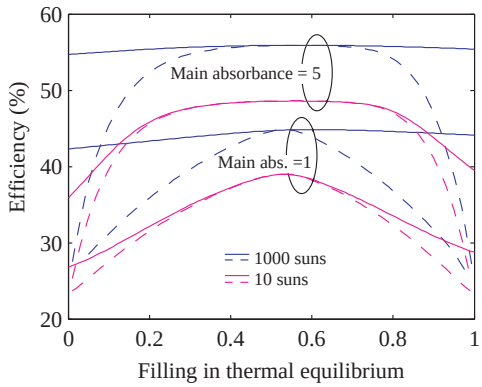

Figure 6: Cell efficiencies as a function of the filling in thermal equilibrium for a cell without photofilling (dashed lines) and a cell with photofilling (solid lines) at 10 and 1000 suns. Results are shown for main absorbances of 1 and 5.

When photofilling is occurring, the negative effect of a non-optimal prefilling can be reduced since the illumination may push the filling closer to the optimal. Higher light intensities will increase this effect, as already shown elsewhere [16]. The possibility of shifting the filling to more favourable levels is an advantage of cells with a low density of IB-states, as compared to cells with a large density of IB-states. On the other side, a high absorbance will also reduce the negative effect of a non-optimal prefilling. Keeping everything else constant, a large density of IB-states will result in large absorption coefficients. This makes it more likely that absorbances that are sufficiently high to compensate for a non-optimal filling can be achieved in a cell with a reasonable thickness.

iii) Overlapping absorption coefficients

When the absorption coefficients are overlapping, additional processes can occur as compared to in the non-overlapping case. For example, photons can be absorbed over a smaller band gap than the largest band gap with energy smaller than the photon energy. When such a transition has taken place and the resulting electron-hole pair thermalizes, an irreversible loss of energy has taken place. The extent of such energy losses can be reduced if the absorption coefficient for transitions over a certain band gap is larger

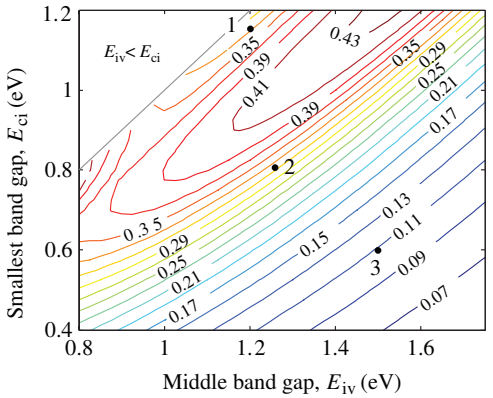

Figure 7: The optimal filling for cells with absorption coefficients overlapping with 0.3 eV.

than the absorption coefficients for transitions over all smaller band gaps [17]. Such a difference between the absorption coefficients also reduces the irreversible photon recycling processes, i.e. processes where a photon emitted in a radiative recombination process is reabsorbed over a smaller band gap leading to an irreversible thermalization loss. The latter processes will also be reduced if the cell thickness is limited, which is why there exist an optimal cell thickness when the absorption coefficients are overlapping [17].

Figure 7 shows the optimal IB-filling, as a function of the sub-band gaps, when the overlap between the absorption coefficients is 0.3 eV. As a general observation, one can see that the optimal filling is lower than in case i) (see figure 3), because with overlapping absorption coefficients it is favourable to reduce α_{ci} relative to α_{vi} for most combinations of band gaps when $E_{ci} < E_{iv}$.

In the lower right area of figure 7, the requests for a maximized net generation and minimized irreversible losses, are pulling in the same direction. The dependence of the optimal filling on the band gaps are therefore showing the same behaviour as in the lower right area of figure 3, but with the optimal filling shifted to lower values. In the upper left area, optimizing the filling with respect to the photon fluxes opposes the optimization with respect the irreversible losses. The optimal filling is thus a compromise between the two effects. Note that with overlapping absorption coefficients, the value of Φ

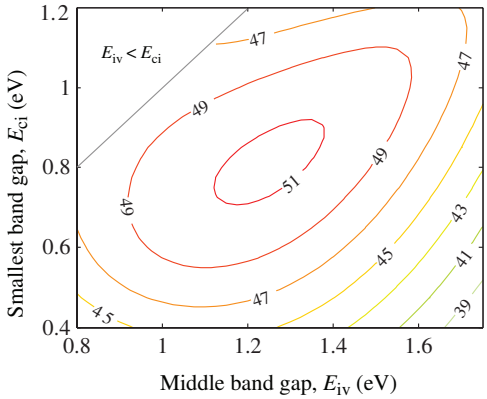

Figure 8: Efficiencies for cells with absorption coefficients overlapping with 0.3 eV.

is shifted from the values plotted in figure 2. The shift is particularly large when the difference between E_{ci} and E_{vi} is small.

The cell efficiency with overlapping absorption coefficients is plotted in figure 8. When moving away from the optimal band gaps, the efficiency does not decrease as much as in case i). With overlapping absorption coefficients, a relatively good balance between the generation rates can be achieved for a larger number of band gap combinations, due to the increased range of photon energies allowed to excite electrons over each sub-band gap. The position of the maximum efficiency is shifted slightly towards higher E_{ci} and lower E_{iv} because of the shift in Φ, and the resulting shift in what combinations of band gaps and filling that results in the most balanced generation rates. For combinations of band gaps near the efficiency peak, the optimal filling is 0.25 to 0.35 for an overlap of 0.3eV.

The dependence of the optimal filling on the degree of overlap is plotted in figure 9. The plot is made for three combinations of band gaps, marked as points 1, 2, and 3 in figure 7. For all three points, the optimal filling is shown to vary rapidly when the overlap increases slightly from 0. For example, for point 2 the optimal filling drops from 0.63 with no overlap to 0.45 when the overlap is 0.01 eV. The rapid decline is due to the fact that much of the photons emitted by the cell have energies close to the band gap energies.

Much of the negative effects caused by overlapping absorption coefficients therefore set in at small degrees of overlap.

Point 3 has $E_{\mathrm{iv}} = 1.5\,\mathrm{eV}$ and $E_{\mathrm{ci}} = 0.6\,\mathrm{eV}$. This combination of band gaps maintains a relatively constant ratio between the number of photons allowed to excite electrons over each sub-band gap when the overlap is increasing. After a decline for small overlaps, due to the onset of irreversible photon recycling, the optimal filling stabilizes for larger overlaps. For point 2, with $E_{\mathrm{iv}} = 1.25\,\mathrm{eV}$ and $E_{\mathrm{ci}} = 0.8\,\mathrm{eV}$, the number of photons allowed to excite electrons over E_{ci} increases relative to the number of photons allowed to excite electrons over E_{iv} when the overlap is increasing. Therefore, the curve for point 2 has a larger decline than the curve for point 3.

For point 1, with $E_{\mathrm{iv}} = 1.2\,\mathrm{eV}$ and $E_{\mathrm{ci}} = 1.15\,\mathrm{eV}$, the situation is a bit different. Here, the difference between the two sub-band gaps is so small that an overlap between the absorption coefficients is increasing the number of electrons that can be excited via the IB. An overlap of 0.3 eV between the absorption coefficients is therefore increasing the efficiency. The irreversible losses are also less destructive for point 1 than for point 2 and 3, since the difference between E_{iv} and E_{ci} is only 0.05 eV. Nevertheless, such losses do have a negative effect which for small overlaps results in a reduction of the optimal filling. When the overlap increases, however, the growing number of photons allowed to excite electrons over E_{ci} makes a higher filling more favourable because it will lead to a larger net generation via the IB. The positive effect of a large absorption over E_{ci} outweighs the negative effect of the irreversible processes.

Figure 10 shows how deviations from the optimal filling affects the cell efficiency for a cell with $E_{\mathrm{ci}} = 0.8\,\mathrm{eV}$ and $E_{\mathrm{iv}} = 1.25\,\mathrm{eV}$ (point 2). Having the right filling is increasingly important with increasing overlap. The larger the overlap, the more photons will be absorbed over E_{ci} which could have been absorbed over E_{vi}, if the filling is too high. With an overlap of 1.0 eV, the efficiency drops over 8 percentage points if the IB is half-filled as compared to an optimally filled cell. For point 1 (not shown in the figure), it is not as important as for point 2 to have the optimal filling, because the amount of energy lost in irreversible processes is smaller.

General discussion

The investigation of the cases i)-iii) have identified several parameters that can affect the optimal filling. Although some general conclusions can be made, an uncritical transfer of the numerical results to real cells should

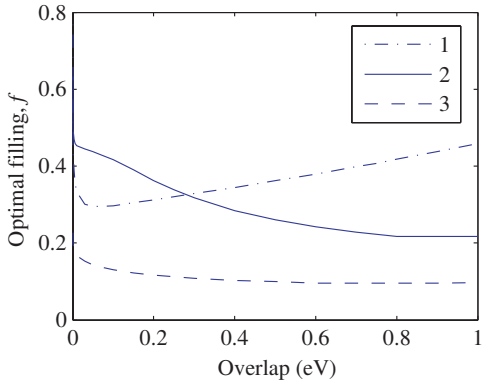

Figure 9: The optimal filling as a function of the overlap between the absorption coefficients. The plot is done for the three points shown in figure 7

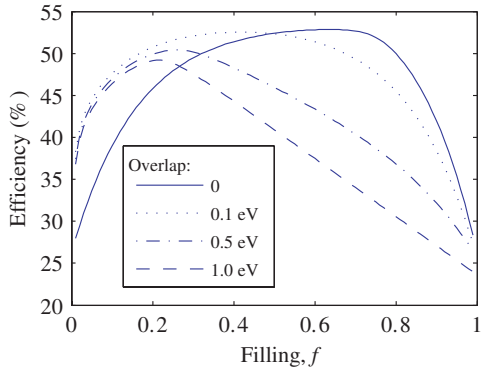

Figure 10: The cell efficiency plotted as a function of the filling of the IB for various overlapping between the absorption coefficients. The plot goes from $f = 0.01$ to $f = 0.99$, since $f = 0$ and $f = 1$ are unphysical. $E_{\mathrm{ci}} = 0.8\,\mathrm{eV}$ and $E_{\mathrm{iv}} = 1.25\,\mathrm{eV}$.

not be done. For real cells, non-radiative recombination, the width of the IB [20, 21] and other non-idealities will most likely affect the optimal filling. The actual energy dependence of the absorption coefficients also needs to be a part of the modeling before any conclusions can be made regarding the optimal filling of a particular cell or of cells made of a specific material.

For several cases it has been shown that deviations from the optimal filling only results in small efficiency degradations. It has also been shown, however, that cases where a non-optimal filling has a very negative effect on the cell efficiency, also exist. A real cell can have properties that make it sensitive to deviations from the optimal filling. This should be noticed when experimental cell performances are evaluated. A low efficiency *can* be due to a non-optimal filling of the intermediate band.

4. Conclusions

Models based on detailed balance principles have been applied to show that the optimal filling of an intermediate band solar cell depends on the band gaps, the light concentration, the degree of overlap between the absorption coefficients as well as the mutual sizes of the absorption cross-sections.

Two effects are identified as main reasons for the existence of an optimal filling. The first is the optimization of the net generation via the IB. The net generation is limited by the smallest generation rate over the sub-band gaps, which should be as large as possible. With non-overlapping absorption coefficients, maximizing the net generation is determining the optimal filling. When the absorption coefficients are overlapping, it is also important to reduce the losses associated with unfavourable absorption and photon recycling processes. The optimal filling is thus determined by the combined impact of the two effects.

It has also been shown that in cases where photofilling is an issue, one has to adjust the optimal prefilling to obtain the optimal filling during operation of the cell. Cases have been identified where the optimal filling can not be reached because the illumination is removing too many electrons from the IB.

Deviations from the optimal filling is not necessarily detrimental to the cell performance, but it *can* be. The negative impact of a non-optimal filling, is found to depend on the degree of overlap between the absorption coefficients, the absorptivity of the cell as well as whether photofilling occurs or not.

Acknowledgements

The authors would like to thank the Research Council of Norway for financial support through project no. 172905/S30.

References

[1] A. Luque and A. Martí, Phys. Rev. Lett. **78**, 5014-5017 (1997).

[2] W. Shockley and H.J. Queisser, J. Appl. Phys. **32**, 510 (1961).

[3] A. Luque and A. Martí, Prog. Photovolt: Res. Appl. **9**, 73-86 (2001).

[4] A. Martí, L. Cuadra, A. Luque, Physica E **14**, 150-157 (2002).

[5] A. Martí, E. Antoln, N. López, P.G. Linares, A. Luque, C.R. Stanley, C.D. Farmer, Thin Solid Films **516**, 6716-6722 (2008).

[6] P. Wahnón and C. Tablero, Phys. Rev. B **65**, 165115 (2002).

[7] K.M. Yu, W. Walukiewicz, J. Wu, W. Shan, J.W. Beemn, M.A. Scarpulla, O.D. Dubon and P. Becla, Physical Review Letters **91**, 246403 (2003)

[8] C. Tablero, Comp. Mat. Sci. **37**, 483-490 (2006)

[9] K.M. Yu, W. Walukiewicz, J.W Ager III, D. Bour, R. Farschi, O.D. Dubon, S.X. Li, I.D Sharp and E.E. Haller, Appl. Phys. Lett. **88**, 092110 (2006)

[10] C. Tablero, Phys. Rev. B **74**, 195203 (2006)

[11] P. Palacios, J.J Fernandez, K. Sánchez, J.C. Conesa and P. Wahnón, Phys. Rev. B **73**, 085206 (2006)

[12] C. Tablero, Solar Energy Materials & Solar Cells **90**, 588-596 (2006)

[13] A. Martí, L. Cuadra, A. Luque, IEEE Transactions on Electron Devices **48**, 2394-2399 (2001).

[14] R. Strandberg and T. Worren Reenaas, J. Appl. Phys **105**, 124512 (2009).

[15] A.S. Lin, W. Wang, J.D. Phillips, Journal of Applied Physics **105**, 064512 (2009).

[16] R. Strandberg and T. Worren Reenaas, *Drift-diffusion model for Intermediate Band Solar Cells including photofilling effects*.

[17] L. Cuadra, A. Martí and A. Luque, IEEE Transactions on Electron Devices **51**, 1002-1007 (2004).

[18] M.Y. Levy, C. Honsberg, Journal of Applied Physics **106**, 073103 (2009).

[19] G.L. Araujo and A. Martí, Sol. Energy Mat. and Sol. Cells **33**, 213-240 (1994).

[20] M.Y. Levy and C. Honsberg, Journal of Applied Physics, **104**, 113103 (2008).

[21] M.Y. Levy and C. Honsberg, Phys. Rev. B **78**, 165122 (2008).